Underwater piling noise

Predicting sound levels in water with
the Underwater Acoustic Simulator

Elisabeth Q. Kasteel

Technische Universiteit Delft

TUDelft

Underwater piling noise

Predicting sound levels in water with the Underwater Acoustic Simulator

by

Elisabeth Q. Kasteel

to obtain the degree of

Master of Science

in Hydraulic Engineering at the Delft University of Technology.

Van Oord

Marine ingenuity

TUDelft

Preface

This master thesis is the final work that completes my MSc in Hydraulic Engineering at the Technical University Delft. The project was conducted in cooperation with Van Oord who provided me with the fascinating topic of underwater acoustics. This gave me the opportunity to be part of the select group of people that are involved in and devoted to underwater acoustics. After nine months of research this thesis contributes to the knowledge there is in this field.

I would like to take the opportunity to thank those who contributed to this research. First I would like to thank my thesis committee for their help during this project. Many thanks to Gerben de Boer, my daily supervisor at Van Oord, for all the help shaping the project by encouraging me with your ideas and for your guidance in teaching me how to write a thesis. I would also like to thank Jeroen Hoving for helping me develop my own simplified sound models to master the physics of sound propagation and for your critic views on my results with the UAS. Also many thanks to Sabine Rijnsburger for your thoughts on a variety of subjects whenever I reached to you for advice. And of course, thanks to Prof. dr. Pietrzak for your help and insights during all our meetings. Furthermore, I would like to thank Niels Kinneging for providing me with various reports on the many aspects related to underwater sound. I would also like to thank Luuk Folkerts for providing me with the Gemini acoustic data. I would like to thank Marten Nijhof, Christ de Jong and Michael Ainslie for inviting my at the TNO office in the Hague and explaining me what their is to know about underwater sound propagation. Finally, I would like to thank Uwe Stöber from the Danish Hydraulic Institute (DHI) for his support and advice about the use of the UAS.

I would like to thank the employees at Van Oord for their interest in this topic during my research. A special thanks goes to Heidi van der Meij for her input on the topic and the fruitful discussions on my findings. Also thanks to Anestis Lioutas and William de Lange for their patience and help with installing the MIKE software and getting me started. Lastly, thanks to Alexander Franck for taking the time and showing me around in Vlissingen where I visited the Svanen. Also, thanks to my fellow graduate students at Van Oord. I really enjoyed sharing our experiences and can't think of a better place to have a coffee break than our office at the Rivium Boulevard.

Last but certainly not least, I would like to thank my parents for supporting me during my studies and for their effort reading this report and helping me improve my writing. I enjoyed working on this project for the last nine months, I hope you enjoy reading it.

Elisabeth Q. Kasteel
Rotterdam, April 2018

Abstract

This thesis investigates the important physical processes related to underwater sound propagation due to offshore pile driving with the first commercially available numerical model called the Underwater Acoustic Simulator (UAS). To make adequately use of noise mitigation measures during offshore wind projects and to protect marine life the prediction of sound levels in water is important. The aim of this thesis is to assess if the UAS is suitable to give insight in the physics contributing to sound propagation and if the UAS is suitable to quantify sound levels in water for the application in future wind park projects. This is done by comparing the predicted sound levels with the UAS with the measured sound levels obtained during the construction of the Gemini wind park.

The results obtained with the UAS identify the parameters related to the seabed properties as the most important for governing the attenuation of the noise levels as function of distance and frequency. In the UAS the seabed is modelled as a fluid which neglects the shear effect of the soil. This leads to underestimation of sound levels at low frequencies. Tsouvalas (2015) showed that the shear rigidity of the soil is important for the prediction of sound levels in water. The seabed is not the only parameter subject to simplifications in the UAS. Also the point source representation neglects important physics regarding the spreading of sound energy from the pile.

The model parameters can be tuned to fit the measured data. Although the UAS is able to predict sound levels in the Gemini area that agree well with the measured sound levels, this is not due to the correct implementation of the physic regarding the seabed and sound source. As a consequence, the model is tweaked to arrive at the measured sound levels. The UAS is therefore not considered suitable for application in future wind park projects.

Executive Summary

With the increasing demand for sustainable energy, the construction of offshore wind parks has developed rapidly. While the parks have a net permanent positive effect on the environment at large, without precautions the construction itself may cause temporary local harm to the environment. Especially the pile driving process during the construction of the wind turbines causes considerable noise. This can lead to sound levels up to 250 dB near the pile, which can cause permanent damage to marine mammals. Sound levels in water spread 10s to 10s of kilometres, due to which its effects cover a large area. Over the past years research into the effect of underwater noise on marine mammals has intensified. With this, ecologists provide answers to the sound levels that are harmful to marine animals. Also, noise generation from impact pile driving is a much-investigated topic. To this end, empirical, physical or numerical models have been developed to predict pile driving noise in the vicinity of the pile. However, to quantify the effect of pile driving noise on marine mammals, knowledge on how the sound propagates trough the sea water is needed as well. Models that investigate this do exist, but are mainly research models from universities and knowledge institutes.

In absence of more detailed knowledge, currently still a more practical way to quantify sound levels in water is used: simple geometrical spreading laws. These spreading laws show a logarithmic decrease in sound level with distance from the sound source. However, these approximations neglect important physical contributions to transmission loss of sound such as reflections from sea surface and seabed, sound absorption by the seabed and bathymetry. Thus this method does not account for, nor gives insight into the effect of the local ocean environment on the sound propagation.

No practical tool is available that has proven to properly account for the sea environment and thus give insight into its contribution on sound propagation. Recently, the first and until now only commercial-off-the shelf numerical model that predicts sound propagation in water has been developed, called the Mike Underwater Acoustic Simulator (UAS). Therefore, this thesis will investigate if the UAS is suitable to give insight into the influence of the local sea environment on underwater sound propagation and to quantify sound levels for application in offshore wind park cases. To this end the following aspects are considered. First, the physical processes contributing to sound propagation underwater are assessed. To place it into context, a literature study is performed to the degree to which impact of underwater sound on marine life has been investigated. Second, the contribution to underwater sound propagation of the processes implemented in the UAS are investigated. To this end, a sensitivity analysis on the model parameters is performed weighing their separate importance and effect on sound propagation. The results of these simulations are analysed using data obtained during the construction of the Gemini wind park in 2015. This wind park is located in the North Sea, 60 kilometres offshore off the Dutch Wadden Sea. During its construction sound levels were measured at 4 distances (750m, 7 km, 32 km and 65 km) from the source of the pile driving activities. This makes the dataset perfect for assessment of propagation models.

The UAS models sound propagation in the 2D vertical plane by using the Parabolic Equation technique. Literature ((Kibblewhite, 1989), (Ainslie, 2010) and (Hamilton, 1980)) shows that the properties of the seabed determine sound propagation in water to a large extent. The lower layers of the seabed impact the propagation of sound in the lower frequency ranges, whereas the upper seabed layers impact the relatively higher frequencies (Kibblewhite, 1989). In the UAS one can model the geological stratification of the seabed by implementing multiple homogeneous layers. These seabed layers are represented in the UAS as a fluid, neglecting the shear effect of the soil. A seabed consisting of two sediment layers is chosen in the model simulations. The upper layer is a sand layer accounting for the sandy sea floor of shallow water areas. The deeper layer is a rock layer accounting for the consolidated deeper seabed layers.

The contribution of the physical processes and model parameters becomes clear, when zooming in on the results displayed in the frequency spectrum. The analysis of the sediment type of the upper sand layer shows that this parameter mainly affects the frequency bands < 800 Hz. For increasing coarseness of the sand the total predicted sound levels increase (blue lines in Figure 5.4). The analysis of the choice of layer thickness of

the upper sand layer shows that this parameter mainly affects the frequency bands < 250 Hz. For a smaller layer thickness the predicted sound levels increase. Overall, the frequencies <800 Hz show a trend of under-estimation of the sound levels compared to the acoustic data. The predicted sound levels that fit the data best are obtained with an upper layer thickness of 2.5 m and a sand type that is classified as coarse. However, almost the same sound levels are reached for an upper layer thickness of 5 m and a sand type classified as very coarse. This shows that no evident choice exists to arrive at the best results compared with the data in the Gemini area. In order to arrive at the final results the model parameters were adjusted to fit the acoustic data measured in the Gemini area. The acoustic data is also used to construct the source spectrum input. The need for data to arrive at results that fit the data makes that the UAS has no predictive value. This diminishes its application to future wind park projects.
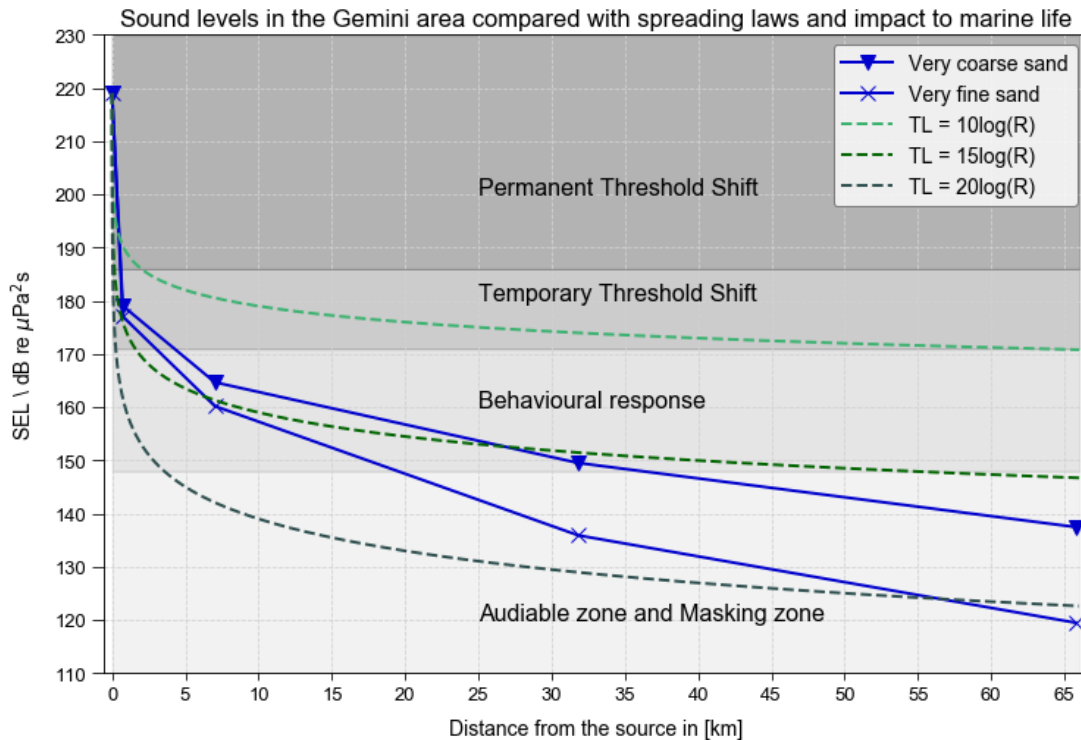

Figure 1: The predicted sound levels in the Gemini area for an upper sand layer consisting of very coarse sand (dark blue triangles) and very fine sand (dark blue squares). These results give a more precise indication of the sound levels than the geometrical spreading laws for shallow water (10log(R)), intermediate water (15log(R)) and deep water (20log(R)). Therefore the degree of impact the piling noise has on marine mammals as a distance from the source is better quantified.

This conclusion is amplified because important physics are not considered in the modelling of the seabed and sound source. An important issue concerning the implementation of the seabed in the UAS is the different wave types the sound takes on as it propagates trough the soil. In water and air sound propagates as compressional waves while in soil the sound propagates as a combination of compressional waves, shear (transverse) waves and Scholte waves. Especially at the lower frequencies the sound propagation is controlled by shear waves and Scholte waves. These types of waves are not included in the UAS physics since the seabed is modelled as a fluid. However, research (Tsouvalas, 2015) shows that the shear rigidity of the soil is the important contributor to the sound levels reached in the soil.

A second important issue concerning the modelling of sound is the vertical representation of the source sound. In reality the sound is emitted over the whole length of the pile. The sound waves spread into the water at an angle referred to as the Mach cone. Also, the pile geometry determines the amount of sound energy released in to the water. In the UAS the source is modelled as a point source that spreads sound equally in all directions. Furthermore, the source level input for the point source is iteratively determined based on the acoustic data available instead of the pile geometry.

Lastly, temperature and salinity determine the 3D sound speed distribution which steers the acoustic energy. Also bathymetry induces refraction in 3D patterns. Considering this, the fact that the UAS is a 2D vertical model implies that these factors cannot be studied. This is another physical process that is not considered in the UAS. Studies show ((Shapiro et al., 2014)) that this does affect the sound propagation resulting from piling noise. Since many offshore wind parks are located in areas with frontal activities this is recommended as a research topic.

Considering the limitations regarding the seabed, sound source and 3D effects, the results of the UAS should be viewed in another light. Exclusion of such essential physics raises questions about the physical validity of the model. Models that include the right physics regarding the seabed and the source, or a combination are available and are recommended to be used.

The results of this thesis are compared with the sound levels obtained when applying geometrical spreading laws (green lines in Figure 5.4). In this comparison the uncertainty introduced by the choice of sediment for the seabed is also considered (blue lines in Figure 5.4). Upto 30 km from the source the predicted sound levels by the UAS come close the to sound levels predicted by the $15log(R)$ law for intermediate water. This means that one can keep on using those. This will lead to conservative predictions, overestimating the sound levels further from the source. The predicted sound levels are also used to give an indication of the impact on marine mammals (Figure 5.4). The grey patches indicate the sound level ranges belonging to the different impact degrees piling noise has on marine life, as found in literature.

Contents

List of Figures

List of Tables

<div align="right">

1

</div>

Introduction

Global warming and air pollution are still steadily increasing. Governments seek to impose measures to reduce the use of fossil fuels that drives both global warming and air pollution. The convenience of fossil fuels is however hard to beat. In order to meet the need for fuels, alternative sources of energy are being developed and wind energy is one of them. Although traditional windmills are pretty and fit well in the countryside, some consider the modern wind turbines as unsightly and noisy. Nobody wants them close to their homes or littering the horizon. Therefore alternative locations are explored and offshore areas in shallow seas are being developed. Since the early development of offshore wind parks in the 1990s their construction continued to grow and growth is expected to continue in the coming years. The cumulative global offshore wind capacity is predicted to reach 74 GW in 2025, more than a sixfold of the current level of 12 GW (Douglas-Westwood, 2017).

An offshore wind park is a collection of wind turbines located in an area offshore, mostly in shallow seas close to the mainland, where the wind turbines can be installed on a substructure. Different types of substructures exist but the monopile is the most common one. In 2016 88% of the installed foundations for wind turbines were monopiles (Ho and Mbistrova, 2017). Monopiles are tubular steel piles with a length up to 70 meter and diameters sometimes exceeding 7 meter. They are driven into the seabed by vibratory hammers or by impact pile driving. The latter is the most popular method. High sound levels are reached underwater during impact pile driving. Sound levels up to 250 dB (peak-to-peak pressure) have been measured close to the pile (Thomsen et al., 2006). Furthermore the sound waves travel over tens of kilometres, affecting a large area. The impact of sound is important to consider for both the bidder and the contractor engaged in the development of offshore wind parks.

Van Oord has been involved in the successful construction of a number of wind parks in the last years. For the coming years several new projects are planned. The environmental impact of construction and operation works needs to be quantified early, to meet legislation and regulations regarding their impact on the environment.

1.1. Legislation, noise mitigation and marine life

In 2002 a European marine strategy was formalized by the European Committee. This led to the Marine Strategy Framework Directive (MSFD) which requires European Member States to develop strategies for their marine waters(Dekeling et al., 2013). European Member States are free to develop and adopt their own legislation within the boundaries of this framework. This has led to varying regulations among the member states. In the German and Belgium seas for instance, these regulations stipulate that the sound levels from impact pile driving are limited to a maximum value at a distance of 750 m from the monopile. In the Dutch sea however no maximum level is prescribed, but the impact pile driving activities are constraint to a seasonal restriction. This restriction focusses on the well being of the harbor porpoise as this species is considered the most sensitive to sound. From January till May more harbor porpoises live in the Dutch North Sea than in other times of the year. To limit the impact of sound on these animals the legislation entails that only a limited amount of piles is allowed to be installed and the duration of the pile driving activities is minimized.

In order to comply with the legislation a variety of noise mitigation measures has been developed by the offshore wind industry. Bubble curtains are the most commonly used noise barrier. This is a system that is deployed around the monopile at the bottom of the sea and releases bubbles of air into the water. The impedance between water and air influences the sound wave propagation in this way reducing the sound levels. Another noise mitigation method is a panel-based noise abatement system. It consist of four panels surrounding the monopile that houses submersible air-filled acoustic resonators (Corp, 2014). This system focusses on the low-frequencies (30-200 Hz) while the bubble curtain mainly filters the higher frequencies. A third system exist which is called the Hydro Sound Damper (HSD). This system consists of nets with air filled elastic balloons and PE-foam elements. The high dissipative effects of these elements damp the impact piling noise (Elmer and Savery, 2014). The performance of the systems mentioned have been tested and reviewed in varying offshore wind park projects. The measured noise reduction varies from 7-12 dB for the bubble curtain (Dähne et al., 2017) to 25 dB for the HSD at 750 m from the monopile (Elmer et al., 2016). For the panel-based system a noise reduction of 36.8 dB at 285 m and 29.6 dB at 750 m from the monopile have been recorded (Corp, 2014). These pilot projects show promising results for application in wind park projects. However the successful implementation depends on many factors, including for example the dependency of the noise reduction on distance and frequency. Furthermore, their application during pile driving activities is expensive. Therefore a precise indication of the desired noise reduction is desirable. Another issue is that these systems focus mainly on the damping of the sound propagating through the water column. The sound energy that propagates through the seabed and is transmitted back into the water is not affected by these measures. Therefore insight in to physics regarding this aspect are important to master.

The legislation and regulations concentrate on impact pile driving as a sound source and the well being of the marine life being exposed to this noise. An Acoustic Deterrent Device (ADD) and a soft start are included in the standard offshore pile driving procedure in all European countries. This must drive away the animals from the proximity of the impact pile driving activities. Van Oord has developed the FaunaGuard, an acoustic device that safely and temporarily deters marine life and uses special underwater acoustics to prevent potential hearing loss to porpoises. To assess the effect that pile driving noise has on these species and to be able to purposeful apply devices as the FaunaGuard, the impact of piling noise on animals is a well studied topic. Ecologists study impact of sound on marine mammals, depending on the distance between the source and receiver. Also, the sound levels related to temporal or permanent damage are subject to extensive research. For marine contractors as Van Oord this information is valuable to assess the environmental impact of their work and to adequately make use of noise mitigation measures. To do that predictions of the sound levels in the construction area are required.

1.2. Sound propagation models
A number of methods to quantify sound levels in water are available. Several numerical models that simulate underwater sound propagation in order to predict sound levels have been developed. Also a lot of research is performed on the development of finite element models that simulate the monopile as a sound source. With such models the sound field and propagation in the vicinity of the monopile as a results of the impact hammer is studied. These numerical models are mainly research models developed and owned by universities or knowledge institutes. These models are thus not in-house available to Van Oord. A more practical method used to calculate sound levels in the sea is based on the estimation of the transmission loss of sound over distance. This is called the principle of geometrical spreading loss. The method assumes that the total amount of energy produced by the sounds source stays constant as the sound waves spread out through the water. With the spreading of the sound over distance the energy produced by the sound source is spread out over an increasing surface. As the energy is conserved, the intensity of the sound will decrease with increasing distance from the source. This is called spherical spreading loss as it describes the sound waves propagating as spheres centred around the sound source. The sound waves cannot propagate uniformly in all directions from a source in the sea forever, especially not when the sea is shallow. Beyond a certain range the sound will hit the sea surface and the seabed, forming lower and upper boundaries. With the cylindrical spreading loss approximation this effect is taken into account. The sound energy produced by the sound source is distributed uniformly over the surface of a cylinder with a radius equal to the range considered and a constant height equal to the water depth of the sea. The calculation of the transmission loss (TL) is expressed in equation 1.1 as a function of distance R from the source,

$$TL = Nlog(R) \qquad (1.1)$$

with the coefficient N being equal to $N = 10, 15, 20$ accounting for the shallow, intermediate and deep water respectively. No precise guidelines exist to determine if one is dealing with shallow, intermediate or deep water. Therefore the use of spreading laws results merely in a range indicating the expected sound levels (Figure 1.1).

An issue regarding this method is that the approach of geometrical spreading neglects al kind of physical processes that are present in the sea and that contribute to transmission loss. Reflections from the sea surface and seabed cause reflection losses (Osborne, 2010). Jensen (2001) mentioned water absorption due to its chemical composition as an other contributor to transmission loss. A varying waterdepth influences the distribution of the sound in the water column. Tronstad and Hovem (2011) showed in a study of the propagation of air gun signals over long distances that even small variations in bathymetry affect the sound propagation in the sea. This study also mentioned the influence of seasonal effects in the sea environment. Temperature, salinity and ambient pressure influence the 3D sound speed distribution and therefore the propagation paths and the transmission loss of the underwater sound (Brekhovskikh et al., 2003). In the shallow regions where offshore wind parks are located these temperature and salinity variations are present which cause stratification of the water column. Several studies ((Rousseau et al., 1982), (Heathershaw et al., 1991), (Lynch et al., 2003) and (Shapiro et al., 2014)) have shown that this impacts the sound levels in the seawater.
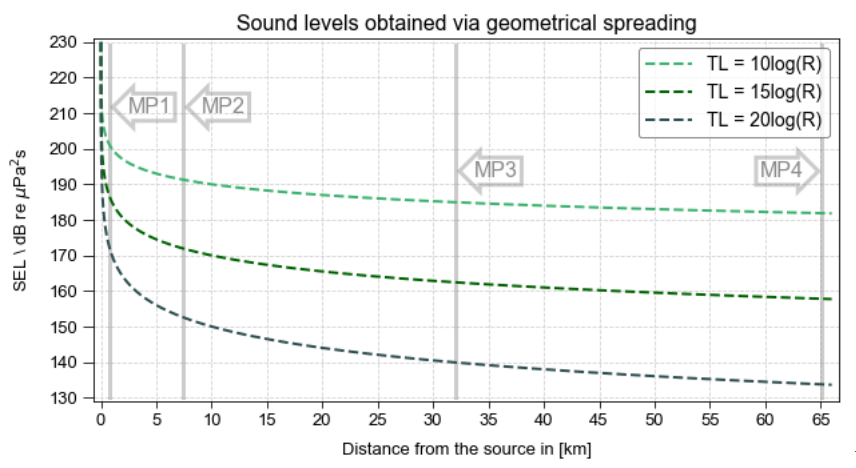
Figure 1.1: The sound levels obtained with the use of the geometrical spreading laws for spherical spreading (10log(R), intermediate spreading (15log(R) an cylindrical spreading (20log(R). The four arrows indicate the locations of the four positions where sound measurements were conducted during the construction of the Gemini wind park. These locations are labelled MP1 to MP4 and are respectivly 750 m, 7 km, 32 km and 65 km from the monopile.

Recently, the Mike Underwater Acoustic Simulator (UAS) has been developed. This is the first and until now only commercial-off-the shelf numerical model that predicts sound propagation under water. The UAS simulates sound propagation in a vertical plane with a seabed modelled as a fluid instead of a solid. This tool is intended to quantify sound levels resulting from human work in the sea. It has however not yet proven its validity for application in offshore wind park projects by marine contractors.

As ecologists provide answers to the degree to which sound levels are harmful to marine animals, a lot of research is put into the development of numerical models simulating the sound field in the vicinity of the monopile. The prediction of sound levels based on the physics influencing sound propagation is needed to adequately use noise mitigation measures and to protect marine life.

1.3. Thesis aim and approach

This thesis aims to investigate the physical processes that contribute to sound propagation in the sea with the Mike Underwater Acoustic Simulator (UAS). Moreover, the suitability of the UAS to unravel the influence of the local sea environment on underwater sound propagation is assessed. In doing so, its suitability to quantify sound levels in construction of offshore wind parks is evaluated.

A literature study is performed into the physical processes contributing to sound propagation underwater. Also, the degree of impact of underwater sound on marine life is investigated to place the research into context.To assess the suitability of the UAS and investigate the important processes a number of scenarios with varying model parameters have been tested. The results are compared with acoustic data obtained during the measurement campaign conducted at the construction of the Gemini wind park. This wind park is located in the Dutch North Sea, 60 km north of the Wadden Sea (area indicated in red in Figure 1.2). The pile driving of the monopiles as foundation for the wind turbines took place in July 2015. At four different distances from the pile (arrows in Figure 1.1) and at two heights above the seabed the sound pressures resulting from the hammering sequence were recorded. This makes the dataset perfect for the assessment of propagation models and therefore the results of the simulations with the UAS will be compared to the measured sound levels at these locations.

1.4. Thesis outline

The literature study of the processes of propagation of underwater sound and its impact on marine life are presented in Chapter 2. The dataset obtained with the measurement campaign at Gemini is analysed. This data and the parameter values used in the model simulations are presented in Chapter 3. The results of the sound propagation simulations are given in Chapter 4 together with a physical interpretation of these results. The conclusions follow which are delineated in Chapter 5. Also in this chapter, the research will be viewed in context with other research and aspects related to underwater sound. Lastly, recommendations are outlined in Chapter 6.
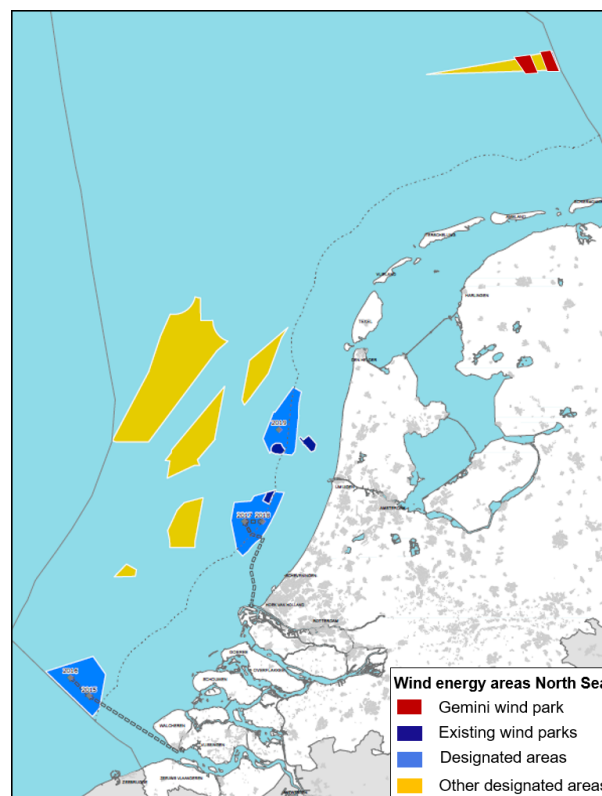
Figure 1.2: A map of the Dutch North Sea indicating the location of the Gemini wind park (red areas). The location of other wind parks and areas that are designated for the construction of future wind parks are indicated with the blue and yellow areas respectively. The figure is based on 'Route kaart op zee 2017-2018'.

2

Physical processes of underwater sound

The literature study presented in this chapter aims at providing the theoretical background related to this master thesis. Sound propagation in water forms the basis of this thesis. It is essential to understand what sound is and what the physical quantities are that describe sound propagation. Therefore this will be treated first. Also, the decibel, the unit used to express sound levels, is shortly addressed. This is done to underline the importance of its correct use and understanding. Second, the impact pile driving as a sound generating source is considered. The physical mechanisms related to this are discussed, just like how these mechanisms affect underwater sound. The third section presents the physical processes in the sea contributing to sound propagation. In the last section a concise overview is given on the impact of underwater sound on marine life, to place it all into context.

2.1. Sound characteristics

Sound is a pressure wave that originates from perturbations which generate local compressions and expansion in the fluid medium the sound wave is travelling through. These compressions and expansions are transferred because of the mediums compressibility. This and the density determine the local sound speed with which the perturbations propagate,

$$c = \sqrt{\frac{K}{\rho}} = \sqrt{\frac{1}{\chi \rho}} \tag{2.1}$$

where ρ is the density of the medium and K is the bulk modulus in Pa. For a fluid K is the inverse quantity of the compressibility χ. This property quantifies the relative variation of volume or density due to pressure variations. Equation 2.1 holds for sound waves in a fluid and differs from sound waves in a solid which support both compression variations and shear effects.

Additionally, the sound wave is characterized by the local motion amplitude of each particle in the medium and by the particle velocity corresponding to this motion[1]. This motion compresses and expands the medium causing the acoustic pressure detected by ear. The strength of the vibrations which defines their amplitude, determines the loudness of the sound experienced. The frequency of the oscillations determines how high or how low the sound is experienced.

2.1.1. Sound notation

Acoustic quantities are expressed in decibels (dB). The decibel is ten times the base-10 logarithm of the ratio of two values of a physical acoustic quantity. The decibel has no physical dimensions since it is a relative unit and not an absolute one. The logarithmic scale is chosen for two reasons. Firstly, to deal with the wide and dynamic range of sound experienced in day to day life. Secondly, it is to acknowledge that the loudness of sound perceived increases in a logarithmic way and not in a linear way (Chapman and Dale, 1998).

---

[1]The particle velocity is not the same velocity as the sound speed at which the sound wave propagates

In a uniform acoustic medium, the magnitude of the acoustic intensity I is proportional to the square of the acoustic pressure,

$$I = \frac{p_0^2}{\rho c} \tag{2.2}$$

with ρc being the specific acoustic impedance. This is a property of the medium that expresses the resistance a sound wave encounters when propagating through this medium. Ten times the base-10 logarithmic ratio of two acoustic intensities results in a certain difference expressed in decibel between the intensities,

$$\Delta dB = 10 \log_{10}\left(\frac{I_1}{I_2}\right) \tag{2.3}$$

Accordingly, the difference expressed in decibel of two sound pressure values follows from equation 2.2 and equation 2.3 and reads,

$$\Delta dB = 10 \log_{10}\left(\frac{I_1}{I_2}\right) = 10 \log_{10}\left(\frac{p_1^2}{p_2^2}\right) = 20 log\left(\frac{p_1}{p_2}\right) \tag{2.4}$$

Absolute decibel levels are obtained when a ratio of an acoustic quantity is defined relatively to the reference level of that quantity. For acoustic pressure this entails,

$$dB = 20 \log\left(\frac{p}{p_{ref}}\right) \tag{2.5}$$

In water the reference level for pressure (p_{ref}) is 1 μPa. In air p_{ref} is 20 μPa. The unit decibel is only used properly when the reference level is stated and when two identical physical quantities are compared. Physical quantities are identical when they describe the same time-domain and frequency-domain.

Underwater sound caused by pile driving are non-continuous or transient sounds. The most common definitions used for expressing transient sounds in decibel levels are:

1. Sound Pressure Level (SPL)

2. Zero-to-peak sound pressure level

3. Sound Exposure level (SEL)

Sound Pressure level
This is the sound level resulting from the variation of the sound pressure over time. The acoustic pressure varies above and below a mean value with time. The Sound Pressure Level allows for this variation by averaging over a certain time interval.

$$SPL = 10 \log \frac{1}{T} \int_0^T \frac{p(t)^2}{p(t)_{ref}^2} dt \tag{2.6}$$

Zero-to-peak sound pressure level
This is the sound level resulting from the square of the peak pressure to the square of the reference pressure. The peak pressure is the maximum absolute value of the instantaneous sound pressure during a stated time interval.

$$L_{peak} = 10 \log \cdot \left(\frac{p_{peak}^2}{p_{ref}^2}\right) \tag{2.7}$$

Sound Exposure Level
This is the sound level resulting from the ratio of the sound exposure (E) to the reference sound exposure (E_{ref}). The sound exposure is the time integral of the time-varying square of the instantaneous sound pressure over a transient sound event: $E = \int_{-\infty}^{+\infty} p(t)^2 dt$. The reference sound exposure is defined as $E_{ref} = p_{ref}^2 T_{ref}$, in which p_{ref} is the reference sound pressure 1 μPa and T_{ref} the reference duration of 1 s.

$$SEL = 10 \log \frac{E}{E_{ref}} \tag{2.8}$$

2.1.2. Sound attenuation

The main effect of sound propagation is the decrease in pressure amplitude. This decrease in amplitude is mainly caused by the spreading of the sound intensity, also referred to as geometrical spreading. The sound intensity becomes weaker the further away it travels from its source. The energy loss in radial distance from the source is distributed over the surface of a hemisphere with area $2\pi r^2$. The intensity of the wave is the energy per unit area of the wave front,

$$I = \frac{E}{2\pi r^2} \tag{2.9}$$

The decrease in intensity with travelled distance is proportional to $1/r^2$. The decrease of pressure amplitude is therefore proportional to $1/r^2$.

2.1.3. Sound wave types

Sound waves can take on different forms as they propagates through different types of medium. This section discusses the sound wave types that are important for sound propagation in water:

1. Longitudinal waves present in fluids and solids

2. Transverse waves present in solids

3. Rayleigh waves along a solids surface

4. Scholte waves present at the soil-water interface

The displacement of the medium in a longitudinal wave is parallel to the direction the wave travels. This results in regions where the mediums particles are spread apart or compressed together, the expansions and compressions discussed earlier. In the expanded regions a low sound pressure occurs, while in the compressed medium high pressures occur. This type of sound wave is able to travel through gasses, fluids and solids. In a transverse wave or shear wave the movements of the particles in the wave are perpendicular to the travel direction of the wave. This requires a material to have shear strength which is not the case for water and air. Both Scholte waves and Rayleigh waves are a combination of a longitudinal wave and a transverse wave. The Scholte wave propagates at the solid-water interface in a water body and the Rayleigh wave travels near the surface of a solid (Zhu et al., 2004).
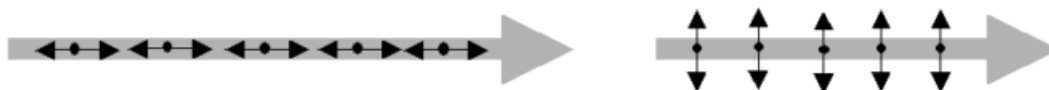
Figure 2.1: Longitudinal waves (left) and transverse waves (right): The motion of the particles (small black arrows) is either parallel or perpendicular to the direction of wave propagation (grey larger arrows).

2.2. The pile driving process

Impact pile driving is a method used to install piles for marine and inland water construction projects using high-energy impact hammers (Dahl et al., 2015). It is the most widely used installation method despite the drawbacks regarding this installation method being a source of high sound levels. The next sections will discuss this sound generation and the paths the sound propagates along after the impact hammer hits.

2.2.1. Sound field resulting from impact pile driving

With impact pile driving a hydraulic hammer is used to induce a series of blows on a monopile to drive it into the soil. The force exerted by the impact hammer on the pile causes a compression at the top of the pile. In a simplified one-dimensional system this compression travels down the pile along the vertical axis of the monopile with a wave speed c_p. When the wave reaches the tip of the monopile the compression wave causes a radial expansion of the pile which pushes the pile into the soil. Then the compressional wave is reflected from the tip of the pile up to the top of the pile (Figure 2.2).
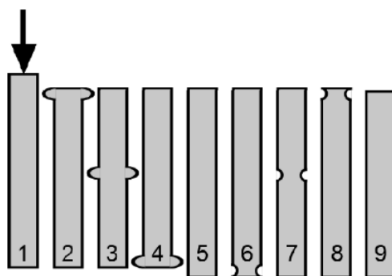
Figure 2.2: Schematic impression of a wave propagation through a monopile as a result of a force exerted by an impact hammer (Rhijn, 2017).

The monopile is surrounded by air, water and soil. The compression wave travelling down the monopile causes a radial expansion. This way the energy from the blows is radiated in the form of longitudinal pressure waves into the air and water. Experiments and model analysis performed by Reinhall and Dahl (2011) have shown that this is the main contribution to the underwater noise from impact pile driving. Not all the energy enters the water and air, a part of the energy enters the soil.

The wave speed in steel is approximately c_p = 5120 m/s, depending on the surrounding medium. This is a substantial higher wave speed than the wave speed in water of c_w = 1500 m/s. As a consequence the wave fronts released from the pile travel under an angle $\phi_w = \sin^{-1}\left(\frac{c_w}{c_p}\right)$ = 17.2° (Figure 2.3(i)). This is the angle between the vertical axis of the pile and the released wave fronts. This angle changes from ϕ_w to $\phi_s = \sin^{-1}\left(\frac{c_s}{c_p}\right)$ = 18.6 ° as the compressional wave in the pile enters the section of the pile surrounded by sediment (Figure 2.3 (ii)). As the deformation of the pile reaches the pile tip it is reflected upward releasing pressure waves into the sediment under angle ϕ_s (Figure 2.3 (iii)). The sound field associated propagates up through the sediment and penetrates into the water where ϕ_s changes to ϕ_{ws} = 30.0 °. This gives a wave field with two wave fronts, one with angle ϕ_w and one with angle ϕ_{ws} (Figure (2.3 (iv)). As a result the acoustic field has the shape of a cone that is symmetric around the pile, also referred to as a Mach-cone (Reinhall and Dahl, 2011).

2.2.2. Sound propagation paths after impact pile driving

After the impact hammer hits the monopile the sound propagates through air, water and soil. Due to direct contact between the monopile and the air and water the sound travels as longitudinal pressure waves through air and water. The sound path through air hardly affects the sound levels under water. The sound path in water is the main contributor to the underwater sound levels (Reinhall and Dahl, 2011). The last noise path is the one propagation through the soil.

Part of the airborne sound waves enter the water. The sound waves in air approach the air-water interface under an incident angle. If this angle with the horizon is < 77° the airborne sound is fully reflected. This is the reason that models by (Young, 1973) predict that the sound levels underwater that originates from the airborne path is only present close to the pile. This, combined with the acoustic impedance of the transfer from air to water, is the reason that the airborne sound contribution is insignificant to the sound levels underwater.

As the compression wave travelling down the pile reaches its tip both shear waves and compressional waves propagate into the soil. A short moment in time later, Scholte waves are observed at the seabed-water interface (Tsouvalas, 2015). The Scholte waves travel at this interface and leak their sound energy into the water thereby contributing to the sound levels in the water. A higher shear rigidity of the soil makes the sound energy propagating in the form of Scholte waves radiate further away from the water-soil interface into the fluid. These waves contain mainly low frequencies. Because the damping factor of soil is much higher than that of water, the high frequency waves are damped out by the soil before entering the water. This is not the only frequency dependant phenomenon in the soil. The deeper parts of the sediment are relevant for low-frequency propagation (<1 kHz), while the upper parts of the sediment column govern the propagation at the higher frequencies (1-10 kHz) (Kibblewhite, 1989).
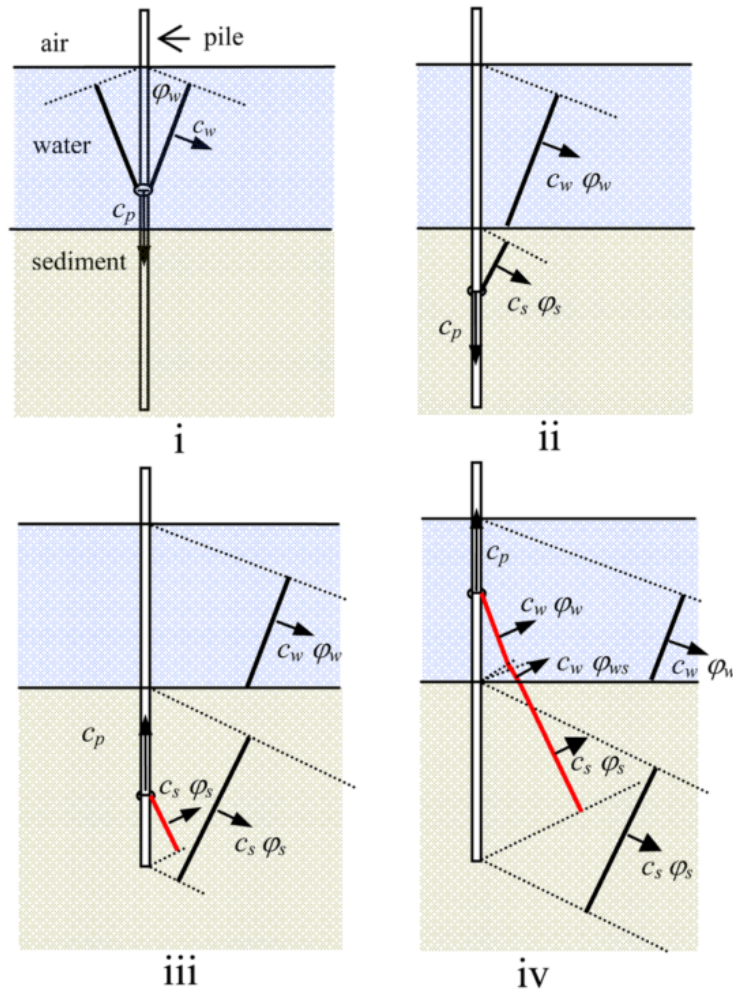
Figure 2.3: Illustration of the propagation of the wave fronts associated with the Mach cone generated by the pile compression wave. (i) Wave front before reaching the sediment. (ii) Wave front after pile deformation wave have reached the sediment. (iii) Wave fronts after the first reflection of deformation wave. (iv) Wave fronts after the reflected deformation wave has reached the water.Reinhall and Dahl (2011)

2.3. Sound propagation in the sea

The change of sound speed over depth, distance and azimuth induce refraction of sound waves. The direction in which the sound energy travels is steered in this way. The sound speed in the sea at a certain depth is given by (Medwin and Clay, 1998),

$$c = 1449.2 + 4.6T - 0.055T^2 + 0.00029T^3 + (1.34 - 0.01T)(S - 35) + 0.016z \qquad (2.10)$$

with T being the temperature of the seawater, S being the salinity of the seawater at a certain depth z. In shallower areas such as continental shelf and slope regions the water is not deep enough for the depth pressure term to be significant (Kuperman and Roux, 2007). Thus, in these regions only the temperature and salinity variations influence the 3D sound speed distribution.

Also variations of the water depth influence the sound in the sea. On an upward sloping bottom the sound energy converges. Due to that slope the incident angle of the sound waves changes. For larger incident angles the propagation path increases and more reflections occur (Figure 2.4). This results in more transmission loss. An inclined seabed profile also makes the sound refract in both horizontal and vertical direction thereby steering the sound energy.
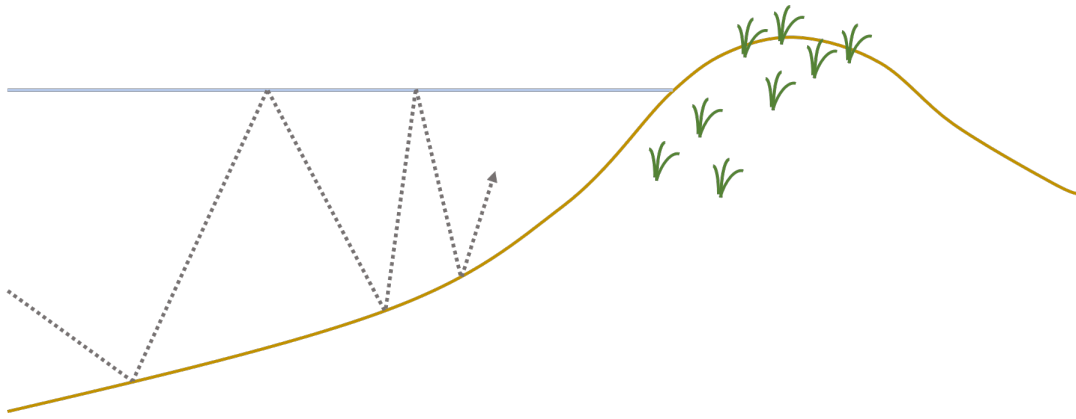
Figure 2.4: Schematization of how a sound wave reflects on a sloping seabed.

2.3.1. Sound absorption in seawater

Sound spreading loss expressions in water are often extended with attenuation losses expressed with the attenuation coefficient of seawater α in dB/km. This coefficient α includes the effects of the attenuation of sound due to the absorption by chemical properties of the seawater and absorption by suspended solid particles in the seawater. The attenuation coefficient is expressed as,

$$\alpha = \alpha_w + \alpha_v + \alpha_s, \tag{2.11}$$

where α_w is the attenuation coefficient of clear seawater, α_v includes the attenuation due to viscous absorption by suspended solid particles and α_s represents the attenuation due to scattering of suspended solid particles.

Attenuation in clear seawater

The attenuation in clear seawater considers the absorption of sound as the sum of the contributions from pure water and processes involving magnesium sulphate and boric acid. Several expressions for this coefficient exist, but the expression by Francois and Garrison appears to be be the most complete and therefore the most widely used, (Richards, 1998),

$$\alpha_w = \frac{A_1 P_1 f_1 f^2}{f_1^2 + f^2} + \frac{A_2 P_2 f_2 f^2}{f_2^2 + f^2} + A_3 P_3 f^2 \tag{2.12}$$

This expression gives a prediction of the absorption of sound in clear seawater in the frequency range of 200 Hz to 1 MHz and to depths of 5000 m. The first two terms in equation 2.12 represent chemical relaxation processes, the first deals with the effects of boric acid and the second with the effects of magnesium sulphate on sound propagation. The third term represents the absorption from pure water, (Francois and Garrison, 1982a). The dependency of α_w on pressure and relaxation frequencies are given by the coefficients P_1, P_2, P_3 and f_1, f_2, f_3, respectively. The coefficients A_1, A_2, A_3 express the contribution of the salinity, temperature, pH of the water and sound speed on the sound propagation.

Attenuation due to suspended particles

The presence of suspended solid particles in the seawater leads to two additional attenuation mechanism. The first mechanism is due to viscous absorption. The suspended solid particles induce frictional heat between the particle and the ambient fluid. Because the particles have higher inertia than an equivalent volume of water, a velocity gradient in the boundary layer between water and particle exist. This velocity gradient in a viscous fluid as water leads to friction and with that to loss of amplitude of the movement of the water particles. The second mechanism is the scattering of sound. The suspended solid particles induce scattering of the sound waves in all directions. This leads to loss of energy in the primary sound wave.

In Francois and Garrison (1982a) and Francois and Garrison (1982b) research is done into the dependencies of frequency ranges on the different absorption and attenuation mechanisms. They found the contribution from boric acid to be dominant for frequencies below 10 kHz. Coefficient A_1 is a function of the value of the pH of the seawater and soundspeed, coefficient P_1 is equal to 1 and coefficient f_1 is a function of salinity and temperature. Francois and Garrison (1982b) found that the pH is the largest contributor to the absorption by boric acid. At frequencies 10-200 kHz the effect of the absorption by magnesium sulphate, expressed in the second term of equation 2.12 is dominant. Since A_2 is mainly a function of salinity and slightly depended on temperature, the value of the salinity of the seawater will dominate the absorption due to magnesium sulphate. At frequencies above 200 kHz the absorption due to pure water, expressed in the third term of equation 2.12 has the largest contribution. Since A_3 is a function of temperature, in these frequency ranges temperature will dominate the absorption due to magnesium sulphate. For frequencies below a few hundred Hz the absorption in clear seawater decreases to a negligible effect.

2.3.2. Sound absorption in the seabed

As a compressional sound wave in water reaches the water-seabed interface, part of the wave is reflected and part of the wave is transmitted into the seabed as a compressional wave and shear wave (Figure 2.5). The amount of reflection or transmission of the sound energy depends on the density of both mediums, the impedance ratio and the angle at which the wave reaches the boundary. This is derived from *Snell's law of refraction* (Jensen et al., 2011),

$$\frac{cos\theta_1}{c_1} = \frac{cos\theta_2}{c_2} \tag{2.13}$$

This law shows that the sound waves bends towards the medium with lower propagation speed and therefore determines the grazing angles at which sound waves reach medium interfaces.

The main loss mechanism for incident sound waves on the seabed is through the transmission into the sediment. The seabed is a layered medium whose acoustical properties vary with depth on length scales from a few millimetres to hundred of meters. Depending on the layering of the seabed or the presence of reflecting boundaries close to the water interface the sound energy is reflected and scattered.
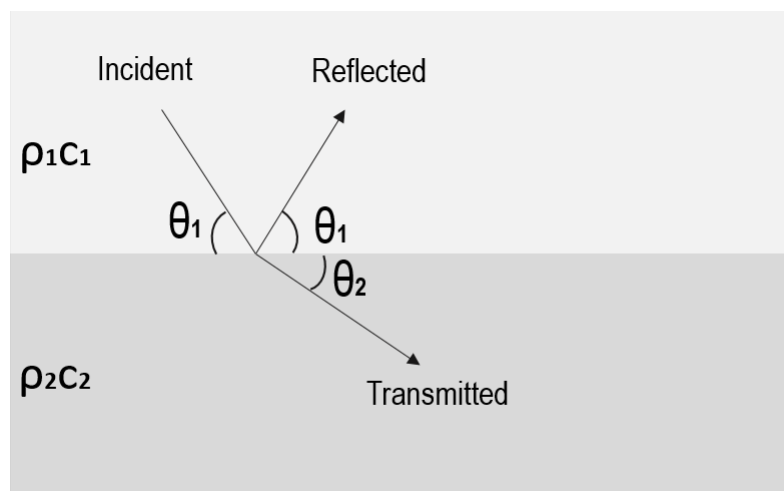
Figure 2.5: An incident sound wave is reflected and transmitted as it reaches the water-seabed interface

The attenuation in the seabed is often expressed with the attenuation coefficient for a sediment in dB/λ. This coefficient is a function of frequency, sediment grain size and sediment density. The losses associated with it arise from viscous drag between the water in the sound field and sediment grains and arise from the scattering of sound by the sediment grains, (Urick, 1948). Buckingham (2002,2005) derived a relation between the porosity and grain size on one hand and their ability to support sound propagation on the other hand. Generally it is observed that more compact sediments cause relatively less attenuation. These sediments have a higher wave sound speed for which less sound penetrates into the sediment, because more sound is reflected. These compacter sediment are in general coarse, thus have a larger grain size. Sediment types are classified in different degrees of coarseness. Gravel is considered a coarse sediment while sand can consist of fine particles (fine sand) and coarser particles (coarse sand).

2.4. Impact of Underwater sound on marine life

The underwater noise as a consequence of impact pile driving, or other sound sources, can affect marine life in many ways. To what extend these sensitive receivers are effected depends on a variety of factors of which the main issue is the specie in question. Furthermore, age, gender and health related factors play a role. Also, sensitieve receivers are effected by the underwater sound in many different ways. The sound can interfere with their communication system, hinder acoustics signal detection or effect their auditory system. More severe impacts are the temporary or even permanent shifts in hearing threshold, concussive effects, physical damage to tissues and organs or stress. These consequences of underwater sound are divided into different degrees of impact, named below in order of increasing severity:

1. Audibility

2. Masking

3. Behavioural responsiveness

4. Temporary Threshold Shift in hearing (TTS)

5. Permanent Threshold Shift in hearing (PTS)

The audibility is defined as the point at which the animal in question is able to detect the sound. This is limited by two factors. Namely, if the noise falls below the animals audiogram or if the noise falls below the ambient noise level (Erbe and Farmer, 2000). An audiogram is a graph that indicates the hearing treshold per frequency. The ambient noise level due to for example shipping in the North Sea is 90 dB (Remmers and Bellmann, 2016). The audiogram of harbour seals and harbour porpoises is very wide (Figure 2.6). For harbour seals the hearing range extends from 75Hz-100kHz with the best hearing approximately between 8-16kHz (two blue lines in Figure 2.6). For harbour porpoises this range is from approximately 100 Hz to 140kHz with the best hearing between 16-140kHz (green line in Figure 2.6), (Kastelein et al., 2002). Thomsen et al. (2006) conclude in their study that the zone of audibility for both harbour porpoises and harbour seals is beyond 80 km from the impact pile driving source.

If the sound intensity is loud enough the underwater noise can mask other sound signals. The masking region defines the range within which noise is strong enough to interfere with detection of other sounds at certain frequencies (Thomsen et al., 2006). For sensitive receivers this means that it interferes with for example communication sounds, echolocation and predator and pre sounds. The range of masking can for some frequencies coincide with the range of audibility and occurs to up to 80 kilometres from the source.

Behavioural responsiveness means that animals show difference in behaviour due to the detection of underwater sound. Change in swim direction and swim speed, dive duration or surfacing duration are indicators of this impact. Harbour seals show behavioural responses for SPLs in the range 135-148 dB re 1 μPa, (Götz and Janik, 2010), (Kastelein et al., 2017), (Southall et al., 2007). For harbor porpoises also levels within this range are foun around SPL 140 dB re 1 μP. (Southall et al., 2007). This corresponds to a distance from the source where behaviour responsiveness is observed that extends atleast up to 15 km, (Tougaard et al., 2003a), (Tougaard et al., 2003b) and (Tougaard et al., 2005).

An auditorial threshold shift is the noise level to which animals are exposed for which loss of hearing sensitivity occurs. A temporary threshold shift (TTS) means that the hearing returns to normal after some time.

Otherwise it is permanent threshold shift (PTS) which is considered an injury. TTS and PTS are not only dependent on the sound levels received by the animals but also dependent on the time the animal is exposed to the sound and if the sound is transient like pile driving noise or continuous. Furthermore, the severity of the TTS and PTS is expressed in the magnitude of the threshold shift in dB and the time its takes for the threshold to recover to normal. The onset of TTS for harbour seals occurs at SELs of 183 to 206 dB in dB re 1 μPa^{2}s, (Kastak et al., 2005). Southall et al. (2007) found an TTS onset of 171 dB re 1 μPa^{2}s and PTS onset of 186 dB re 1 μPa^{2}s for harbour seals. In their study Kastelein et al. (2012) found a maximum TTS of around 15 dB at an SEL of 190 dB re 1 μPa^{2}s for harbor porpoises. The exposure lasted 240 minutes at a 4 kHz signal. The occurrence of PTS for harbor seals could be prevented if seals are outside a range of 100 to 200 meter from the source, (Kastelein et al., 2017). For the harbor porpoise this is 1.8 km, (Thomsen et al., 2006).
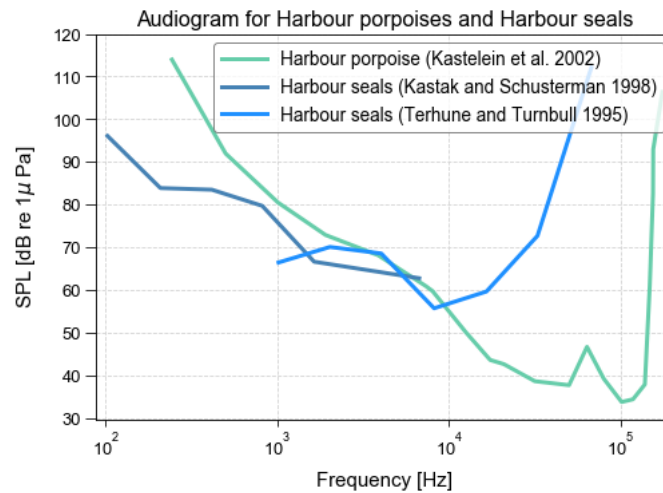
Figure 2.6: Audiograms of harbour porpoises and harbour seals, adopted from (Thomsen et al., 2006)

3

Methods

This chapter explains how the UAS is used to identify the important physical processes of sound propagation. Each model parameter is subject to a number of simulations to determine their effect on the results. The values used for each simulation is discussed in this chapter. The results of these simulations will be compared with measured sound levels, to relate them to the physical reality. Therefore this chapter will start with a detailed explanation of the available acoustic dataset obtained during the construction of the Gemini wind park. Subsequently, the specifications of the UAS are discussed. The algorithm used to model the sound propagation is shortly highlighted as well as the model assumptions and limitations. This is followed by the explanation of the used values of the model parameters in the different scenarios.

3.1. Acoustic data from the Gemini area

The acoustic dataset used in this thesis is obtained during the construction of the Gemini wind park. This wind park consist of two smaller wind parks, each with 75 offshore wind turbines. The offshore wind turbines are fixed into the seabed by monopiles. Each wind farm has its own offshore high voltage station. Such a station is fixed in the seabed by a jacket-construction with pin-piles. During the construction the Intitute for technical and applied Physics GmbH (ITAP) performed measurements to monitor the underwater sound. Itap is a German company that provides technical-scientific services in the field of underwater acoustics.

The monopiles of the different wind parks and the pinpile have different diameters. Measurements are performed for all the different pile types. The selected monopiles are labelled U8 and Z2, respectively and the pinpile is labelled B3. The sound measurements are performed at four distances of each pile and at two height above the seabed, 2 m and 10 m. The four distances from the source are labelled MP1 to MP4 and are respectivly 750 m, 7 km, 32 km and 65 km from each pile. The location of MP1 differs for every pile so that the distance to that pile is approximately 750 m. The locations of MP2 to MP4 are fixed and thus the same for every pile.

The measurements are conducted with hydrophones which record sound pressure levels. The measurement devices used are have a sampling frequency of 48 kHz. These devices have a high reproducibility of ≤+1 dB concerning the hydrophones. However, an unsystematic measurement uncertainty in repeated measurements in the range of ≥ 2 dB is generally to be expected during field measurements under offshore conditions. (ITAP) reported the results of the underwater sound measurements and provided the raw and processed data for the hammering sequence of each pile U8, Z2 and B3. For this thesis the hammering sequence the processed data of monopile U8 is analysed.

3.1.1. Sound levels monopile U8

The hammering sequence of monopile U8 started 21 July 2015 at 11:10h UTC and lasted 2 hours and 54 minutes. The used acoustical parameter in this analysis is the Sound Exposure Level (SEL) expressed in dB re $\mu\,\text{Pa}^2\text{s}$. The results as processed by ITAP are presented in one-third octave frequency bands. A third octave band is a bandwidth of frequencies where the difference between the lower limit and the upper limit of the band is equal to one-third octave and the centre frequencies of the bands are spaced by a ratio of $10^{0.1}$ such that ten one-third octaves make precisely one decade (Ainslie, 2011). A decade is a logarithmic unit of frequency ratio defined such that a factor 10 change in frequency corresponds to one decade (Ainslie, 2011). An octave is a logarithmic unit of frequency ratio defined such that a factro 2 change in frequency corresponds to one octave (Ainslie, 2011). In Table 3.1 the exact locations of the measurement positions MP1 to MP4 and the distances to monopile U8 are indicated. To be able to do an analysis a well-defined hammer strike is selected from the piling sequence of pile U8. The selected strike is chosen taking into account that a pause is present in the piling activities just before the strike. This is because at larger distances from the pile reverberations from a single strike can overlap with the sound of the previous strike.

Position	Latitude	Longitude	to U8 [m]
MP1$_{U8}$	54° 04,835' N	006° 03,446' E	732
MP2	54° 02,306' N	005° 57,949' E	7,017
MP3	53° 56,096' N	005° 37,816' E	31,816
MP4	53° 46,922' N	005° 11,029' E	65,764

Table 3.1: Measurement locations

The Sound Exposure Level for a single strike is determined with the procedure discussed in section 2.1.1 using equation 2.8. t_0 and t_1 in equation 2.8 are the start and end times of the integration interval selected for the single strike (Remmers and Bellmann, 2016):

- t_0 is selected 200 ms before the moment of the maximum magnitude of the sound pressure.

- t_1 is selected 800 ms after the moment of the maximum magnitude of the sound pressure.

This results in the integration window for a single strike of $t_1 - t_0 = 1000$ ms. The SEL for a single strike is expressed in the total SEL level in dB re $\mu\,\text{Pa}^2\text{s}$ and the distribution of the contributions of separate frequency bands to this total SEL, the SEL frequency spectrum.

Figure 3.1 shows the SEL spectrum at the four measurement locations at 2 meter and 10 meter height above the seabed. The main energy of the piling sound occurs in the 31.5 Hz to 1 kHz one-third octave bands, with a maximum at the 125 Hz third-octave band for MP1 to MP4. The levels at 2 meter above the sea bed are slightly lower than at 10 meter above the sea bed. The shape of the spectra at the four measurement position MP1 to MP4 is generally the same. The frequencies ≥ 1 kHz dampen out faster than frequencies < 1 kHz. This is reflected in a faster decrease in sound levels when moving away from the monopile. The difference between the sound levels measured at 2 meter above the seabed and 10 meter above the seabed becomes larger further away from the monopile.

3.2. The Underwater Acoustic Simulator

The model used for this thesis is the Underwater Acoustic Simulator (UAS). This is a module of the MIKE software developed by the Danish Hydraulic Institue (DHI). The UAS is a two-dimensional model that calculates sound transmission loss in the vertical plane, from now on called a transect. Within such a transect the UAS takes into account the attenuation of sound in sea water as derived by Francois and Garrison (1982a) and Francois and Garrison (1982b). The UAS calculates transmission loss in the vertical water plane and in the seabed. The seabed is modelled as one or multiple uniform sediment layers which behave as a fluid. This means that the propagating sound waves are modelled as compressional waves only. The sound propagation in the seabed is governed by the compressed wave speed, the density of the sediment and the sound attenuation coefficient in the sediment. Also, the sound speed distribution over depth can be included. The sound source is modelled as an omnidirectional point source at a depth specified by the user. This implies that from
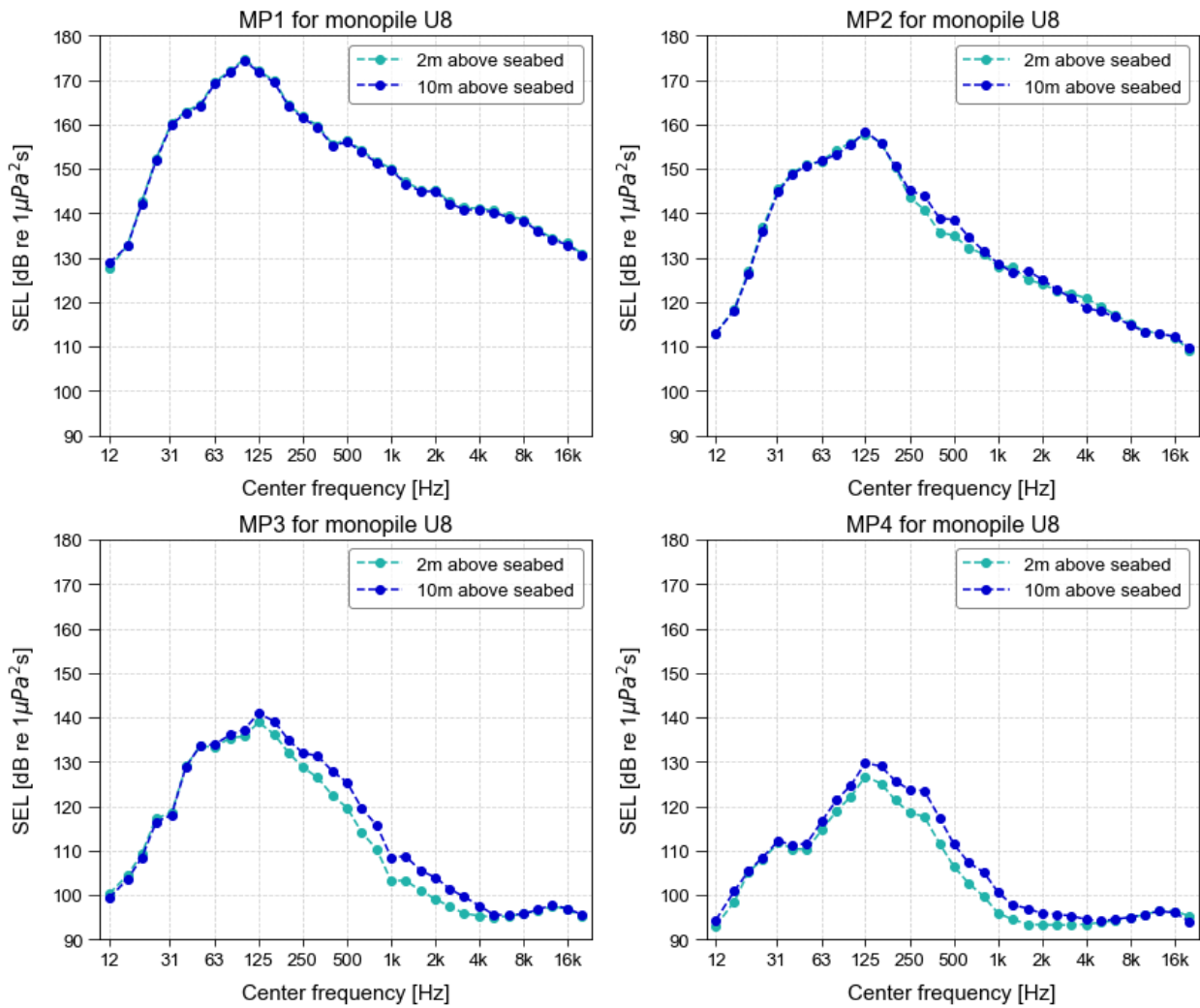
Figure 3.1: One-third octave band spectra of the sound exposure level for the selected piling strike as record by two hydrophones at 2m and 10m above the seabed at the measurement location MP1, MP2, MP3 and MP4 for Gemini pile U8

the source the sound spreads equally in all directions.

The UAS is a Range dependent Acoustic Model (RAM) based on the Parabolic Equation (PE) technique as described by Collins (1989) and Collins (1993). Using this approach the UAS determines the transmission loss over range and depth per frequency by taking the sound levels from the source input. With the outcome from these calculations the sound level per frequency and the total sound level at every location in the transect are determined.

The model is based on the following model assumptions:

- The PE approach used is based on the assumption that outgoing energy dominates back-scattered energy to obtain an outgoing wave equation (Collins, 999a). Hence, the back-scattered sound energy is ignored in the UAS.

- The PE approach used is based on the far-field assumption $k_0 r \gg 1$.

- The sea states accounting for the influence of wind and waves are ignored.

- The seabed is modelled as a fluid. Hence, the physical contribution of shear waves and Scholte waves is ignored.

- The UAS only accounts for large-scale bathymetry. Localised area with for example large stones are not resolved.

- The near-field acoustics effects associated with the propagation of the sound under the Mach-cone angle are ignored because of the point source representation.

Modelling of sound propagation can be done with normal modes. A normal mode is a pattern of motion for which all parts of the system move with the same frequency. The normal mode solution is obtained by a superposition of the up-and down going plane wave of equal amplitude and vertical wave number (Jensen et al., 2011). The complete acoustic field is then constructed by summing up contributions of each of the modes.
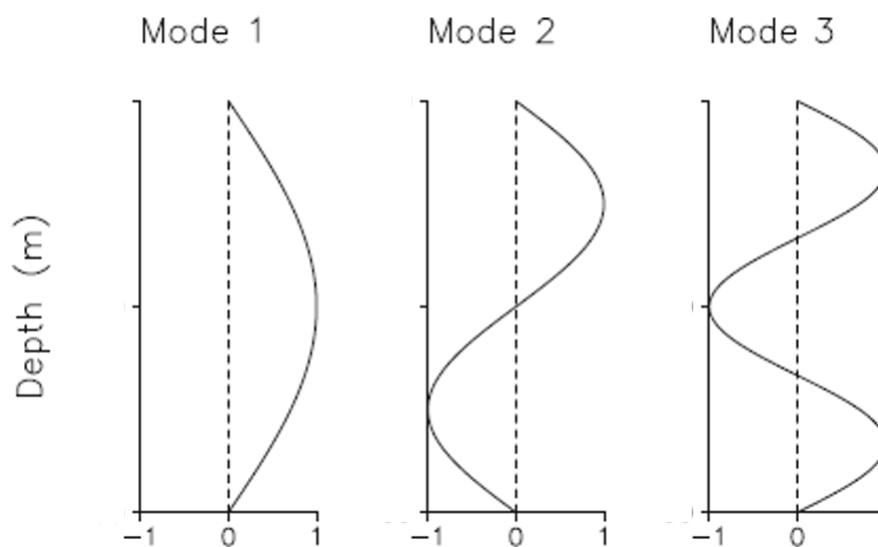
Figure 3.2: The first three normal modes

3.3. The UAS parameters

3.3.1. The modelled transect

The modelled domain is the part of the North Sea where the Gemini wind park is situated (Figure 1.2). The modelled transect starts at the location of monopile U8. The start of the transect is where the sound source is located. The transect reaches over a distance of 66 km covering all measurements locations (Figure 3.4). Based on Binnerts et al. (2016b) the modelled transect is chosen to have a constant water depth of 34 m.

It is possible with the UAS to use the local bathymetry in the modelled transect. This input bathymetry is linearly interpolated in the UAS to each location in the transect. This way the algorithm determines for each grid point if it is in the water or if it is part of the seabed. After studying the results of the UAS simulations it became clear that the implemented bathymetry is not modelled in a satisfactory manner and affects the results. Therefore it was chosen to use a constant water depth.

3.3.2. The source level input

The source level (SL) symbolizes the measure of radiated sound power or sound energy by the source. In the case of offshore pile driving this is the sound level emitted at the monopile surface caused by the impact of the hammer. The Gemini data discussed in section 3.1.1 consists of sound level measurements at four different locations from the monopile. A measure for the source level is not included in these measurements. This is because the source level in the UAS is a virtual value that cannot be determined by measurements due to the physical sound spreading mechanism at the monopile. Additionally, in the acoustic near field, measurements of the sound pressure and the sound velocity are needed to characterize the strength of sound, but sound velocity sensors for underwater noise are not available or not accurate (Remmers and Bellmann, 2016). However, this value is needed to use as input for the simulations.
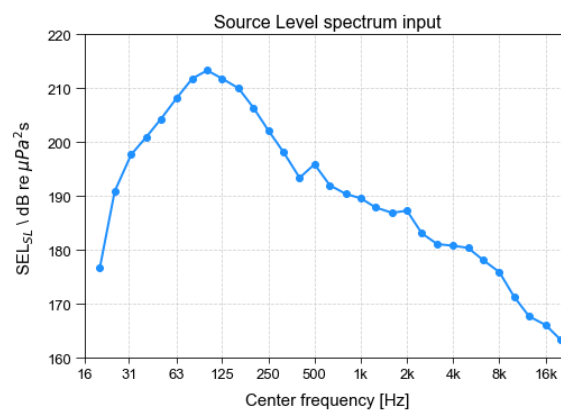
Figure 3.3: The estimated one-third octave band source level spectrum expressed in Sound Exposure Level that is used as the input for the simulations with the UAS

The source level can be estimated using a physical or numerical source model or by using field measurements of received level to back-calculate the source level using an appropriate propagation model[1]. This is because in shallow water sound propagation is dominated by the interaction of the sound with the seabed and water surface and the extrapolation approach does not take these boundary interactions into account, (Farcas et al., 2015). Since realistic physical or numerical models are complex and not at the disposal for this thesis, the acoustic data from section 3.1.1 is used. To calculate the source level, measurements of the sound level received at a certain distance r are combined with an estimate of the propagation loss between the source and receiver: $SL = SEL_{data}(r) + TL(r)$, (Lepper et al., 2012), (Farcas et al., 2015) and (Robinson et al., 2014). An estimate of the propagation loss is made with the UAS itself, thereby the source level input is determined iteratively. The source level is expressed in Sound Exposure Levels (SEL) in the one-third octave frequency band spectrum (Figure 3.3).

---

[1]To calculate the transmission loss by extrapolating the available data back to the source via a simple logarithmic spreading law is not regarded as an appropriate approach, (Robinson et al., 2014)

Figure 3.4: The locations of the four measurement positions MP1, MP2, MP3 and MP4.

3.3.3. The water phase

Temperature, salinity and pH

The temperature and salinity values together with the pH value determine the attenuation of sound in the water in dB/km via the expression derived by Francois and Garrison (1982a) and Francois and Garrison (1982b) discussed. Temperature and salinity are measured in the area around Gemini. The sea surface temperature is measured by a TRIAXYS measurement buoy at the Gemini location. Additionally, 32 km north east from this buoy a measurement ship TW/EMS performed measurements on temperature and salinity in the year 2015. The water temperature is measured on 3, 6, 10, 15, 20, 25 and 30 m water depth. Salinity is recorded at 6 and 30 m water depth. Claessens (2016) interpolated the values from these measurements. The temperature distribution over depth and the salinity at 6 and 30 m water depth are shown in Figure 3.5. Since the data gives no indication of the value for the pH this value is derived using Beare et al. (2013). In this paper the variability of ocean parameters in the North Sea is indicated. These values are used as guideline in the analysis to calibrate the model for the correct pH value. In Table 3.2 the definite values are presented. Using these parameters results in values of the attenuation coefficient α_w ranging from 0.011 dB/km for f = 200 Hz to 3.05 dB/km for f = 20 kHz.
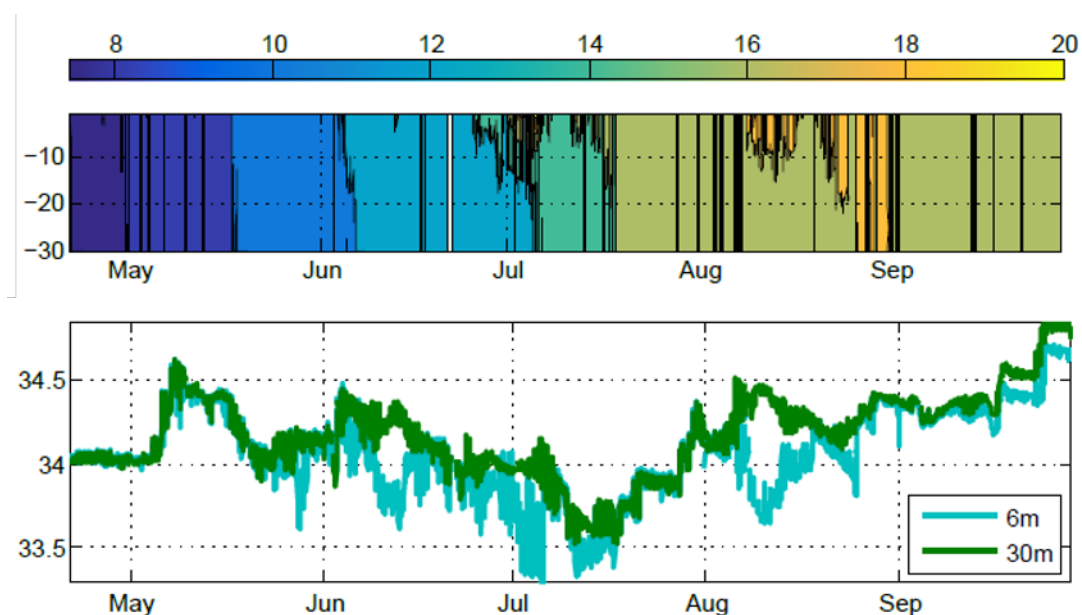
Figure 3.5: Temperature and salinity measurements through depth made by the TW/EMS station in 2015. Temperature measurements during 2015 in a contour plot (top). Salinity measurements during 2015 at 6 and 30 meter depth (bottom), from (Claessens, 2016)

Parameter	Value [unit]
Temperature	14 ^{o}C
Salinity	33.5 PSU
pH	8.5

Table 3.2: Model parameters for the water phase

Other values for these parameters are used to test the sensitivity of the UAS to uncertainties in the used values. These scenarios are in further detail presented in Appendix D.

Sound speed distribution

The speed of sound is determined by the water temperature, salinity and because of shallow water to a lesser extend depth. The water temperature and salinity values from Figure 3.5 are used to determine the sound speed distribution via equation 2.10. This results in a sound speed of c = 1501 m/s. It is assumed that the sound speec is constant over depth.

3.3.4. The seabed

The seabed in the UAS is modelled as a fluid. One or multiple homogeneous sediment layers can be applied. Each soil layer is characterized by four geoacoutic parameters: the density of the specific soil layer, the compressed wave speed in this layer, the compressional attenuation in this layer and the thickness of this layer. According to Hamilton (1980) a geoacoustic model represents the true thickness and properties of the sediment layers. This includes the uppermost few meters of sediment that mainly consists of unconsolidated sediments. Additionally, this also includes the lower consolidated sedimentary rock layers in the seabed at a few 100 meters depth. The layering of the seabed in the Gemini area is not known. Therefore, based on the description by Hamilton (1980) it is assumed that the seabed in the UAS consist of two geo-acoustic layers. The first and upper layer is a layer that represents the unconsolidated sediments and the second and deeper layer is a rock layer that represents the consolidated sedimentary rock.

Upper layer sediment type

The soil type of the upper sand layer is determined using the Seabed Substrate map by EMODnet Geology (MVe). The sediment in the modelled domain is classified as sand according to the Folk classification[2]. A range of possible values for the density, compressed wave speed and compressional attenuation coefficient for the found sediment classification exist and is described in Ainslie (2010). The geoacoustic properties are frequency dependent and devided in three frequency ranges. The high-frequency properties are important for the propagation at frequencies > 10 kHz and represent the uppermost few centimeters of the seabed. The mid-frequencies are applicable to the range 1 - 10 kHz en respresent the first meters of the seabed. Altough this must be done carefully, these geo-acoustic properties can also be applied to the ranges < 1 kHz. Because low-frequency properties are not evident to derive for a fluid seabed as in the UAS, the mid-frequency properties are used.

Sand comes in different classifications based on its coarseness. The different types of sand are investigated with the UAS. The geoacoustic parameters compressed wave speed and sediment density are expressed as a ratio with their equivalent value in water[3]. An overview of the investigated sediment types is given in Table 3.3. For al the simulations performed the used layer thickness of the upper sediment layer is 5 m.

Sediment type	Compressed wave speed	Sediment density	Sediment attenuation [dB/λ]
Very coarse sand	1961 m/s	2470 kg/m^3	0.89
Coarse sand	1835 m/s	2224 kg/m^3	0.87
Medium sand	1797 m/s	2146 kg/m^3	0.88
Fine sand	1685 m/s	2001 kg/m^3	0.89
Very fine sand	1669 m/s	1870 kg/m^3	1.05

Table 3.3: Geo-acoustic parameters of the various sediments types used in analysis of the upper seabed layer composition based on (Ainslie, 2010).

The second and lower layer is a rock layer. Ainslie (2010) provides the information on the geoacoustic parameters several rock types. The chosen values are presented in Table 3.4. These values parameters are the maximum values possible in the UAS. The deeper rock layer is made as rigid as possible. This way it reflects the most sound energy to obtain the best results.

Sediment type	Compressed wave speed	Sediment density	Sediment attenuation [dB/λ]
Rock	5500 m/s	3000 kg/m^3	0.10

Table 3.4: Geo-acoustic parameters of the used rock layer.

Upper layer thickness

The thickness of sediment layers impacts the sound propagation. The influence of the layer thickness is related to the ability of the seabed to absorb the sound. A number of values for the layer thickness are used

---

[2]The Folk classification is a common classification derived by Folk (1954). It groups grains into mud, sand and gravel on the basis of their diameter with the boundary between mud and sand size grains at 63 μm and the boundary between sand and gravel size grains at 2 mm. The relative proportion of the grains in the three categories is then used to describe the sediment

[3]The sound speed in water is discussed in section 3.3.3. Therefore, the density of the water is calculated by inserting the data on temperature, salinity and pH in the Ocean Density Calculator

and presented in Table 3.5. All these simulations are performed with the sediment type classified as coarse sand in Table 3.3.

Layer thickness
160 m
80 m
40 m
10 m
5 m
4 m
2.5 m

Table 3.5: The layer thickness used for the different scenarios

Sediment type and layer thickness combined

Scenarios with different combinations of layer thickness and sediment type are studied, to asses its effect on the predicted sound levels. In Table 3.6 the different scenarios are displayed. The geoacoustic properties belonging to the sediment type are as indicated in Table 3.3.

Sediment type	Layer thickness
Very coarse	5 m
Very coarse	2.5 m
Coarse	5 m
Coarse	2.5 m

Table 3.6: The layer thickness and sediment types used for the different scenarios

Cut off frequency

In shallow water sound propagation a critical frequency exist below which the energy propagates directly in to the seabed. This is referred to as the low-frequency cut off. This frequency is dependent on the acoustic soil properties and is therefore treated in this section. The propagation at frequencies below the cut off frequency is controlled by the Scholte waves at the interface of water and seabed (Kibblewhite, 1989). However, these type of waves are not included in the UAS. Therefore, the propagation below this cut off frequency cannot be accounted for in the UAS.

The cut off frequency for a homogeneous water column is given by

$$f_0 = \frac{c + w}{4D\sqrt{1 - (\frac{c_w}{c_b}^2)}} \tag{3.1}$$

where D is the depth of the water column, c_w is the sound speed in the water colomn and c_b is the sound speed of the seabed. The cut off frequency for the situation described above is $f_0 = 18$ Hz. Therefore, in this thesis only the frequencies above this cut off are evaluated.

3.4. The UAS output settings

The UAS simulates the transmission loss per frequency. The modelled frequencies are the center frequencies of the one-third octave frequency bands. The UAS solves the used equations with a resolution Δr and Δz. This resolution is determined by the algorithm of the UAS. The results of the UAS simulations are then generated on a mother grid which is defined by means of horizontal and vertical spacing and a maximum depth. This resolution is user defined and should be chosen to adequately resolve the relevant characteristics of the simulated sound field pattern. When the calculations are finished the results on the mother grid are saved to the output files. For the output files horizontal and vertical intervals are chosen defining the resolution of the output relative to the mother grid. Also these intervals are user defined. The predicted sound levels in the output files are discretized in the transect. These results are linearly interpolated to be able to compare the UAS predicted sound levels with the measured sound levels at the exact measurement locations.

<div align="right">

4

</div>

<div align="right">

Results

</div>

In this chapter the results of the modelling of the sound propagation with the UAS are presented. The seabed is the key factor in the obtained results and is therefore treated extensively. The other scenarios that are simulated are addressed shortly. Table 4.1 gives an overview of the scenario groups and the tested variables. The focus is twofold when looking at the results. First, the behaviour of the sound levels in the frequency spectrum is observed and compared with the measured sound levels. This will be done for every measurement location, MP1, MP2, MP3 and MP4. Second, the effect on the total received sound levels over the range of the modelled transect is examined. Subsequently, the sound levels that fit the acoustic data best are discussed, as well as the parameter values used. For these results also the frequency spectrum and total received sound levels are observed. In the last section of this chapter the results are related to the physics contributing to the observed behaviour.

Scenario groups	Variables
The seabed	Varied sediment type upper layer
	Varied thickness upper layer
	Rock upper layer
The water phase	Varied temperature, salinity and pH
Source and receiver	Varied locations

Table 4.1: The scenario groups with corresponding description of the simulated and analysed variables

4.1. Results for the separate parameters

4.1.1. The Seabed

Sediment type upper layer

At MP1 the sound levels for 20 -63 Hz are the same fro all sediment types (upper left panel Figure 4.1). For frequencies > 63 Hz the modelled sound levels differ from the measured sound levels. The frequency distribution of the Sound Exposure Level (SEL) shows an irregular pattern. A clear difference between the sound levels reached per frequency band per sediment type is visible from MP2 (upper right panel Figure 4.1). For the frequency bands (≤ 800 Hz) concerned the magnitude of the difference between the predicted sound levels increases with distance from the source.

At MP2 for frequency bands < 250 Hz the very fine sediment (grey line in Figure 4.1) predicts the lowest sound levels and very coarse sediment (black line) predict the highest sound levels. For both sediment types the highest sound level is reached at frequency band 100 Hz. For very coarse sand the sound level is 160 Hz and for very fine sand the sound level is 153 Hz. The other simulated sediment types, fine sand (blue line), sand (green line) and coarse sand (yellow line), result in sound levels between the very fine sand and very coarse sand, increasing in loudness with increasing coarseness (Figure 4.2).

At MP3 and MP4 the same behaviour is observed for the frequency bands ≤ 500 Hz and ≤ 800 Hz respectively. At MP3, the highest sound level for very fine sand is 120 dB at frequency band 500 Hz and for very coarse sand

is 141 dB at frequency band 100 Hz. Also the sound levels of frequency bands 20-50 Hz for very fine sand (grey line) are below the ambient noise level. This is not reflected in the measured data at this locations (red line in Figure 4.1). For fine sand (blue line) the sound level of frequency band 20 Hz is below the ambient noise level.

At MP4 the highest sound level for very fine sand is 110 dB at frequency band 500 Hz and for very coarse sand is 128 dB for frequency band 160 Hz. Here the sound level for frequency bands 20-200 Hz for very fine sand (grey line), 20-160 Hz for fine sand (blue line), 20-80 Hz for sand (green line), 20-50 Hz for coarse sand (yellow line) and 20-31.5 Hz for very coarse sand (black line) are below the ambient noise level of 90 dB. This is not reflected in the measured data at this locations (red solid line). At all the measurement locations the very coarse (black line) show the best agreement with the data (red solid line).
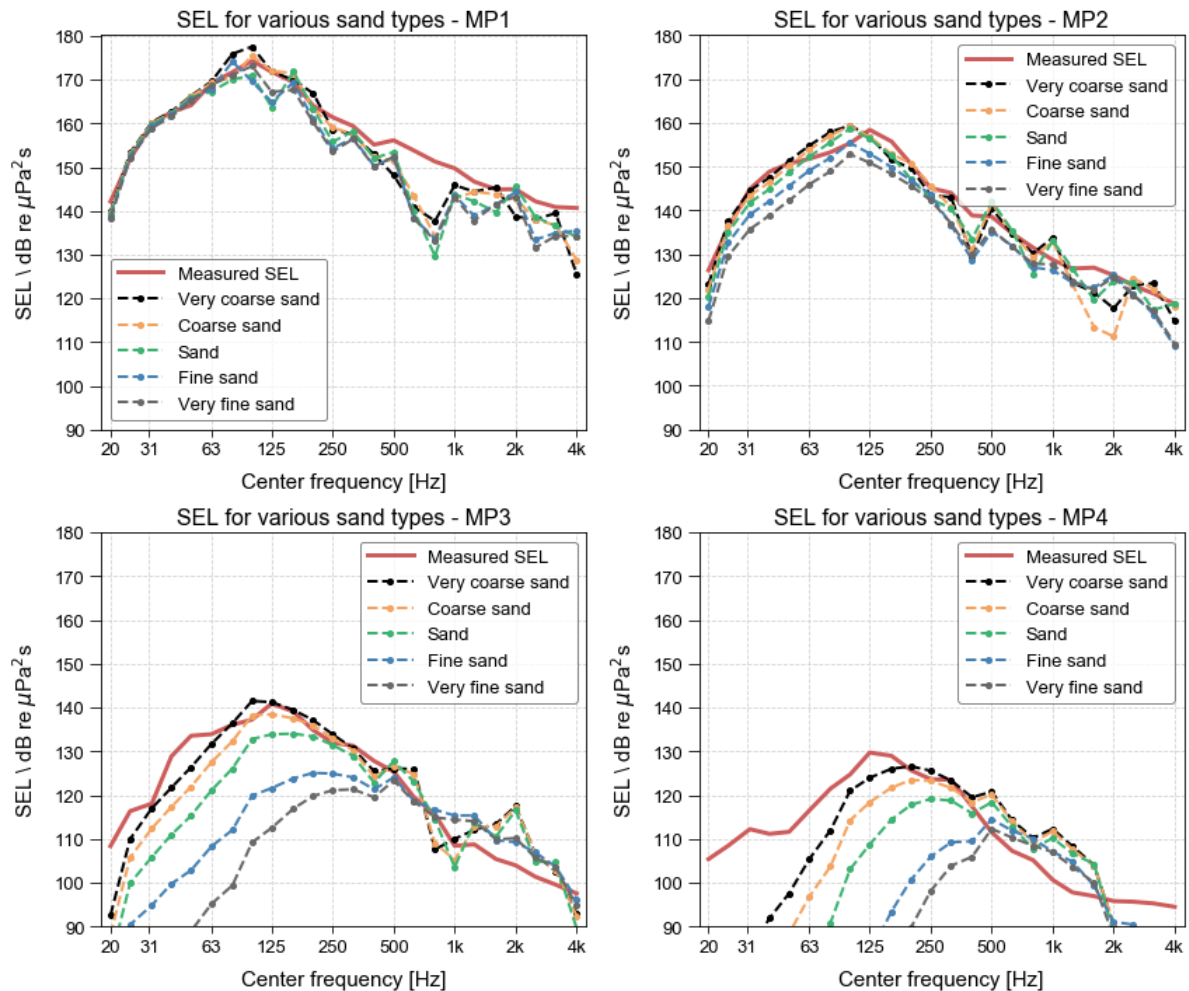
Figure 4.1: The SEL per frequency band as simulated by the UAS at measurement locations MP1, MP2, MP3 and MP4 for a varied upper sediment layer thickness upto 5 m.

The effect of the sediment type on the total sound levels is reflected in Figure 4.2: the Sound Exposure Levels for very coarse sand (black line) are the highest over the whole modelled range and the sound levels for very fine sand (grey line) are the lowest. The difference between the predicted levels for the various sediment types increases with range. At MP2, the sound level is 165 dB for very coarse sand and 160 dB for very fine sand. At MP3 very coarse sand gives a sound level of 150 dB and very fine sand a sound level of 135 dB. At MP4, very coarse sand gives a sound level of 137 dB and very fine sand gives a sound level of 120 dB. The results for the other types of sand vary between these two limits with increasing sound level for increasing coarseness of the sediment.
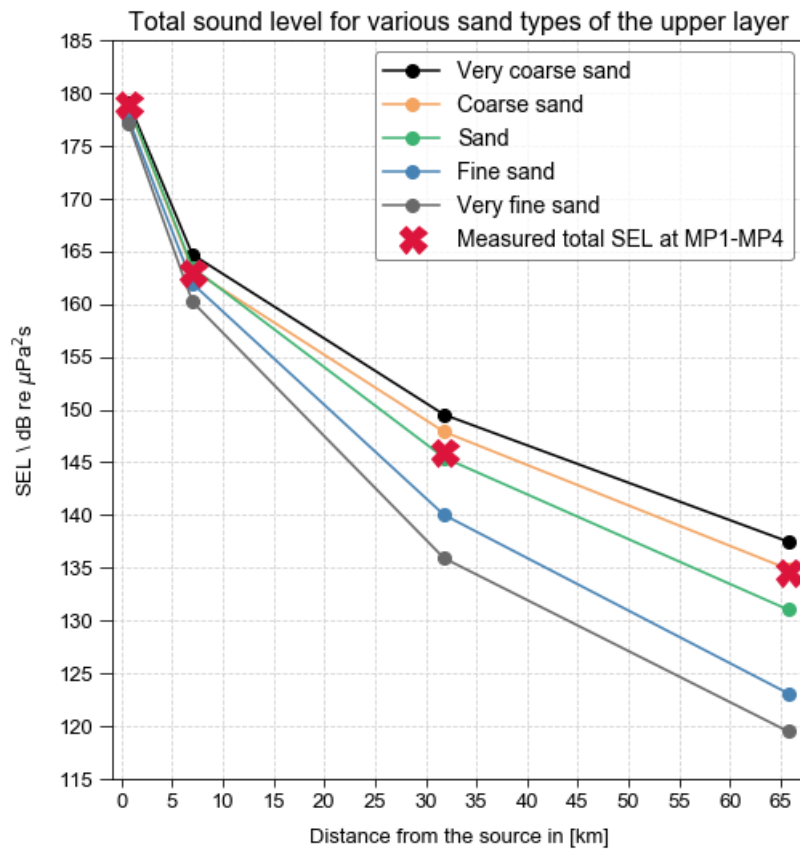
Figure 4.2: The total SEL over distance as simulated by the UAS. The circles indicated the predicted sound levels at measurement locations MP1, MP2, MP3 and MP4 for the varied upper sediment layer thickness. The red crosses indicate the measured sound levels.

Upper layer thickness

At MP1 the predicted sound levels for frequency bands 20 - 50 Hz and 125 Hz - 4 kHz are the same for the each layer thickness. For frequency bands 63 Hz - 100 Hz the following is observed: Layer thickness 5 m (grey line in Figure 4.3) predicts the highest sound levels that agree best with the measured sound levels (red line). The sound levels obtained with layer thickness 10 m (yellow line), 40 m (green line) and 80 m (blue line) are comparable.

At MP2, for frequency bands < 100 Hz, the seabed with an upper layer of 80 m (blue line) predicts the lowest sound levels and the seabed with upper layer of 5 m (grey line) predicts the highest sound levels. A seabed with upper layer of 80 m (blue line) and 40 m (green line) predicts the same sound levels for frequency bands ≥ 31.5 Hz. For all the implemented upper sand layers the maximum the sound levels are reached at 100 Hz with a value of 160 dB.

At MP3 the upper sand layer of 40 m and 80 m predicts the same sound levels for every frequency band modelled. The maximum level is 140 dB for frequency band 125 Hz. The sand layer of 10 m (yellow line) and 5 m (grey line) thick both reach a maximum sound level for frequency band 125 dB as well. These values are 138 dB and 137 dB for 5 m and 10 m respectively. For frequency bands ≤ 160 Hz the results for a layer of 5 m are the highest and the results for a layer of 40 m and 80 m are the lowest. For the seabed with an upper layer of 10 m (yellow line) the frequency bands ≤ 25 Hz are below the ambient noise level. For a seabed with upper layer of 40 m (green line) and 80 m (blue line) the frequency bands ≤ 31.5 Hz are below the ambient noise level. At MP3 the measured sound levels (red solid line) are never below the ambient noise level. For frequency bands ≥ 500 Hz the seabed with layer thickness of 80 m (blue line) predicts higher sound levels than the others.

At MP4 the same behaviour is observed for frequency bands ≥ 400 Hz. Furthermore, a layer thickness of 80 m (blue line), 40 m (green line) and 10 m (yellow line) predict the same sound levels for every frequency band. For these layers the sound levels of the frequency bands ≤ 63 Hz are below the ambient noise levels. This is not the case for the measured sound levels (red solid line). For the seabed with layer thickness 5 m the sound levels are the highest and are below the ambient noise level for frequency bands ≤ 50 Hz. For all applied layers the maximum level is 125 dB for frequency band 250 Hz.

The effect of the applied layer thickness on the total sound levels is reflected in the total sound levels received. The difference between the predicted levels increases with range. At MP1 and MP2 the sound levels for a layer thickness of 80 m (blue line in Figure 4.5) are 178 dB and 163 dB receptively. For a layer thickness of 5 m (green line in Figure 4.5) the sound levels at these locations are 176 dB and 162 dB respectively. At MP3 and MP4 the sound levels reached are 146 dB and 133 dB for a layer thickness of 5 m and 143 dB and 132 dB for a layer thickness of 80 m.

At MP1 and MP2 a seabed with layer thickness 2.5 m (blue line in Figure 4.4) and a seabed with layer thickness 5 m (green line in Figure 4.4) results in the same sound levels for the observed frequency bands. At MP3 and MP4, an upper layer of 2.5 m (blue line in Figure 4.4) results in higher sound levels compared with an upper layer of 5 m (green line in Figure 4.4). All the measurement locations considered, a layer thickness of 2.5 m complies best with the measured data.

Upper layer sediment type and thickness combinations

Very coarse sand applied to an upper layer of 2.5 m (green line in Figure 4.6) results in the highest predicted sound levels at MP4. Coarse sand applied to an upper layer of 5 m (yellow line in Figure 4.6) results in the lowest predicted sound levels at MP4. The simulation with coarse sand and a layer thickness of 2.5 m (blue line in Figure 4.6) almost show the same results as the simulation with very coarse sand and a layer thickness of 5 m (green line in Figure 4.6) for the frequency bands 63 - 400 Hz at MP4. A combination of the coarse sand and layer thickness of 2.5 meters (blue line in Figure 4.6) complies the best with the measured data (red solid line).
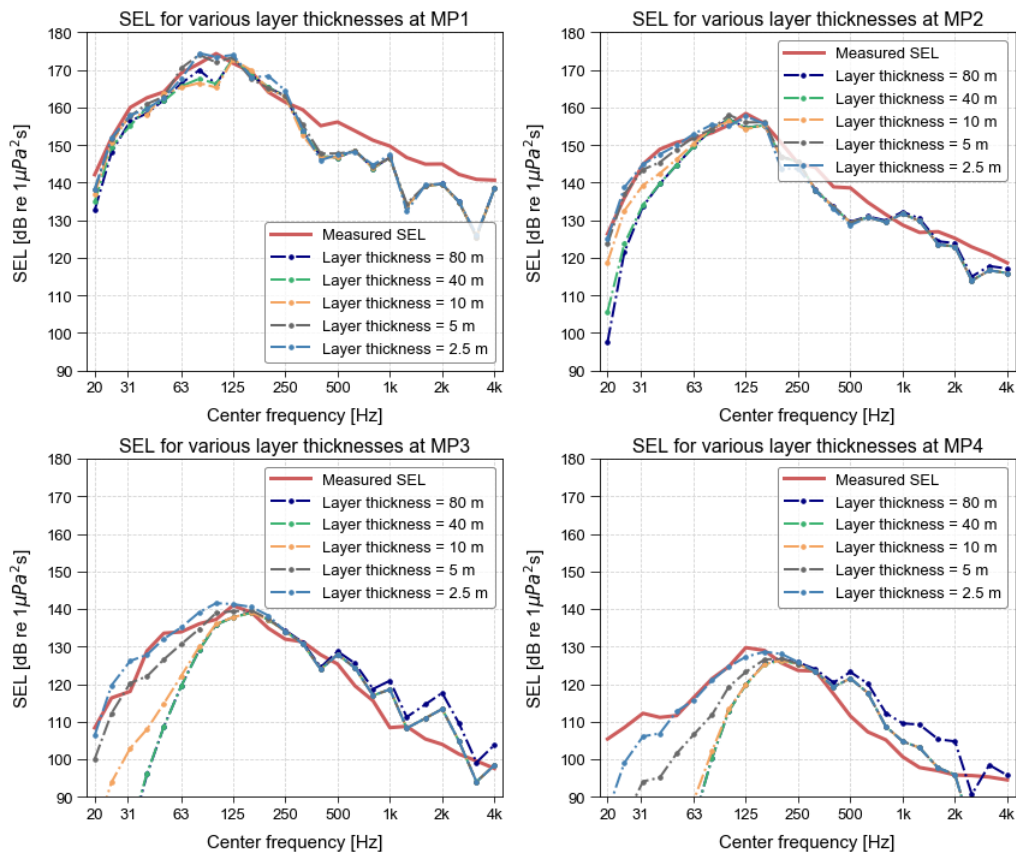
Figure 4.3: The UAS results compared with the acoustic data (red line) for an upper layer thickness of 80 m (pink) 40 m (blue) 10 m (light green) and 5 m (dark green). The results are displayed in the one-third octave band spectra of the Sound Exposure Level at 10m above the seabed at the measurement locations MP1 till MP4.
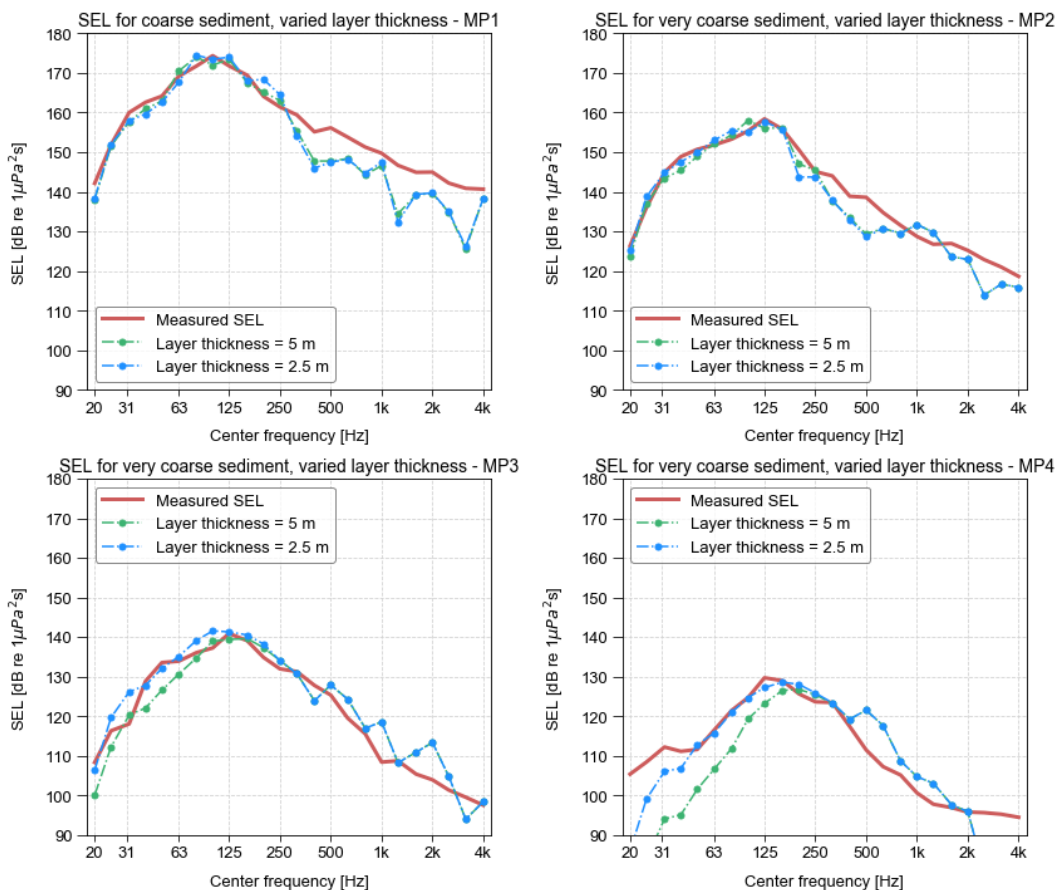
Figure 4.4: The UAS results compared with the acoustic data for an upper layer thickness of 2.5 m and 5 m. The results are displayed in the one-third octave band spectra of the Sound Exposure Level at 10 m above the seabed at the measurement locations MP1 till MP4
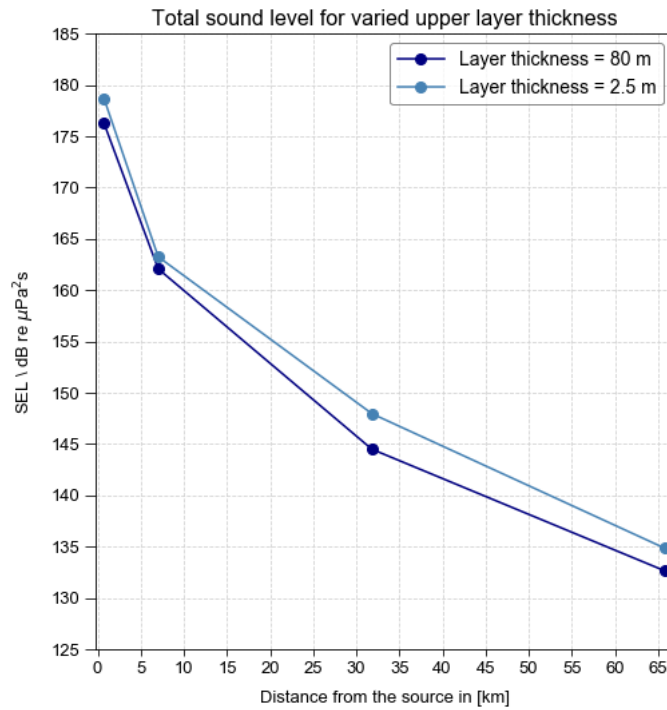
Figure 4.5: The total SEL over distance from the source as predicted by the UAS for the different implemented layer values of the thickness. The circles indicate the total predicted SEL at measurement location MP1 till MP4.
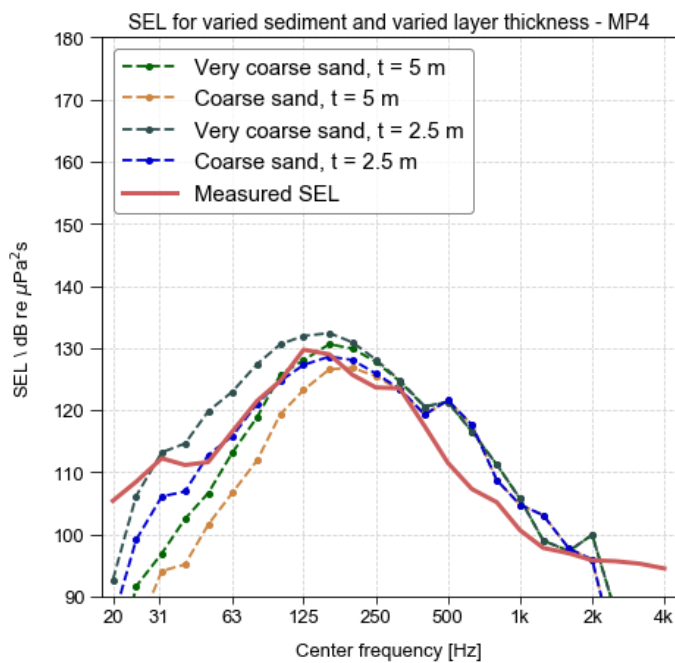
Figure 4.6: The UAS results compared with the acoustic data for the simulated combinations of layer thickness (*t*) and sediment type of the upper sand layer. The results are displayed in the one-third octave band spectra of the Sound Exposure Level at 10 m above the seabed at the measurement locations MP1 till MP4.

Rock seabed

The predicted sound levels in the frequency spectrum for a rock seabed agree well with the measured sound levels at MP1. For frequencies > 125 Hz alternation of underestimation and overestimation of the predicted sound levels compared to the measured ones is observed. At MP2 the frequency bands ≤ 315 Hz are overestimated compared to the measured sound levels. For frequencies bands > 315 Hz underestimation and overestimation alternate. At MP3 and MP4 the sound levels over the entire modelled frequency range are overestimated. The difference between measured sound levels and predicted sound levels increases with distance from the source. What stands out is that the sound levels of the frequency bands ≤ 100 Hz are over estimated at MP2, MP3 and MP4, whereas the sound levels for these frequencies with a sandy seabed (Figure 4.1) are underestimated.
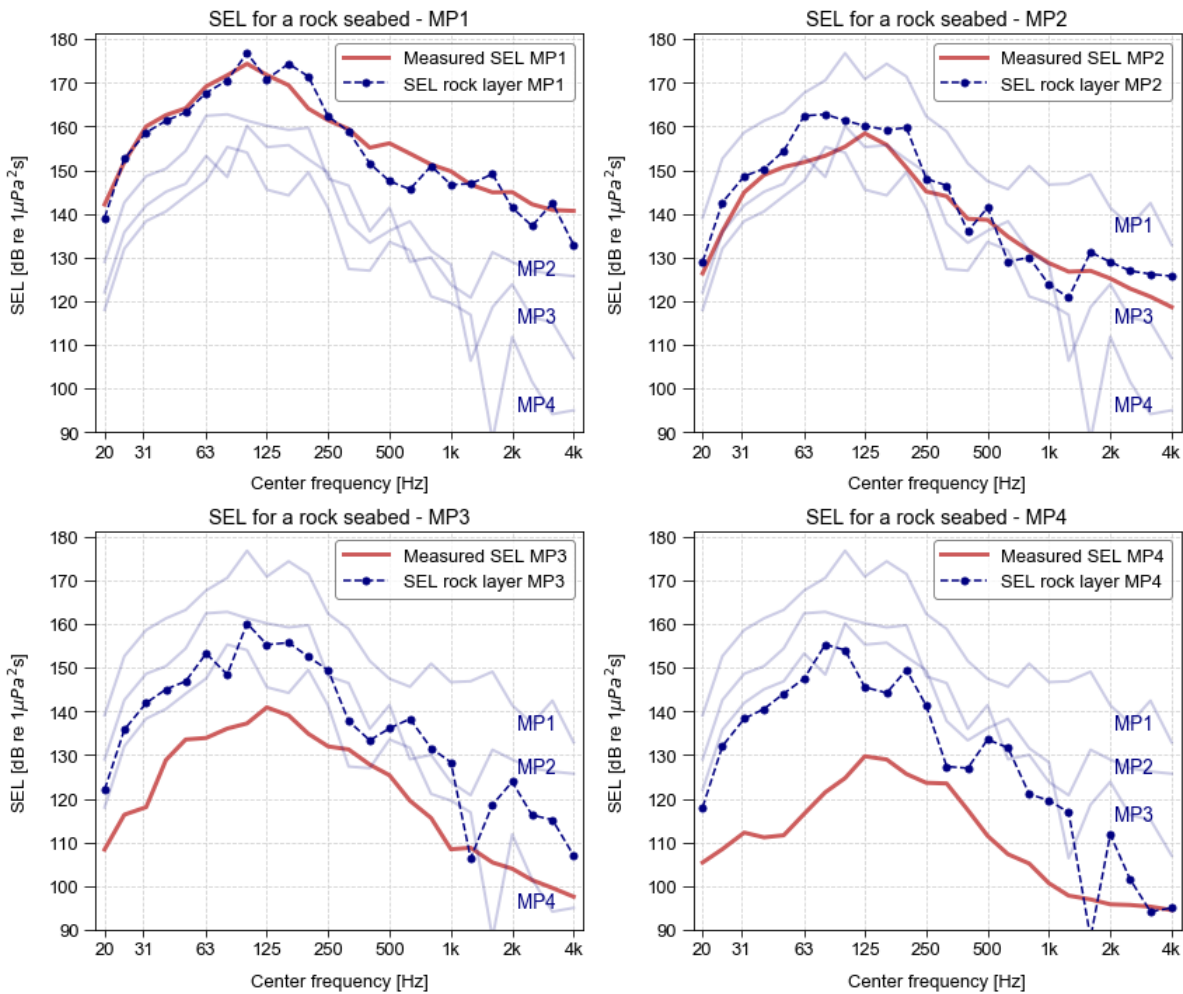
Figure 4.7: The UAS results at every measurement position (blue lines) compared with the acoustic data (red line) for a rock seabed. The results are displayed in the one-third octave band spectra of the Sound Exposure Level at 10m above the seabed at the measurement locations MP1 till MP4.
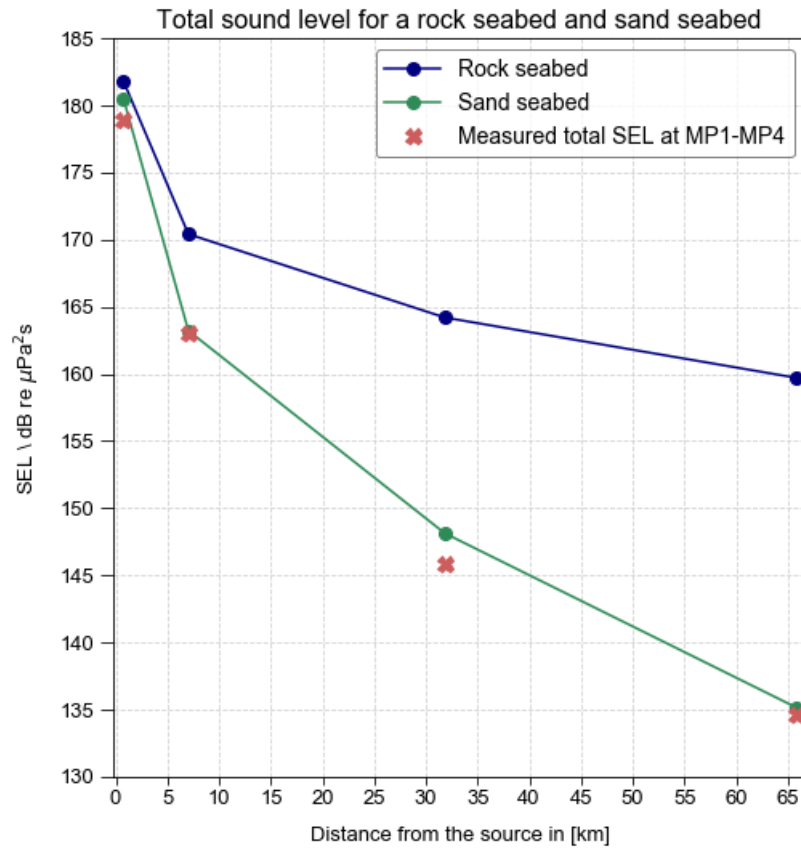
Figure 4.8: The total SEL over distance from the source as predicted by the UAS for a rock seabed and a sand seabed. The circles indicate the total predicted SEL at measurement location MP1 till MP4.

4.1.2. The Waterphase

The temperature, salinity and pH has negligible influence on the predicted SELs for the frequency ranges studied. The effect on the total sound levels over distance is negligible. The same holds for the implementation of the varying water depth. The results of these simulations are presented in Appendix D.

4.1.3. The Source and Receiver

The implementation of a different source spectrum brings uncertainty into the predicted sound levels. For the compared source spectrum the difference in total SEL reaches a maximum of 10 dB at MP4. This is presented in Appendix D.

The results of the choice of source location depth are presented in Appendix D. Also the results with a different source spectrum is presented there. Subsequently, the variation of receiver depth and location from the source brings has no effect on the predicted sound levels. The results regarding the parameters discussed in this section are presented in Appendix D.

4.2. Results with best fit

The total received sound levels at 10 m (blue line in Figure 4.10) and 2 m (green line in Figure 4.9 above the seabed shows a logaritmic decrease with distance from the source. The sound levels 10 m above the bed reach values of 178 dB at MP1, 163.24 dB at MP2, 147.94 dB at MP3 and 134.84 dB at MP4 (blue circles in Figure 4.9. These sound levels deviate 0.30 dB, 0.23 dB, 2.02 dB and 0.23 dB from the measured values at these locations (red crosses in Figure 4.9. The sound levels 2 m above the bed reach values of 177.02 dB at MP1, 162 68 dB at MP2, 144.93 dB at MP3 and 130.81 at MP4 (green circles in Figure 4.9). These sound levels deviate from the measured data with 2.30 dB, 0.33 dB, 0.86dB and 0.27 dB at MP1 till MP4 respectively.

Underestimation and overestimation of the sound levels alternate over range for both measured heights above the bed. At MP2, MP3 and MP4 the sound levels are overestimated compared to the data while at MP1 the SEL is underestimated. For 2 m above the bed only the sound level at MP3 is overestimated. The sound levels at MP1, MP2 and MP4 are underestimated.

The sound levels in the frequency spectrum (blue lines in Figure 4.10) follow the distribution of the measured sound levels (red lines in Figure 4.10) at a height 10 m above the seabed. At MP1 the sound levels are underestimated for frequency bands ≥ 100 Hz. At MP2 sound levels agree with the data for all the modelled frequency bands execpt 400 Hz. An underestimation of 10 dB is observed. At MP3 frequency band 25 Hz is over predicted with 5 dB, frequency band 31,5 Hz is over predcited with 8 dB, frequency band 80 Hz is over predicted with 3 dB and frequency band 100 Hz is over predicted with 5 dB. At MP4 the frequency bands ≤ 50 Hz are under predicted compared with the measured sound levels. The difference between the predicted sound levels and measured sound levels reaches a maximum of 15 dB for frequency band 20 Hz. Frequency bands ≥ 500 Hz and < 2 kHz are over predicted with a maximum 10 dB at 500 Hz and a minimum of 2 dB.

The sound levels displayed in the frequency spectrum (green lines in Figure 4.11 show a wide distribution compared with the measured sound levels (red lines in Figure 4.11 at a height 2 m above the seabed. At MP1 the sound levels for the frequency bands ≥ 80 Hz are under predicted. Subsequent frequency bands show deviations in sound level in the order of magnitude of several dB's. The largest deviation is 15 dB between the subsequent frequency bands 160 Hz and 200 Hz. At MP2 sound levels are underestimated for frequency bands 125 Hz and 160 Hz with 8 dB. For frequency bands ≥ 1 kHz and ≤ 2 kHz the sound levels are over predicted, while for frequency bands > 2 kHz the SELs are under predicted with a maximum of 8 dB at 2.5 kHz. At MP3 the frequency spectrum shows a smooth distribution for frequency bands ≤ 250 Hz. Only 31,5 Hz shows a significant over prediction of 8 dB. Frequency bands ≥ 315 Hz show a noisy distribution with alternating over predictions and under predictions of the sound levels. The difference between the subsequent frequency bands 500 Hz and 630Hz is 10 dB. At MP4 the frequency bands ≤ 50 Hz are under predicted compared with the measured sound levels with a deviation increasing to 15 dB for frequency band 20 Hz. Frequency bands ≥ 500 Hz and < 1.25 kHz are over predicted with a maximum 8 dB at 500 Hz and a minimum of 2 dB at 1 kHz.

The sound levels as discussed here (Figure 4.9, Figure 4.10 and Figure 4.11) are the results of a simulation with an upper layer thickness of 2.5 m. The geo-acoustic parameters of the upper sediment layer and the deeper rock layer used are presented in Table 4.2.
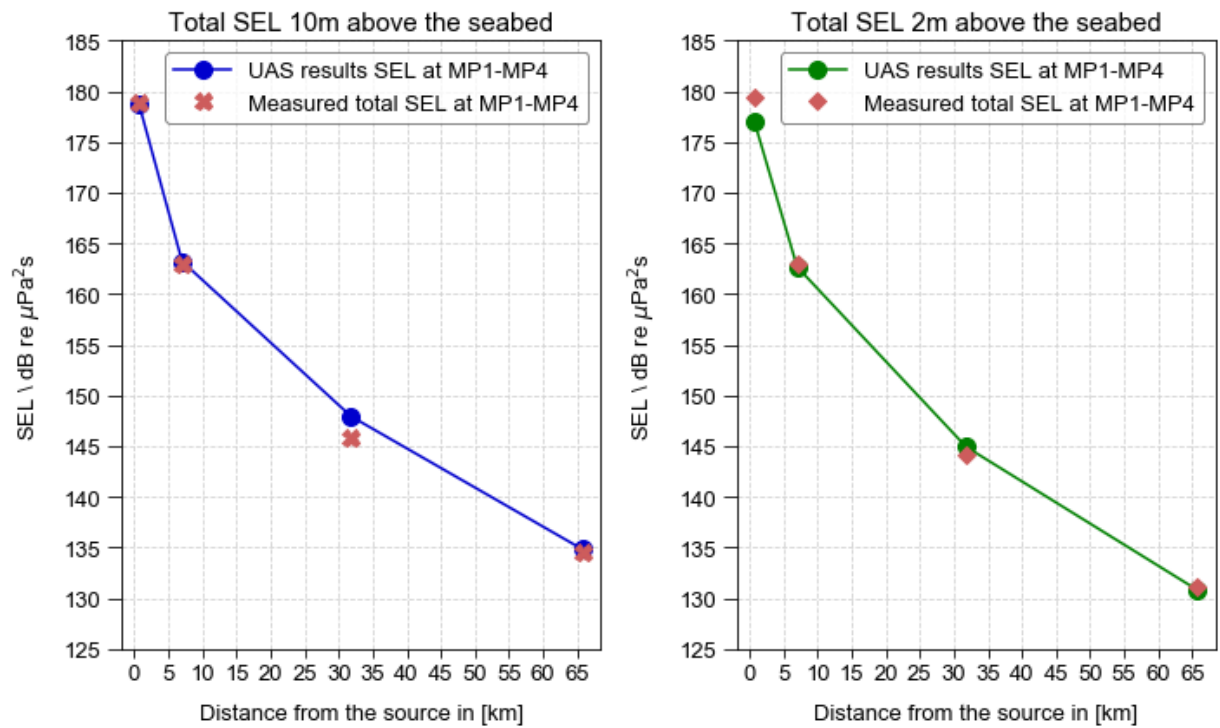
Figure 4.9: The total Sound Exposure Levels at every measurement location as predicted by the UAS 10 m above the bed (blue solid line) and 2 m above the bed (green solid line) compared with measured sound levels 10 m above the bed (red crosses) and 2 m above the bed (red diamonds) during the pile driving for pile U8.

Parameter	Value$_{layer1}$ [unit]
Compressional wave speed sediment	1877 m/s
Sediment density	2297 kg/m^3
Attenuation sediment	0.88 dB/λ
Parameter	**Value$_{layer2}$ [unit]**
Compressional wave speed rock	3000 m/s
Rock density	5500 kg/m^3
Attenuation rock	0.10 dB/λ

Table 4.2: Geo-acoustic parameters of the first and upper sediment layer and the second and deeper rock layer in the modelled domain
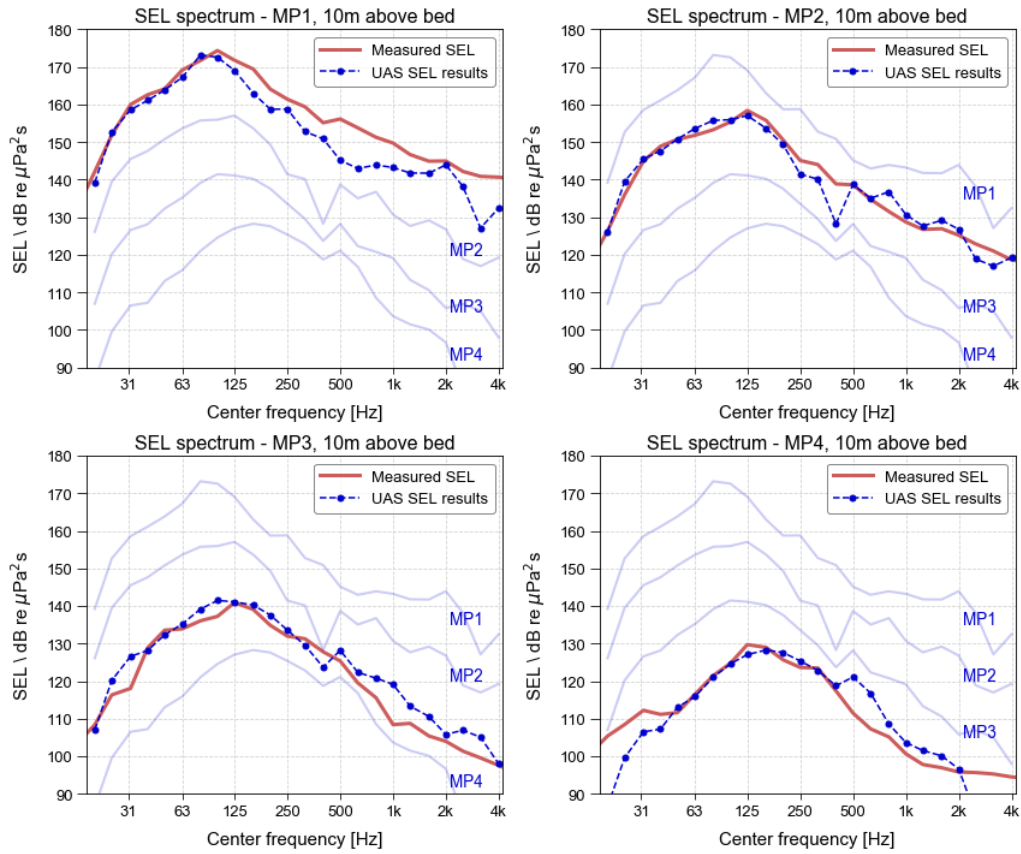
Figure 4.10: The one-third octave band spectrum of the UAS predicted SEL (blue lines with triangles) compared with the measured sound levels (red lines with circles) 10 m above the seabed at the measurement locations MP1 till MP4
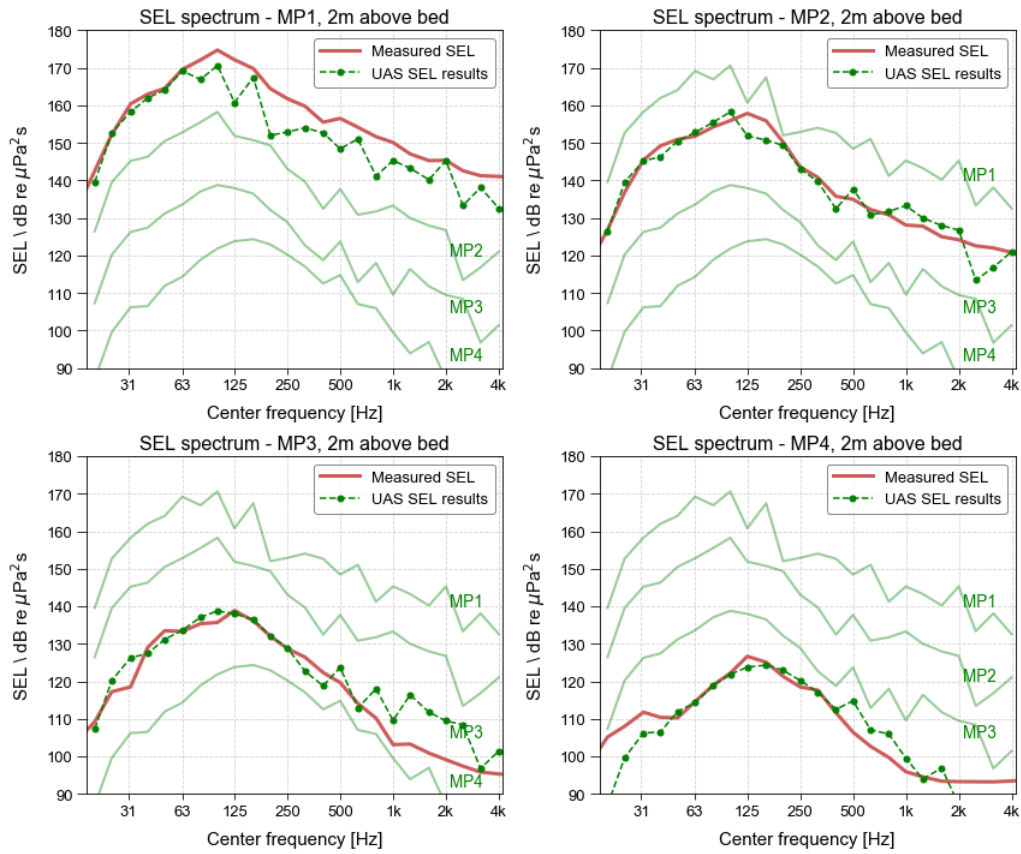
Figure 4.11: The one-third octave band spectrum of the UAS predicted SEL (green lines with triangles) compared with the measured sound levels (red lines with circles) 2 m above the seabed at the measurement locations MP1 till MP4

4.3. Physical interpretation of the UAS results

4.3.1. The seabed

The results of the simulations with the UAS show us that the seabed plays a key role in underwater sound modelling. In the UAS the seabed is modelled as a fluid. With this assumption the shear effect of the soil is neglected. Especially the relatively lower modelled frequencies are sensitive to the possible values of the geo-acoucstic parameters of the soil representing this fluid seabed. This behaviour is related to the choice of sediment type and to the choice of layer thickness of the upper layer in the seabed.

Sandy seabed

The explanation of the observed response of the UAS to the chosen sand type is twofold. The first issue entails the validity of the geo-acoustic parameter values used. The sound propagation in in the seabed is depth and frequency dependent. This is reflected in the geo-acoustic parameter values. The chosen values are determined based on mid-frequency propagation properties (1-10 kHz) of the soil. These values can be applied for lower frequency propagation but that may come with complications. Low-frequencies penetrate deeper into the seabed where the sediment composition changes and shear effects start to have more effect. However, these effects can not be modelled in the fluid seabed of the UAS and therefore can not be reflected in the geo-acoustic parameters. The large spread in predicted sound levels for the various sand types for the frequency bands < 800 Hz (Figure 4.1) is a result of this limitation.

A second issue is the relation between the coarseness of the sediment and the height of the predicted sound levels in the water. For coarser sediment higher sound levels are observed. The amount of sound energy that is transmitted into the seabed or reflected back into the water depends on the ratio between density and wave speed of both propagation mediums. These two parameters increase in value for increasing coarseness (K in equation 2.1). The larger this ratio, the larger the difference between the properties of the medium and the more sound is reflected back into the water. For a higher compressional wave speed and density the sediment type behaves more rigid and reflects more sound into the water (Figure 4.1).

Rock seabed

The high rigidity of the rock seabed makes it a reflective layer rather than an absorbing one. The sound propagation is dominated by reflection losses at the sea surface and seabed interface. The sound wares are not transmitted through the seabed and therefore are not affected by the damping in the seabed. This effects mainly the low frequencies ≤ 100 Hz. The sound levels for these frequency bands are hardly affected by damping resulting in overestimated sound levels compared to the measured data (Figure 4.7), whereas for a sandy seabed the sound levels are over damped resulting in underestimation (Figure 4.1). This accentuates the influence of a sandy seabed on the propagation of the lower frequency ranges.

Layer thickness

For the sandy seabed, the layer thickness of the upper sand layer influences to the ability of the seabed to absorb sound. As this thickness decreases its sound absorbing ability decreases as well. This results in more sound reflection by the lower rock layer which behaves as a reflective layer rather than an absorbing one. The results in Figure 4.3 and 4.4 show that mainly the frequencies ≤ 250 Hz respond to the choice of layer thickness. This behaviour is explained by the fact that the layer thickness relative to the wave length influences the amount of sound absorption relative to the sound reflection. The smaller the sediment layer is compared to the wave length, the less sound is absorbed at the moment the sound wave is reflected from the layer interface. Lower frequencies have a larger wave length than higher frequencies (Figure 4.12). Therefore, larger wave lengths need a thicker sediment layer to be absorbed. This explains why the sound levels for the lower frequency bands increase by decreasing the layer thickness in the UAS.

Combined parameter choice

The final results (Figure 4.9, Figure 4.10 and Figure 4.11) are obtained with an upper sand layer thickness of 2.5 m and a sand type classified as coarse sand. A layer thickness of 5 m and a sand type classified as very coarse give almost the same predicted sound levels (Figure 4.6) and also agree well with the measured data. The ambiguous choice of geo-acoustic parameter values makes clear that no evident implementation of the seabed exists to arrive at predicted sound levels that agree with measured data.
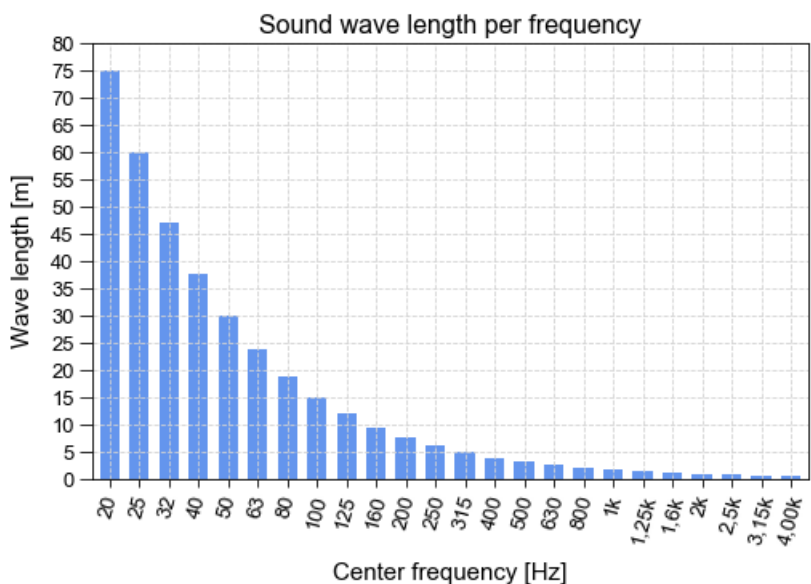
Figure 4.12: The wave length in meter for each center frequency in Hz

4.3.2. The point source representation

The source is described as a point source. A point source spreads the sound in al directions at one location in the water column. The individual sound waves propagate through the water column under different angles with the horizon. Sound waves travelling at large angles reach the sea surface relatively close to the source and experience much reflections (red arrow in Figure 4.13). Or, the sound waves reach the seabed relatively close to the source and are affected by the influence of geo-acoustic parameters of the seabed (green arrow in Figure 4.13). These sound waves encounter the frequency dependent effect of the sediment choice and layer thickness. However a part of the sound waves travels with angles that are close to the horizon. These sound waves propagate over large distances without undergoing any reflection losses or damping by the seabed (blue arrows in Figure 4.13) in this way contributing to the sound levels at larger distances from the source.
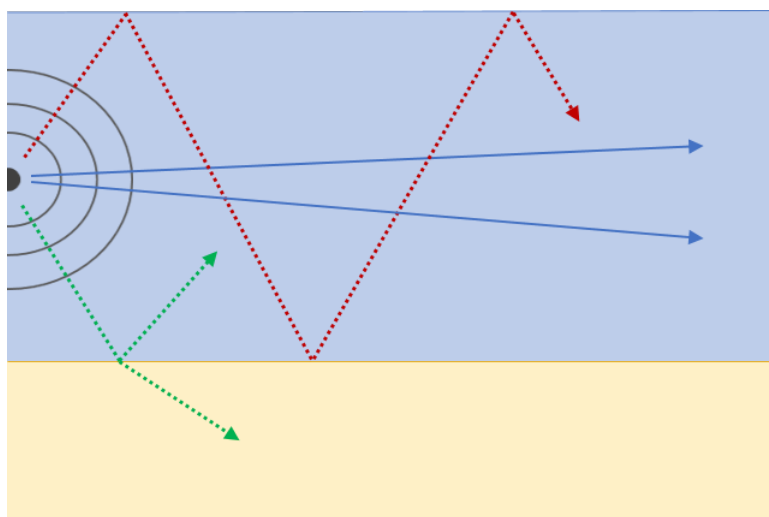
Figure 4.13: A schematization of the different effects the sound waves emitted from a point source undergo

4.3.3. Spectral discretization

An observation regarding the relatively higher frequency bands ($\geq$ 315 Hz) is the irregular distribution of the the sound levels in the spectrum. For subsequent frequency bands relative large differences between sound levels are observed that do not show in the measured sound levels. This behaviour is mainly contributed to the fact that in the UAS the transmission loss is calculated for the center frequencies that represent a complete one-third octave bandwidth. In reality such a one-third octave band contains multiple frequencies ranging from a lower limit to an upper limit belonging to that bandwidth. The hydrophones used measure all the existing frequencies. The variation of the sound levels of subsequent frequencies within a frequency band can be considerable. With the spectral discretization of the measured sound levels these variations are averaged. This results in a smooth distribution of the sound levels in the frequency spectrum. In the UAS not all the frequencies within in the discretized bands are modelled, but only the center frequency. This results in a different propagation pattern. For higher frequencies constructive and destructive patterns are observed. This results in frequency ranges with higher sound levels (constructive interference) followed by areas with lower sound levels (destructive interference). For subsequent frequencies these patterns differ with large difference in sound level as a results.

5

Discussion & Conclusions

The increasing demand for sustainable energy sources has stimulated the development of offshore wind parks. The high sound levels reached in the water during the pile driving activities for the construction of offshore wind parks have impact on the environment. The prediction of sound levels underwater is essential to quantify this impact in order to take the appropriate noise mitigation measures. The aim of this research is to assess whether the first commercially available sound propagation model, the Underwater Acoustic Simulator (UAS), is able to predict these sound levels for application in wind farm cases and to give insight into the physical processes contributing to sound propagation in the sea. The measured sound levels at the four measurement positions obtained during the pile driving activities for the Gemini wind park are used to assess the sound propagation predictions of the UAS. This assessment shows us that the UAS is able to predict sound levels that agree with the measured data (Figure 5.1 and Figure 5.2). The representation of the seabed plays a key factor in underwater sound propagation. However, in the UAS some important physics regarding the seabed are not included. Also the physics related to the sound source and 3D sound propagation effects are not considered in the UAS. This diminishes the value of the UAS for application in future wind park projects, especially considering the method used to obtain the results.
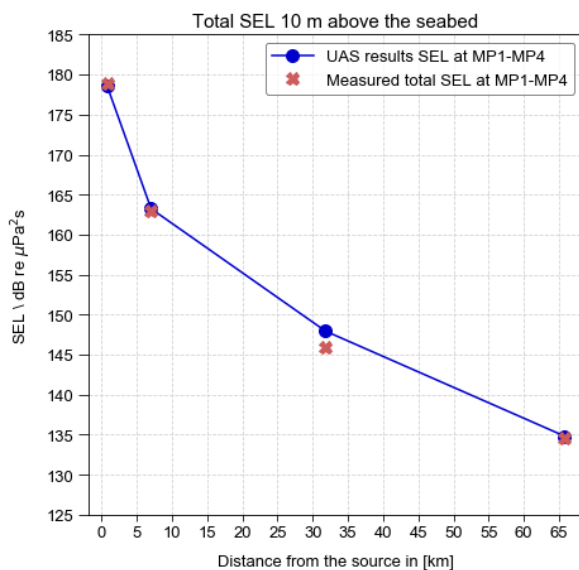
Figure 5.1: Total sound levels over distance
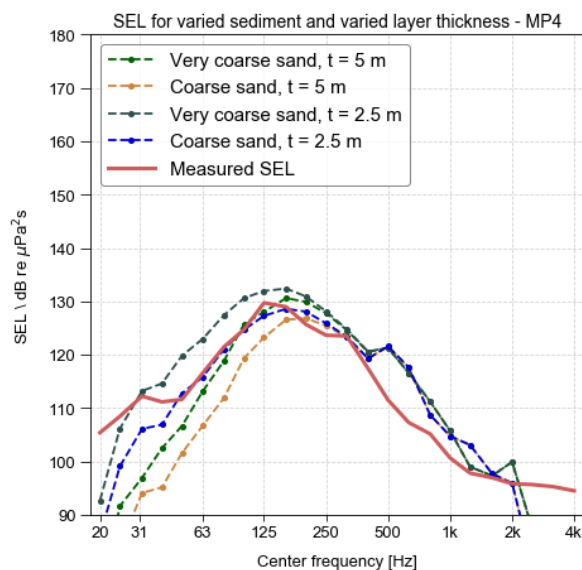
Figure 5.2: Sound levels in the frequency spectrum

The importance of the shear properties of the seabed in underwater sound propagation
The predicted sound levels with the UAS are most sensitive to the values of the parameters related to the seabed properties. Based on findings in literature the seabed is chosen to consist of an upper sand layer and lower rock layer. The sediment type and layer thickness of the modelled upper sand layer cause the most uncertainty in the sound level predictions. A trend of underestimated sound levels is observed especially for the relatively lower frequencies modelled (< 800 Hz). These frequencies show a large spread in predicted sound levels in the frequency spectrum for different sand types. The reason for this is that with the fluid seabed representation in the UAS the effect of shear waves and Scholte waves on sound propagation are not represented.

In the UAS the seabed is described as a fluid instead of a solid. This means that only the compressional acoustic waves are modelled while in a solid also shear waves and Scholte waves are present. This fluid assumption of the seabed without the shear effect is an often used approach in acoustic modelling. It is mainly implemented to improve the computational speed. Low frequency sound waves propagate deep into the seabed where shear effects play a more pronounced role than in the upper parts. Part of the low frequency sound energy propagates in the form of Scholte waves at the interface between seabed and water in this way contributing to the sound levels in the water. A parametric study by Tsouvalas (2015) looked into the effect of shear and Scholte waves. The shear rigidity of the soil was found to be crucial for the correct estimation of the sound levels, especially regarding the low frequencies.

The reason the UAS is still able to predict sound levels that agree with the measured sound levels despite this exclusion of essential physics is contributed to the combination of the chosen layer thickness and sand type of the upper sand layer. The results that fit the measured data best are obtained with an upper layer thickness of 2.5 m and a sand type classified as coarse. The deeper rock layer is close to the seabed-water interface because of the small thickness of the upper sand layer. The rock layer therefore reflects sufficient sound energy to arrive at sound levels corresponding with the measured sound levels. However, such a thin upper sand layer is not considered realistic. A depth scale of a few wave lengths (several 100 m) should be implemented to represent the true thickness of the sediment layers (Ainslie, 2010), (Hamilton, 1980). This is another indication that the results that fit the data best are not because the right implementation of the physics. The small layer thickness compensates for the absence of the shear wave effect by reflecting the sound energy back into the water.

The reason the sound levels propagating at low frequencies are underestimated by the fluid seabed is the last topic discussed here. In a fluid seabed as implemented in the UAS the damping effects associated with shear-waves are included in the geo-acoustic parameters describing the seabed (Li and Hodgson, 1998). This assumption that comes with a fluid seabed can be applied when the real seabed has a low shear rigidity (low shear wave speed) and thus hardly supports shear wave propagation. This means that in such a case the bottom losses due to excitation of shear waves can be simulated by a fluid seabed described by adjusted geo-acoustic parameters. However, for a seabed with high shear rigidity (high shear wave speed) one cannot apply the adjusted geo-acoustic parameters of a fluid seabed without taking into account the contribution of the sound wave energy propagation as shear and Scholte waves. In such a case the damping associated with shear waves is considered, but not the propagation in the form of shear waves and its contribution to the sound levels.

Another reason that could contribute to the underestimated sound levels of the low frequencies is the trapping of the sound energy in the fluid seabed layer. The amount of sound energy in the seabed that is transmitted into the water or reflected back into the seabed depends on several geo-acoustic parameters and the grazing angle of the sound waves. For angles smaller than the critical angle the reflection coefficient of a fluid seabed is $R = 1$ (Li and Hodgson, 1998), (Jensen et al., 2011). This means that all the sound energy is reflected back into the medium (Figure 5.3). If this occurs in the seabed, the sound is trapped there and does not contribute to the sound levels in the water.
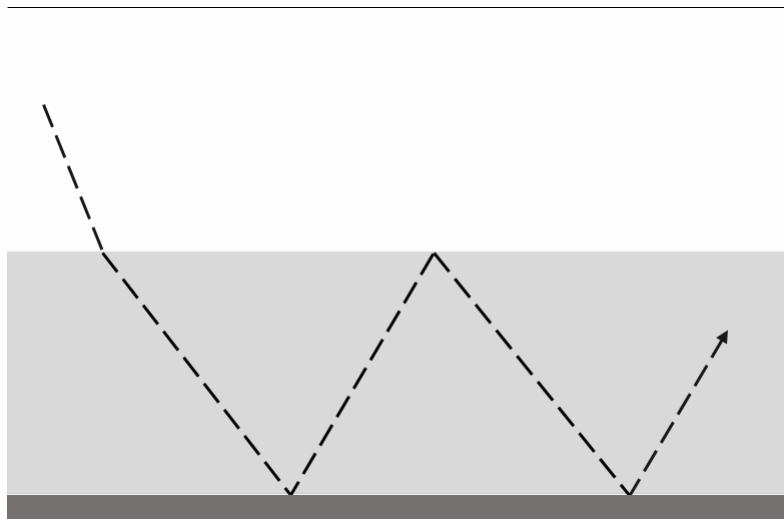
Figure 5.3: A schematization of the trapping of a sound wave in a fluid layer.

The importance of the source in underwater sound propagation

Another issue concerning the modelling of sound is the vertical representation of the source sound. In the UAS this is a points source. This simplification does not account for the actual physics of the sound radiation from the pile. A point source spreads the sound in al directions at one location in the water column while in reality the sound is emitted over the whole length of the pile and the sound energy is radiated in the direction of the Mach-cone as found by Reinhall and Dahl (2011). After the impact hammer hits the monopile, a sound wave travels through the pile. This sound wave releases pressure waves into the water under an angle referred to as the Mach cone. The effect of this simplification is studied and found to be range dependent and frequency dependent. The assumption of a point source is only acceptable for some frequencies and at some range from the source. This is because the sound at these frequencies follows horizontal propagation paths, instead of the paths following the angles of the Mach-cone.

Not only the way the sound spreads from the source is important, but also the aspects that determine the amount of sound energy spread. In the UAS this source level is implemented as a sound spectrum and based on acoustic data. In reality the hammer impact, the pile diameter and pile length underwater are the most important parameters influencing the loudness and frequency distribution of the radiated sound. Additionally, the soil composition around the monopile and the type of hammer and anvil used also contribute to the initial spreading of the source energy. The use of a source spectrum based on data neglects the effects of these parameters on the source energy.

The importance of the seawater composition in underwater sound propagation

Although the seabed plays a key role in underwater acoustics the local sea environment is elaborated on here as well. The temperature, salinity and pH of the sea in the Gemini area are used in the sound predictions via a process called volume attenuation. This is related to the chemical composition of the water. Suspended particles induce scattering losses and absorption. Via this mechanism the variation of the contributing parameters does not affect the sound levels and thus has no impact in the Gemini area. In the case of the frequencies modelled in this thesis (20 Hz - 4 kHz) these properties do not have an effect on the predicted sound levels in the water for the frequency ranges modelled (20 Hz - 4kHz).

Temperature and salinity influence sound propagation via another process as well. In shallow seas mainly the temperature and to a lesser extend the salinity effects the 3D sound speed distribution. The option to include a 1D sound speed distribution over depth based on the temperature and salinity distribution in the UAS simulations is not investigated in this thesis. The effect of such a profile on shipping noise showed no important contribution to the obtained sound levels, (Sertlek et al., 2016). However, it is known that in the Gemini area stratification occurs as results of surface heating and fresh water discharge during certain periods in the year, (Claessens, 2016). Studies of the effect of ocean front and stratification on piling noise are limited, but the results doe show that when present they affect sound propagation (Shapiro et al., 2014).
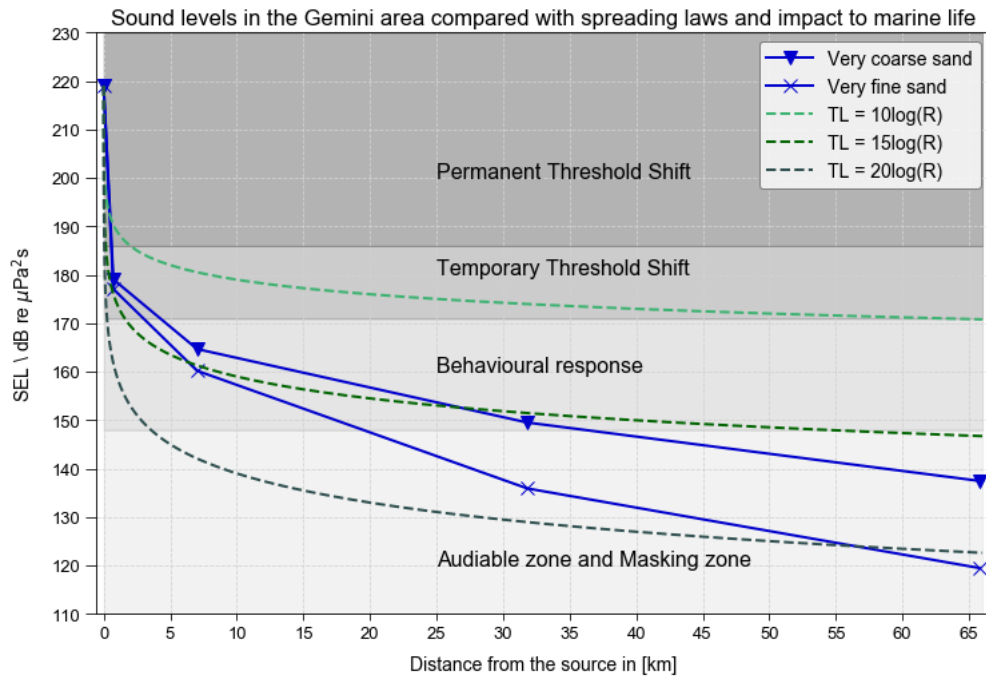
Figure 5.4: The predicted sound levels in the Gemini area for an upper sand layer consisting of very coarse sand (dark blue triangles) and very fine sand (dark blue squares). These results give a more precise indication of the sound levels than the geometrical spreading laws for shallow water (10log(R)), intermediate water (15log(R)) and deep water (20log(R)). Therefore the degree of impact the piling noise has on marine mammals as a distance from the source is better quantified.

Application to wind farm cases

In order to arrive at the final results the model parameters were adjusted to fit the acoustic data measured in the Gemini area. The predicted sound levels that fit the data best are obtained with an upper layer thickness of 2.5 m and a sand type that is classified as coarse. However, almost the same sound levels are reached for an upper layer thickness of 5 m and a sand type classified as very coarse. This shows that no evident choice exists to arrive at the best results to match the data in the Gemini area. Other combinations of sediment type and layer thickness give results that are comparable to the final ones presented in this thesis.

Multiple combinations of two parameters (thickness and sediment types) give the right behaviour of the fluid soil layer to match the data. However, without data no guarantees exist that this is indeed the case. In the case of the seabed the choice of parameters is ambiguous. This means that the model has no predictive value. The soil parameters relate in no way to the actual soil properties. Near Gemini the soil is indeed coarse (MVe), but the thickness of the sand layer is tens of meters, (Balson et al., 2002).

The acoustic data is also used for the iterative determination of the source spectrum. The need of the acoustic data to arrive at the measured sound levels diminishes the applicability of the UAS as a tool to predict sound levels from piling noise for future wind park projects. Given the many parameters related to pile geometry, local environment and impact hammer specifications influencing the source energy, the construction of a suitable source spectrum without acoustics data is not considered realistic. This means that also regarding this aspect, the UAS has no predictive value.

Other sound propagation models

The results of this thesis are compared with the sound levels obtained when applying geometrical spreading laws (green lines in Figure 5.4). In this comparison the uncertainty introduced by the choice of sediment for the seabed is also considered (blue lines in Figure 5.4). The predictions of the UAS in the Gemini area give a more precise indication of the received sound levels in the water compared with the existing geometrical spreading laws. Upto 30 km from the source the predicted sound levels by the UAS come close the to sound levels predicted by the $15log(R)$ law for intermediate water. For distances further away from the source the predicted sound levels by the UAS are between $15log(R)$ and $20log(R)$ depending on the used type of sand.

This means that environmental departments can keep on using those. This will lead to conservative predictions, overestimating the sound levels further from the source.

The remarks made on the valid application of the UAS to wind park cases in general arouse our interest in other underwater sound prediction models. Binnerts et al. (2016a) developed sound propagation models and validated them with the same Gemini acoustic data set. These models also calculate sound propagation in the vertical plane and model the seabed as a fluid. A quick analysis of the results at the four measurement positions learns us that the this model shows an underprediction of the sound levels at lower frequencies (Figure 5.6). This is due to the same reason that underestimation is observed in the UAS. The overdamping is related to the fluid seabed representation. In their study Binnerts et al. (2016a) chose to apply a layer thickness that represents the true thickness of the seabed layers instead of a layer thickness of 2.5 m as in the thesis (Figure 5.5). Neither the optimization in this thesis, nor as their free run, give a satisfactory result. It is a trade off between the true representation of the seabed which results in over damping of low frequencies on the one hand. Or on the other hand, an unrealistic representation of the seabed resulting with the right predicted sound levels, but is has no predictive value for application to other wind farm projects.

Sound impact on marine mammals

The results of this thesis are applied to the impact that pile driving sound has on marine mammals. The piling noise stays above the lower limit of the audiable range over the modelled distance of 66 km. This is consistent with the study performed by Thomsen et al. (2006) who identified a distance of at least 80 km from the source. The distance at which behavioural response occurs lays between 20 and 30 km from the source. This gives an indication of how the uncertainty of the sediment choice reflects on the application of the model to marine life. A shifting of hearing ability, temporal or permanent, occurs within a distance of 3.5 km from the source. This agrees with studies of the impact on marine life (amongst others (Thomsen et al., 2006) and (Kastelein et al., 2017)).

An important reason to be able to quantify sound levels is the aimed application of mitigation measures. Not only is the UAS not suitable to quantitatively predict the effect of such measures, also a qualitative analysis is not possible because the physics are not represented well. This is because mitigation measures not only influence the sound paths in the water but also in the seabed. More sound energy propagates through the seabed when such measures are present (Nijhof, M. (2017, October 10). Personal interview). This highlights the importance of the correct physical implementation of the seabed in a sound propagation model and disqualifies the UAS as such a model.

In summary, although the UAS is able to predict sound levels in the Gemini area that agree well with the measured sound levels, this is not due to the correct implementation of the physic regarding the seabed and sound emission from the source. As a consequence, the model is tweaked of the model to arrive at the measured sound levels. The UAS is therefore not considered suitable for application in wind park cases.
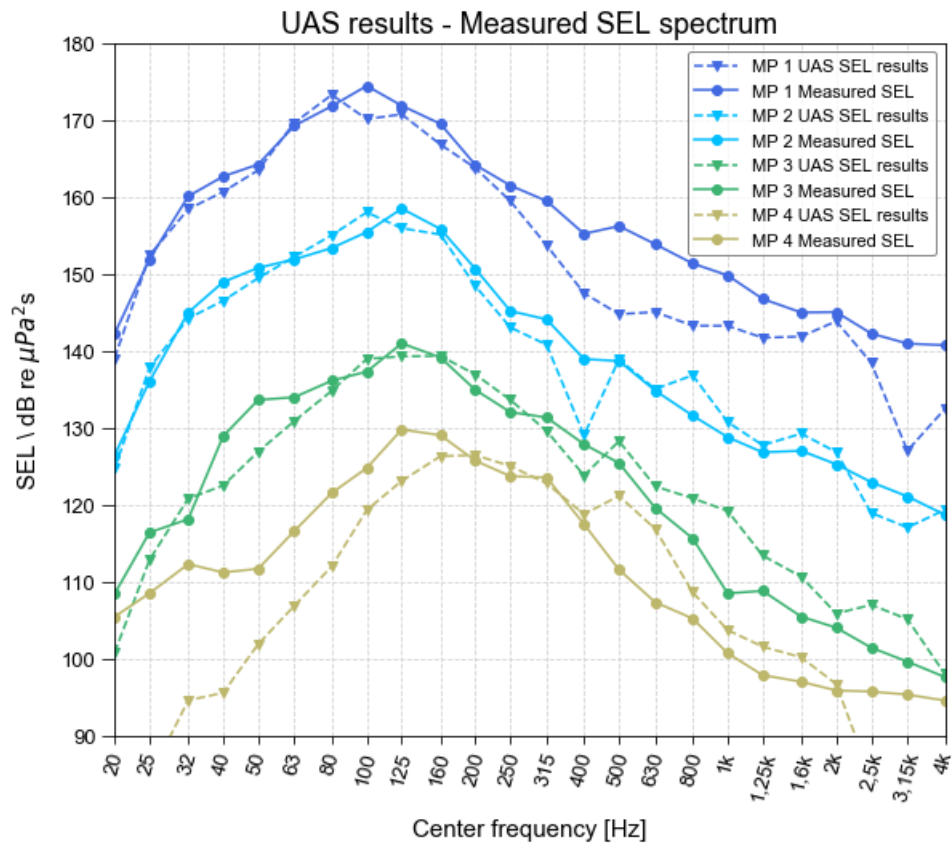
Figure 5.5: UAS results and Gemini data compared: The one-third octave band spectra of the sound exposure level at 10m above the seabed at the measurement locations MP1 till MP4

Confidential

Figure 5.6: Aquarius 1.0 results by Binnerts et al. (2016a) and Gemini data compared: The one-third octave band spectra of the sound exposure level at 10m above the seabed at the measurement locations MP1 till MP4

6

Recommendations

Predicting underwater sound levels is important to determine the impact on marine life and assess whether mitigation measures are required during the pile driving activities for offshore wind parks. Based on the findings in this thesis some issues need to be addressed regarding the future effort into underwater sound modelling. First, the recommendations for Van Oord are discussed. The remainder of this chapter focusses on future research into the physics of underwater sound propagation.

Van Oord

Underwater sound propagation is a complex subject and is influenced by a variety of factors. This thesis made clear that the use of the UAS is not suitable for the proper application in wind park cases. This is amplified by the fact that the prediction of sound levels by using numerical models in general requires specialist knowledge on how to use such models. At this moment Van Oord is lacking experience in the field of underwater acoustics to make adequately use of such models. Additionally, the use of the geometrical spreading law for intermediate water ($15log(R)$) proves to predicts sound levels over range comparable to the behaviour predicted by the UAS. Both approaches have limitations, but the uncertainty that comes with the use of spreading laws is qualitatively better to assess and less time consuming. It is therefore recommended to Van Oord to use the geometrical spreading method to estimate the sound levels. Additionally, it is recommended to outsource the sound modelling to a third party like ITAP in case more precise predictions are required.

Acoustic soil modelling

The first issue addressed is the model representation of the seabed. This thesis showed that the effect of a fluid seabed is that the sound levels at the lower frequencies are underestimated. This is an effect of the fluid seabed which negelcts the shear effect of the sol. Research shows that the shear rigidity of the soil is important for the sound energy propagation at the lower frequencies. Tsouvalas (2015) developed an acoustic model that does consider the effect of the shear of the soil. This Elastic Medium model is a parametric model which requires only relative simple input parameters (Rhijn, 2017). With such a model the following issues could be assessed.

In the Elastic Medium model the shear effect of the seabed is included, but it also contains a function to describe the soil as a fluid. With the use of this function the effect of the exclusion of the shear effect in the soil on sound propagation can be investigated quantitatively. Additionally, the contribution of the Scholte waves at the soil-water interface to the sound levels in water can be investigated. This will contribute to the knowledge on the effect of the seabed on sound propagation in water.

The recommendation above can be extended with a validation of the Elastic Medium model with an acoustic data set, for example the one used in this thesis. This will help increase the understanding of the different available numerical sound models and their specifications. Also, the suitability of this Elastic Medium model can be assessed to predict sound levels for application in offshore wind park projects. Because the shear effect of the soil is incorporated in this model, the implementation of noise mitigation measures can be studied as well.

Source modelling

A second important issue is the modelling of the sound source. The fact that many parameters determine the sound energy emitted from the monopile asks for a more thorough investigation. A variety of methods have been used to model the pile acoustics. The output from such models can be coupled to an acoustic model. Such models could help understand the contribution of the many parameters that effect the sound radiation from the pile. A parametric into this topic is therefore recommended.

The possibility to couple a source model to an acoustic propagation model could contribute to the ability of Van Oord to do sound propagation predictions in-house in the future. Therefore it is recommended to investigate this possibility, but not before more knowledge is gained about the topics addressed above.

Oceanography

The third and last aspect addressed in this thesis is regarding the effect of three-dimensional oceanographic variations. Bathymetric variations and the distribution of the sound speed profile steer the acoustic energy. With the increasing demand for offshore wind energy the interest of oceanographers is aroused. Little research is put into the effect of the local sea environment on the propagation of sound from offshore pile driving in shallow water areas. The studies available on this topic do show a significant effect. Since many offshore wind parks are located in areas with this frontal activities it is interesting to investigate this. For this purpose a 3-D ocean model should be coupled to an acoustic propagation model.

Bibliography

Map viewer emodnet. Accessed: 09-01-2018 via : http://www.emodnet-geology.eu/map-viewer.

Ainslie, M. (2010). *Principles of Sonar Performance Modelling.* Springer-Praxis.

Ainslie, M. (2011). Standard for measurement and monitoring of underwater noise, part i. physical quantities and their units. Technical report, TNO.

Balson, P., Butcher, A., Holmes, R., Johnson, H., Lewis, M., and Musson, R. (2002). North sea geology. Technical report, British Geological Survey.

Beare, D., McQuatters-Gollop, A., Hammen, T. v. d., Machiels, M., Hall-Spencer, J., and Teoh, S. (2013). Long-term trends in calcifying plankton and ph in the north sea. *PLoS One*, 8(5).

Binnerts, B., de Jong, C., Ainslie, M., Nijhof, M., Muller, R., and Jansen, E. (2016a). Validation of the aquarius models for prediction of marine pile driving sound. Technical report, TNO.

Binnerts, B., Jong, C. d., Ainslie, M., Nijhof, M., Muller, R., and Heijningen, A. (2016b). Validatie heigeluid-modellen - wp1 - inventaristatie gegevens - 2016. Technical report, TNO.

Brekhovskikh, C., Lysanov, and Yu, P. (2003). *Fundamentals in Ocean Acoustics.* Springer New York.

Chapman, D. and Dale, D. (1998). The elusive decibel: thoughts on sonarrs and marine mammals. *Canadian Acoustics*, 26(2):29–31.

Claessens, C. (2016). Episodic density-induced current velocities at the gemini offshore wind park. Msc. thesis, TU Delft.

Collins, M. (1989). Applications and time-domain solution of higher-order parabolic equations in underwater acoustics. *The Journal of the Acoustical Society of America*, 86(3).

Collins, M. (1993). A split-step padé solution for the parabolic equation method. *The Journal of the Acoustical Society of America*, 93(4).

Collins, M. (1999a). *User's Guide for RAM Versions 1.0 and 1.0p.* Naval research Laboratory.

Collins, M. and Westwood, E. (1991). A higher-order energy-conserving parabolic enquation for range-dependent ocean depth, sound speed, and density. *The Journal of the Acoustical Society of America*, 89(3):1736–1742.

Corp, A. (2014). Adbm buitendiek demonstration report. Technical report.

Dahl, P., de Jong, C., and Popper, A. (2015). The underwater sound field from impact pile driving and its potential effects on marine life. *Acoustics Today*, 11(2).

Dähne, M., Tougaard, J., Carstensen, J., Rose, A., and Nabe-Nielsen, J. (2017). Bubble curtains attenuate noise from offshore wind farm construction and reduce temporary habitat loss for harbour porpoises. *Marine Ecology Progress Series*, 580:221–237.

Dekeling, R., Tasker, M., Van der Graaf, A., Ainslie, M., Andersson, M., Andre, M., Borsani, J., Brensing, K., Castellote, M., Cronin, D., Dalen, J., Folegot, T., Leaper, R., Pajala, J., Redman, P., Robinson, S., Sigray, P., Sutton, G., Thomsen, F., Werner, S., Wittekind, D., and Young, J. (2013). Monitoring guidance for underwater noise in european seas - executive summary. 2nd report of the technical subgroup on underater noise (tsg noise). Technical report.

DHI (2016). *UAS in MIKE: Underwater Acoustic Simulator Module, Scientific Documentation.* MIKE Powered by DHI.

Douglas-Westwood (2017). World offshore wind market forecast 2017-2025. Technical report, Douglas-Westwood Ltd.

Elmer, K.-H., Bruns, B., and Kuhn, C. (2016). Offshore piling noise attenuation: theory and new applications on monopiles and jacket foundations.

Elmer, K.-H. and Savery, J. (2014). New hydro sound dampers to reduce piling underwater noise.

Erbe, C. and Farmer, D. (2000). A software model to estimate zones of impact on marin mammals around antrhopogenic noise. *Insitute of Ocean Science*, pages 1327–1331.

Farcas, A., Thompson, P., and Merchant, N. (2015). Underwater noise modelling for environmental impact assessment. *Environmental Impac Assessment Review*, 57:114–122.

Francois, R. and Garrison, G. (1982a). Sound absorption based on ocean measurements: Part i: Pure water and magnesium sulfate contributions. *The Journal of the Acoustical Society of America*, 72(3).

Francois, R. and Garrison, G. (1982b). Sound absorption based on ocean measurements. part ii: Boric acid contribution and equation for total absoption. *The Journal of the Acoustical Society of America*, 72(6).

Götz, T. and Janik, V. (2010). Aversiveness of sounds in phocid seals: psycho-physiological factors, learning processes and motivation. *The Journal of Experimental Biology 213*, pages 1536–1548.

Hamilton, E. (1980). Geoacoustic modeling of the sea floor. *The Journal of the Acoustical Society of America*, 68(5).

Heathershaw, A., Stretchs, C., and Maskell, J. (1991). Coupled ocean-acoustic model studies of sound propagation through a front. *The Journal of the Acoustical Society of America*, 89(1):155–156.

Ho, A. and Mbistrova, S. (2017). The european offshore wind industry, key trends and statistics 2016. Technical report, Wind Europe.

Jensen, F. (2001). Acoustics, shallow water. *Encyclopedia of Ocean Sciences*, 1:89–96.

Jensen, F., Kuperman, W., Porter, M., and Schmidt, H. (2011). *Computational Ocean Acoustics*. Springer New York Dordrecht Heidelberg Londen.

Kastak, D., Southall, B., Schusterman, R., and Reichmut Kastak, C. (2005). Underwater temporary threshold shifts in pinnipeds: Effects of noise level and duration. *The Journal of the Acoustical Society of America*, 118:3154–3163.

Kastelein, R., Bunskoek, P., Hagedoorn, M., Au, W., and de Haan, D. (2002). Audiogram of a harbor porpoise measured with narrow-band frequency-modulated signals. *The Journal of the Acoustical Society of America*, 112:334–344.

Kastelein, R., Gransier, R., Hoek, L., and Olthuis, J. (2012). Temporary thresholds shifts and recovery in a harbor porpoise (*phocoena phocoena*) after octave-band noise at 4 khz. *The Journal of the Acoustical Society of America*, 132(5):3525–3537.

Kastelein, R., Horvers, M., Helder-Hoek, L., Voorde, S. v. d., Hofstede, R. t., and Meij, H. v. d. (2017). Behvioral responses of harbor seal (*Phoca vitulina*) to faunaguard seal module sounds at two background noise levels. *Aquatic Mammals*, 43(4):347–363.

Kibblewhite, A. (1989). Attenuation of sound in marine sediments. *The Journal of the Acoustical Society of America*, 86(2):716–738.

Kuperman, W. and Roux, P. (2007). *Springer Handbook of Acoustics*. Springer New York.

Lepper, P., Aisnlie, M., Jongh, C. d., and Robinson, S. (2012). What is the source level of pile-driving noise in water. In Popper, A. and Hopkins, A., editors, *The effects of Noise on Aquatic Life*. Springer.

Li, J.-F. and Hodgson, M. (1998). Development and evaluation of equivalent-fluid approximation for sea-bottom sound reflection. *Canadian Acoustics*, 1(26):3–11.

Lynch, J. F., Newhall, A. E., Sperry, B., Gawarkiewicz, G., Gawarkiewicz, G., Fredricks, A., Tyack, P., Chiu, C. S., and Abbot, P. (2003). Spatial and temporal variations in acoustic propagation characteristics at the new england shelfbreak front. *IEEE Journal of Oceanic Engineering*, 28(1).

Medwin, H. and Clay, C. (1998). *Fundamentals of Acoustical Oceanography*. Academic Press.

Nilsson, A. and Liu, B. (2015). *Vibro-Acoustics, Volume 1*. Springer-Verlag Berlin Heidelberg.

Osborne, A. (2010). *An Introduction to Underwater Acoustics*, chapter Underwater acoustic wave propagation, pages 623–684. Springer.

Reinhall, P. and Dahl, P. (2011). Underwater mach wave radiation from impact pile driving: Theory and observation. *The Journal of the Acoustical Society of America*, 130(3):1209–1216.

Remmers, P. and Bellmann, M. (2016). Ecological monitoring of underwater noise during piling at offshore wind farm gemini. Technical report, ITAP.

Rhijn, J. v. (2017). Reduction of underwater piling noise: An optimization of the impact force to reduce underwater noise during the installation of a large sized monopile. Msc. thesis, TU Delft.

Richards, S. (1998). The effect of teperature, pressure and salinity on sound attenuation in turbid seawater. *The Journal of the Acoustical Society of America*, 103(1):205–211.

Robinson, S., Lepper, P., and R.A., H. (2014). Good practice guide for underwater noise measurement. Technical report, National Measurement Office, Marine Scotland, The Crown Estate.

Rousseau, T. H., Siegmann, W. L., and Jacobson, M. J. (1982). Acoustic propagation through a model of shallow fronts in the deep ocean. *The Journal of the Acoustical Society of America*, 72(3):924–936.

Sertlek, H., Binnerts, B., and Ainslie, M. (2016). The effect of sound speed profile on shallow water shipping sound maps. *The Journal of the Acoustical Society of America*, 140(1).

Shapiro, G., Chen, F., and Thain, R. (2014). The effect of ocean fronts on acoustic wave propagation in the celtic sea. *Journal of Marine Systems*, 139:217–226.

Southall, B., Bowles, A., Ellision, W., Finneran, J., Gentry, R., Greene Jr., C., Kastak, D., Ketten, D., Miller, J., Nachtigall, P., Richardson, W., Thomas, J., and Tyack, P. (2007). Marine mammal noise exposure criteria: initial scientific recommendations. *Aquatic Mammals*, 33(4):437–444.

Tappert, F. (1977). The parabolic approximation method. In Keller, J. and Papadakis, J., editors, *Wave Propagation and Underwater Acoustics*, volume 70, pages 224–287. Springer Berlin / Heidelberg.

Thomsen, F., Luedemann, K., Kafemann, R., and Piper, W. (2006). Effects of offshore wind farm noise on marine mammals and fish. Technical report, COWRIE Ltd.

Tougaard, J., Carstensen, J., Henriksen, O., Skov, H., and Teilmann, J. (2003a). Short-term effects of the construction of wind turbines on harbour porpoises at horns reef. Technical report, Techwise A/S. Hedeselskabet.

Tougaard, J., Carstensen, J., Teilmann, J., Bech, N., Skov, H., and Henriksen, O. (2005). Effects of the nysted offshore wind farm on harbour porpoises. Technical report, Energi E2 A/S. NERI.

Tougaard, J., Ebbesen, I., Tougaard, S., Jensen, T., and Teilmann, J. (2003b). Satellite tracking of harbour seals on horns reef. use of the horns reef wind farm area and the north sea. Technical report, Techwise A/S. Fisheries and Maritime Museum.

Tronstad, T. and Hovem, J. (2011). Bathymetric and seasonal effects on the propagation of airgun signals to long distances in the ocean. *OCEANS'11*, pages 1–8.

Tsouvalas, A. (2015). *Underwater noise generated by offshore pile driving*. PhD thesis, Delft University of Technology.

Urick, R. (1948). The absorption of sond in suspensions of irregular particles. *The Journal of the Acoustical Society of America*, 20(3).

Young, R. (1973). The sound pressure in water resulting from a point source in air. *The Journal of the Acoustical Society of America*, 53(6):1708–1716.

Zhu, J., Popovics, J., and Schubert, F. (2004). Leaky rayleigh and scholte waves at the fluid-solid interface subjected to transient point loading. *The Journal of the Acousitcal Society of America*, 116(4):2101–2110.

<div align="right">

A

</div>
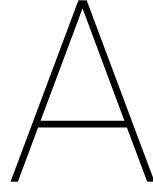
The Wave Equation

A.1. The 2D wave equation for sound

The propagation of acoustic waves in a fluid is described by the wave equation. The wave equation for displacement potential ψ is as follows (Jensen et al., 2011),

$$\nabla^2 \psi - \frac{1}{c^2}\frac{\partial^2 \psi}{\partial t^2} = 0 \tag{A.1}$$

The first term in equation A.1 is independent of time. Therefore the dimensions of the wave equation can be reduced to three by the use of the frequency-time Fourier transform pair. This function transforms the wave equation for displacement potential (equation A.1) to the frequency-domain wave equation, or the Helmholtz equation,

$$[\nabla^2 + k^2(r)]\psi(r,\omega) = 0 \tag{A.2}$$

where $k(r)$ is the medium wave-number at radial frequency ω,

$$k(r) = \frac{\omega}{c(r)} \tag{A.3}$$

Equation A.2 is a three-dimensional partial differential equation and is an easier to solve problem than the original problem of equation A.1.

To model sound propagation in a 2-D transect, azimuthal symmetry is assumed. When there is no dependence on the ψ-coordinate, equation A.2 reduces to the standard 2-D Helmholtz equation,

$$\frac{\partial^2 p}{\partial r^2} + \frac{1}{r}\frac{\partial p}{\partial r} + \frac{\partial^2 p}{\partial z^2} + k_0^2 n^2 p = 0 \tag{A.4}$$

where $p(r,z)$ is the acoustic pressure, $k_0 = \omega/c_0$ is a reference wave number, and $n(r,z) = c_0/c(r,z)$ is the index of refraction.

Several methods exist to derive a solution to equation A.4. the Parabolic Equation from the 2-D Helmholtz equation. The MIKE UAS follows the method derivation developed by Tappert (1977). In this method it is assumed that the general solution to equation A.4 takes the form

$$p(r,z) = \psi(r,z)H_0^{(1)}(k_0 r), \tag{A.5}$$

which is an outgoing cylindrical wave solution. This general solution consist of $\psi(r,z)$, called the envelope function, and the Hankel function $H_0(k_0 r)$. The Hankel function contains the effect of geometrical spreading loss $1/r$,

$$H_0^{(1)}(kr) \simeq \sqrt{\frac{2}{\pi k r}}\exp i(kr - \pi/4) \tag{A.6}$$

The general solution in equation (A.5) is substituted into the 2-D Helmholtz equation (A.4). The Hankel function property is used to obtain the solution to the simplified elliptic wave equation. Next, the far-field assumption is made, $k_0 r \gg 1$ and used to obtain the simplified elliptic wave equation,

$$\frac{\partial^2 \psi}{\partial r} + 2i k_0 \frac{\partial \psi}{\partial r} + 2i k_0 \frac{\partial \psi}{\partial r} + k_0^2 (n^2 - 1)\psi = 0 \tag{A.7}$$

A.2. Solution to the wave equation in the UAS

An infinity of parabolic approximations to the equation A.7 exist, (Jensen et al., 2011). The difference between the various techniques is the mathematical manipulation applied, before the actual implementation of the solution. Here the approxiamtion developed by Collins (1993) as used in the UAS is described. This approximation defines a depth operator,

$$X = k_0^{-2}\left(\rho \frac{\partial}{\partial z} \frac{1}{\rho} \frac{\partial}{\partial z} + k^2 - k_0^2\right) \tag{A.8}$$

With this depth operator, the elliptic wave equation (A.7) is factored into the following form,

$$\left(\frac{\partial}{\partial r} + i k_0 (1 + X)^{1/2}\right)\left(\frac{\partial}{\partial r} - i k_0 (1 + X)^{1/2}\right)p = 0 \tag{A.9}$$

with $k_0 = \omega/c_0$ and c_0 as the representing phase speed. Now is assumed that the outgoing energy is dominating the back-scattered energy. The outgoing wave equation can be written as:

$$\frac{\partial p}{\partial r} = i k_0 (1 + X)^{1/2} p \tag{A.10}$$

The solution of equation A.10 at the range $r + \Delta r$ is

$$p(r + \Delta r) = exp\left[i\sigma(-1 + \sqrt{1 + X})\right]p(r) \tag{A.11}$$

where $\sigma = k_0 \Delta r$. To implement equation A.11 the following approximation is applied,

$$exp\left[i\sigma(-1 + \sqrt{1 + X})\right] \cong 1 + \sum_{j=1}^{n} \frac{a_{j,n}X}{1 + b_{j,n}X} = \prod_{j=1}^{n} \frac{1 + \lambda_{j,n}X}{1 + \mu_{j,n}X} \tag{A.12}$$

By substituting equation A.12 into equation A.11 the so called split-step Padé solution is obtained,

$$p(r + \Delta r) = p(r) + \sum_{j=1}^{n} a_{j,n}(1 + b_{j,n}X)^{-1}Xp(r). \tag{A.13}$$

The work done on this approximation was complemented with the development of a Range-dependent Acoustic Model (RAM) and a corresponding algorithm of the split-step Padé solution. This algorithm forms the basis for the UAS, (DHI, 2016). The advantage of this model is that it can be solved by a range-marching solution technique, step by step from the source, (DHI, 2016). The depth operator from equation A.8 is first discretized using Galerkin's method as described by Collins and Westwood (1991). Then, the UAS uses a forward-marching finite difference scheme to solve the acoustics fields in discretised steps of range and depth, (DHI, 2016).

B

1D lattice sound model

In this chapter a model is proposed to examine the propagating behaviour of the sound underwater radiated from offshore pile driving activities. In this model the sound is represented as pressure or displacement vibrations propagating in horizontal direction. The ocean environment is modelled as a finite string of masses, springs and dampers, a so called lattice model. The properties of these masses, springs and dampers embody the properties of the ocean. In such a domain the sound source representing the monopile is located at the beginning of the domain at $r = 0$ m. The model used in this thesis to simulate sound waves in water is a one-dimensional stacked lattice model. It consist of a number of N masses linked to each other over range with $N + 1$ springs and $N + 1$ dampers. The properties of the water volume are represented by the masses and the behaviour of the environment is represented by the properties of the springs and dampers.

B.1. Equation of motion of a single mass in the 1D lattice model

For each of the masses in the model the equation of motion can be derived to eventually solve the calculations. In the one-dimensional lattice an arbitrary mass n with mass M^n is related to masses $n - 1$ and $n + 1$ by linear springs, that have stiffness's $K_e^{n-1,n}$ and $K_e^{n,n+1}$. Following Newton's second law with the only forces working on mass n represented by the springs, the equation of motion for an arbitrary mass n expressed for the displacement x^n is as follows:

$$M^n \ddot{x}^n + \hat{K}^{n,n-1}(x^n - x^{n-1}) + \hat{K}^{n+1,n}(x^n - x^{n+1}) = 0 \tag{B.1}$$

In equation B.1 the damping of the the motion is incorporated in the equivalent stiffness $\hat{K}^{n,n-1}$. The equivalent stiffness between any two adjacent masses n and $n + 1$ is defined as:

$$\hat{K}^{n,n+1} = K^{n,n+1} + C^{n,n+1}\frac{\partial}{\partial t} \tag{B.2}$$

Here, $C^{n,n+1}$ is the damping element between any two adjacent masses n and $n + 1$. With expression B.2 substituted into equation B.1 and assuming the lattices to be homogeneous with all spring stiffness's equal to K the equation of motion becomes:

$$M^n \ddot{x}^n + K(2x^n - x^{n+1} - x^{n-1} + C(2\dot{x}^n - \dot{x}^{n-1} - \dot{x}^{n+1}) = 0 \tag{B.3}$$

B.2. Equation of motion in the frequency domain

The equation of motion for an arbitraty mass n defined with equation B.3is expressed in the time domain. Calculations with numerical models in the time domain are generally more time consuming that calculations performed in the frequency domain. Furthermore, for the purpose of this thesis the displacment of the masses as function of time are not of particular interest. For sound propagation the response of the model as a function of frequency is much more interesting. The excitation of a linear system of differential equation such as equation B.3 by means of a certain force or initial displacement results in a certain response. Thsi response can be expanded in a Fourrier series. Each term in the series corresponds to a certain frequency. In the frequency domain this is equivalent to a line spectrum. Each line corresponds to a component in the

Fourier series Nilsson and Liu (2015).

Using the general expression for the Fourier transforms $x(t) = \mathscr{F}(x(\omega))$ the function $x(t)$ can be expressed as

$$x(t) = \frac{1}{2\pi} \int_{-\infty}^{+\infty} \tilde{x}(\omega) e^{i\omega t} d\omega \tag{B.4}$$

where $\tilde{x}(\omega)$ is the Fourier transform of $x(t)$. Inversely $x(\omega) = \mathscr{F}(x(t))$ can be defined as

$$\tilde{x}(\omega) = \int_{-\infty}^{+\infty} x(t) e^{-i\omega t} \tag{B.5}$$

Now equation B.5 is used to transform equation B.3 to the frequency domain. This is done by besides rewriting the displacement $x(t)$ also rewriting the velocity $\dot{x}(t)$ and acceleration $\ddot{x}(t)$ in equation B.3 as a function of frequency instead of a functions of time. For the velocity the expression in the frequency domain becomes

$$\mathscr{F}(\dot{x}(t)) = \dot{x}(\omega) = i\omega \int_{-\infty}^{+\infty} x(t) e^{-i\omega t} dt = i\omega \tilde{x}(\omega) \tag{B.6}$$

and for the acceleration the expression in the frequency domain becomes

$$\mathscr{F}(\ddot{x}(t)) = \ddot{x}(\omega) = i\omega \cdot i\omega \int_{-\infty}^{+\infty} x(t) e^{-i\omega t} dt = -\omega^2 \tilde{x}(\omega) \tag{B.7}$$

Substituting equation B.6 and equation B.7 into equation B.3 results in the equation of motion of mass n in the frequency domain

$$-M^n \omega^2 \tilde{x}^n + K(2\tilde{x}^n - \tilde{x}^{n+1} - \tilde{x}^{n-1}) + i\omega C(2\tilde{x}^n - \tilde{x}^{n+1} - \tilde{x}^{n-1}) = 0 \tag{B.8}$$

B.3. Equations of motion for the first and last mass in the system

The equation of motion derived in section B.2 holds for an arbitrary mass n that is related to mass $n-1$ and mass $n+1$ via springs with stiffness $K^{n-1,n} = K^{n,n+1} = K$. However, in this 1D lattice model the motion of the first and last mass of the system deviate from the other masses.

The first mass in the system is underfluence of a force representing the pressure pulses released into the water as a result of the hammer impact on the monopile. This first mass is connected to only its subsequent mass instead of being connected to its subsequent mass and previous mass, like the other masses. Therefore the equation of motion for this mass becomes

$$-M^n \omega^2 \tilde{x}^n + (K + i\omega C)(\tilde{x}^n - \tilde{x}^{n+1}) = F(\omega) \tag{B.9}$$

The modelled domain is finite while in reality the sound propagates over range until the sound hits an obstacle, for example shoaling land. It is not the purpose of this thesis to look into the effect associated with this phenomenon. Therefore a boundary condition needs to be applied at the end of the domain. This should be a non-reflective boundary condition. Hence, for the last mass in the system the equation of motion is as follows:

$$-M^n \omega^2 \tilde{x}^n + K(\tilde{x}^n - \tilde{u}^{n-1}) + i\omega C(\tilde{x}^n - \tilde{u}^{n-1}) + \chi(\omega)\tilde{u}^n = 0 \tag{B.10}$$

with $\chi(\omega)$ being the dynamic stiffness

$$\chi(\omega) = Ki\frac{\omega}{\omega_0}\sqrt{2 + 2\zeta_e i\omega - \frac{\omega^2}{\omega_0^2}} \tag{B.11}$$

The above results in a system of equations that can be solved with respect to $\tilde{\mathbf{x}}$ using linear algebra,

$$\tilde{\mathbf{x}} = \left[-\omega^2 \tilde{\mathbf{M}} + \tilde{\mathbf{K}} + \tilde{\mathbf{C}} \right]^{-1} \tilde{F} \tag{B.12}$$

B.4. Matrix notation

In this system of equations the matrix $\tilde{\mathbf{M}}$ accounts for the mass of the fluid particles vibrating in the system.

$$\tilde{\mathbf{M}} = \begin{bmatrix} m_1 & 0 & \dots & \dots & 0 \\ 0 & m_2 & 0 & 0 & \vdots \\ \vdots & \ddots & \ddots & \ddots & \vdots \\ \vdots & \ddots & 0 & m_{n-1} & 0 \\ 0 & \dots & \dots & 0 & m_n \end{bmatrix}$$

The complex matrix $\tilde{\mathbf{K}}$ accounts for the compressibility of the fluid. This is expressed with the terms $k_{1..n}$ that correspond to the bulk modulus of the fluid. The complex matrix $\tilde{\mathbf{C}}$ accounts for the damping in the fluid. The damping considered here is transmission loss of sound due to geometrical spreading. The terms $c_{1..n}$ account for this loss as a function of distance from the source.

$$\tilde{\mathbf{K}} = \begin{bmatrix} k_1 & -k_1 & 0 & \dots & 0 \\ -k_1 & k_1+k_2 & -k_2 & \ddots & \vdots \\ 0 & -k_2 & k_2+k_3 & \ddots & 0 \\ \vdots & \ddots & \ddots & \ddots & -k_n \\ 0 & \dots & 0 & -k_n & k_n+\chi_n(\omega) \end{bmatrix}, \tilde{\mathbf{C}} = \begin{bmatrix} i\omega c_1 & -i\omega c_1 & 0 & \dots & 0 \\ -i\omega c_1 & i\omega(c_1+c_2) & -i\omega c_2 & \ddots & \vdots \\ 0 & -i\omega c_2 & i\omega(c_2+c_3) & \ddots & 0 \\ \vdots & \ddots & \ddots & \ddots & -i\omega c_n \\ 0 & \dots & 0 & -i\omega c_n & i\omega c_n \end{bmatrix}$$

The vector $\tilde{\mathbf{x}}$ is the displacement vector representing the displacement of each mass or equivalently the pressure in the fluid caused by the displacement. The vector $\tilde{\mathbf{F}}$ represents the force on the first mass.

$$\tilde{\mathbf{x}} = \begin{bmatrix} x_1 \\ 0 \\ \vdots \\ \vdots \\ x_n \end{bmatrix}, \tilde{\mathbf{F}} = \begin{bmatrix} F(\omega) \\ 0 \\ \vdots \\ \vdots \\ 0 \end{bmatrix}$$

B.5. Derivation of the force function

This force accounts for the pressure pulses the monopile radiates into the water which is a time function applied at the first mass. The monopile radiates pressure pulses of a certain duration and with a certain frequency into the water. The pressure in the water is caused by the movement of the water particles. Compressions and dilatations with respect to the equilibrium occur. The force on the first mass in the system must account for this movement as a function of frequency. In the time domain the force function can be seen as a function that lasts a certain period of time $0 < t \le t_1$,

$$f(t) = \begin{cases} f(t), & 0 < t \le t_1 \\ 0, & 0 \ge t_1 \end{cases} \tag{B.13}$$

with $f(t) = \mathscr{F}^{-1} F(\omega)$.

The pressure waves can be reproduced as $F(t) = \Sigma a_i sin(\omega t)$. A Fourier analysis performed on this system gives $F(\omega) = \Sigma \frac{a_i \pi}{i}$, with a_i being the maximum amplitude per frequency. The system is solved with respect to $\tilde{\mathbf{x}}$ for each frequency $\omega = 2\pi f_i$ with f_i = 12 Hz - 4 kHz separated in third octave bands. For each frequency the complex matrices $\tilde{\mathbf{K}}$, $\tilde{\mathbf{C}}$ and $\tilde{\mathbf{F}}$ differ.

C

1D model Notebook

Appendix 1D lattice model with n masses

March 19, 2018

```
In [1]: import h5py
        import numpy as np
        import os

        import cmath
        import matplotlib.pyplot as plt
        %matplotlib inline

        root = r'C:\Checkouts\VOMSC\hyc\Afstuderen Onderwatergeluid\Data Gemini\Gemini\Gemini\(
```

```
In [2]: file = os.path.join(root,r'GM_MP1_1557_piling_nl_ch2.h5')
        os.path.exists(file)
```

```
Out[2]: True
```

```
In [3]: fl = h5py.File(file, 'r')
```

```
In [4]: #Number of masses
        n = 4
        l = np.arange(1,n+1)
        n_length = l.astype(str)
```

```
In [5]: lmin = 10 # min wave length analyzed
        mwv = 7 # no. masses per lmin
```

```
In [6]: #System parameters
        pref = 10**-12 #in Pa
        tref = 1 #in seconds

        T = 14 #temperature in degrees celsius
        S = 33 #salinity in psu
        c_sp = 1501 #soundspeed in m/s

        rho = 1029 #kg/m3
        B = rho*c_sp**2 #Bulk modulus in GPa
        g = 9.81

        dx = mwv/lmin #length of one mass and spring
```

1

```
          dz = 1 #depth of one mass and spring
          l_domain = dx*n + dx*0.5 #length model domain in meters
          T_p = 1 #integration period force

In [7]:  #Definition parameters
          m = rho*dz*dx #water mass in kg
          m_l = 0.5*m #water mass last mass

          k = B #spring stiffness
          k_l = 0.5*B #spring stiffness last spring

          c_d = 0 #damping coefficient

In [8]:  #SEL for displacement amplitude construction
          sl = fl['sel_data_singleblow/block0_values'][1261,:]

          p_sp =[]
          for i in sl:
              p = (10**(i/10)*pref**2)
              p_sp.append(p)

          p_t = p_sp[0]
          p_w = p_sp[1:17]

In [9]:  #Frequency related parameters
          f_range = [12,16,20,25,32,40,50,63,80,100,125,160,200,250,315,400] #frequency range

          #Angular frequency in rad/s
          omega = []
          for f in f_range:
              y = 2*np.pi*f
              omega.append(y)

          #Wave number in rad/m
          k_wave =[]
          for f in f_range:
              u = (2*np.pi)/(c_sp/f)
              k_wave.append(u)

          #Acoustic impendance in N*s/m3
          Z = []
          for w, k in zip(omega,k_wave):
              zi = (B*k)/w
              Z.append(zi)

          #Displacement amplitude spectrum
          a_m = []
          for p,w,zi in zip(p_w,omega,Z):
```

2

```
        a = p/(zi*w)
        a_m.append(a)
```

1   Matrix definition

In [10]:
```
#Critical damping, damping coefficient and natural frequency last mass
c_cr = np.sqrt(k_l*m_l) # critical damping
zeta = c_d/c_cr # damping coefficent
w0_d = cmath.sqrt(k_l/m_l) # natural frequency last mass in rad/s
```

In [11]:
```
# Definition frequency dependent parameters
chi_t = []
for b in (omega):
    ct = complex(0,(b/w0_d)*cmath.sqrt(2+complex(0,2*zeta*b)-(b**2/w0_d**2))) #coeffi
    chi_t.append(ct)
```

In [12]:
```
#Force function
fw = []
for a,w in zip(a_m,omega):
    force_w = a/(complex(0,2))*(T_p+1/(complex(0,2)*w)-1/(complex(0,-2)*w)*np.exp(comp
    fw.append(force_w)
```

In [13]:
```
# Mass matrix
mass = np.zeros(n)
for i in range(len(mass)):
    mass[i] = m

M = np.zeros((n,n))
for j in mass:
    np.fill_diagonal(M,j)
```

In [14]:
```
# Stiffness matrix
K = []
for c in (chi_t):
    g = np.zeros((n,n),dtype=complex)
    g[0,0] = k
    g[0,1] = -k
    g[-1,-2] = -k
    for j,i in zip(range(1,n-1),range(0,(n-2))): #for i in range(0,(n-2)):
        g[j,i-1] = 0
        g[j,i] = -k
        g[j,i+1] = 2*k
        g[j,i+2] = -k
    g[-1,-1] = k+k*c
    K.append(g)
```

In [15]:
```
# Damping matrix
C = []
```

```
        C = np.zeros((n,n))
        C[0,0] = c_d
        C[0,1] = -c_d
        C[-1,-2] = -c_d
        for j,i in zip(range(1,n-1),range(0,(n-2))):
            C[j,i-1] = 0
            C[j,i] = -c_d
            C[j,i+1] = 2*c_d
            C[j,i+2] = -c_d
            C[-1,-1] = c_d

        C_matrix = []

        for w in omega:
            j = complex(0,1)*w*C
            C_matrix.append(j)
```

In [16]:
```
# Construction of the complex K-matrix with damping and stiffness
K_matrix = []

for st,dp in zip(K,C_matrix):
    x = st + dp
    K_matrix.append(x)
```

In [17]:
```
# Construction of the total matrix to be solved: T = (-w^2*M+K-matrix)
Total = []
for j,w in zip(K_matrix,omega):
    t_temp = -w**2*M+j
    Total.append(t_temp)
```

In [18]:
```
# Construction of matrix with force function
F_matrix = np.zeros([33,n], dtype=complex)

for l,r in zip(range(len(F_matrix)),fw):
    F_matrix[l,0] = r
```

2 Solve system of equations

In [19]:
```
#Solves the system of equation and results in displacement matrix X_def for each mass
X_def = []
for t,f in zip(Total,F_matrix):
    x = np.linalg.solve(t,f)
    X_def.append(x)
```

4

3   Plot Solution

```
In [20]: # Displacment spectrum per mass
         X_mass = []
         for j in range(len(X_def[0])):
             x_temp = []
             for i in range(len(X_def)):
                 p = X_def[i][j]
                 x_temp.append(p)
             X_mass.append(x_temp)
```

4   Calc check

```
In [21]: for t,u,f in zip(Total,X_def,F_matrix):
             l = np.allclose(np.dot(t,u),f)
             print(l)
```

```
True
True
True
True
True
True
True
True
True
True
True
True
True
True
True
True
```

D

Sensitivity Analysis of model parameters

D.1. Sediment type lower layer

The sediment type of the lower layer is tested. The results in the frequency spectrum at MP1 till MP4 are presented in Figure D.1. The lower layer is simulated as a rock to account for the lowest consolidated layers in the real seabed. The influence of the choice of sediment type for this lower layer is investigated here. If the lower layer consists of coarse sand the seabed absorbs more sound than for a rock layer (green line and pink line in Figure D.1). If the lower layer consist of fine sediment the seabed absorbs more sound than for a rock layer as well (green line and blue line in Figure D.1). A clear relation between the coarseness of the sediment and the predicted sound levels is observed. For a coarser sediment type of the lower layer higher sound level in the water are reached.
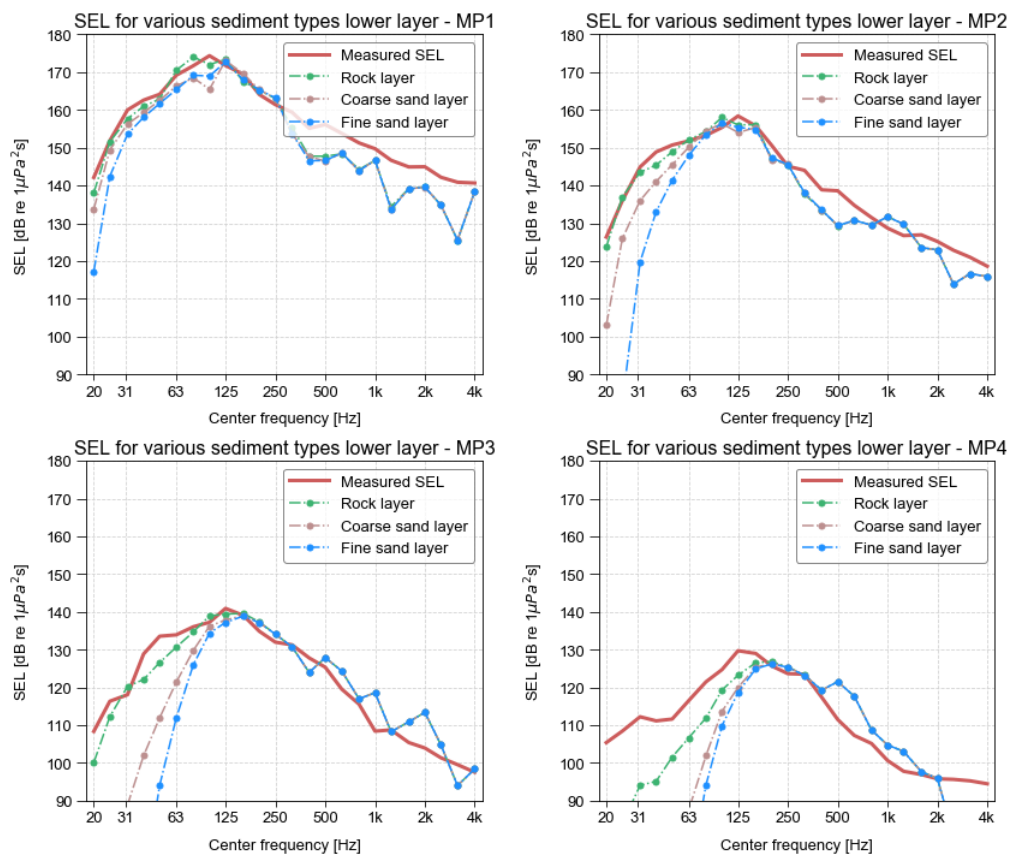
Figure D.1: Model results and Gemini data compared: The one-third octave band spectra of the sound exposure level at 10m above the seabed at the measurement locations MP1 till MP4

D.2. Upper rock layer

The effect of different types of rock for a rock seabed has been tested. The results in the frequency spectrum at MP1 till MP4 are presented in Figure D.2. Both rock types show an overprediction of the sound levels. The difference of between the sound levels for the different types is not significant.
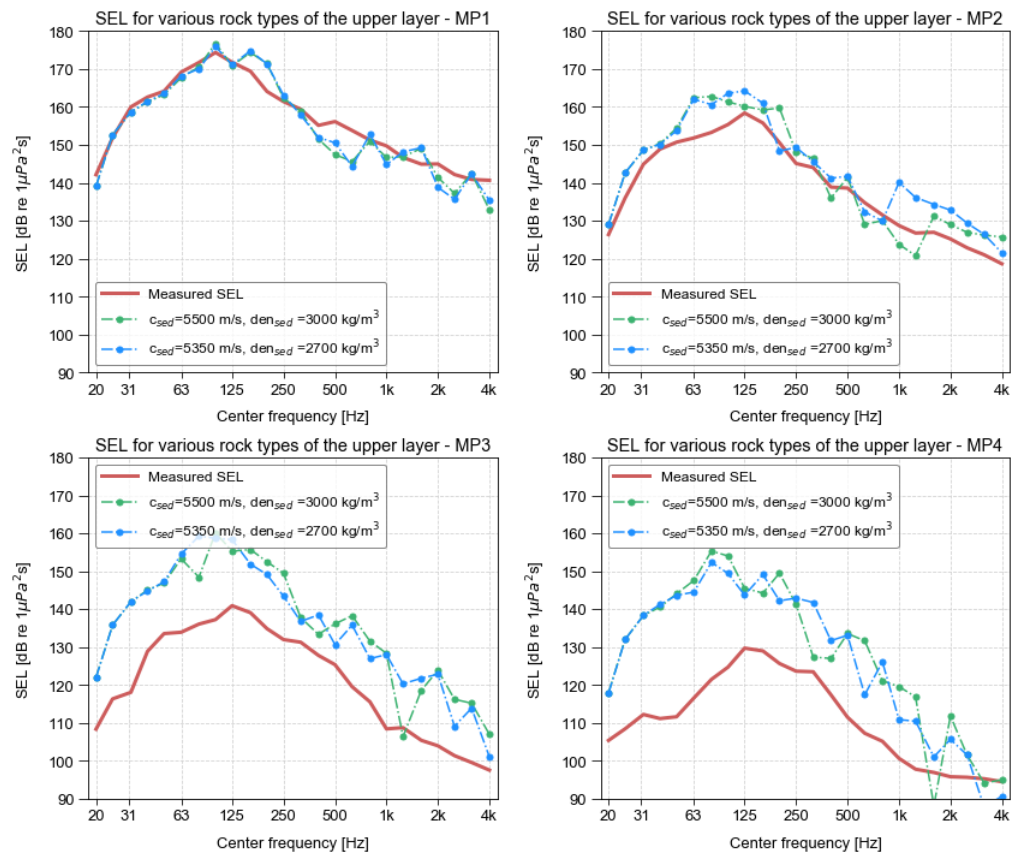
Figure D.2: Model results and Gemini data compared: The one-third octave band spectra of the sound exposure level at 10m above the seabed at the measurement locations MP1 till MP4

D.3. pH value

The effect of different values of the pH of the water has been tested. The results in the frequency spectrum at MP1 till MP4 are presented in Figure D.3. For distances larger than 30 km this starts to make a difference in predicted sound levels. However, the variation expressed in the used values of the pH is not considered realistic. In reality the variation of the pH of the water is really small.
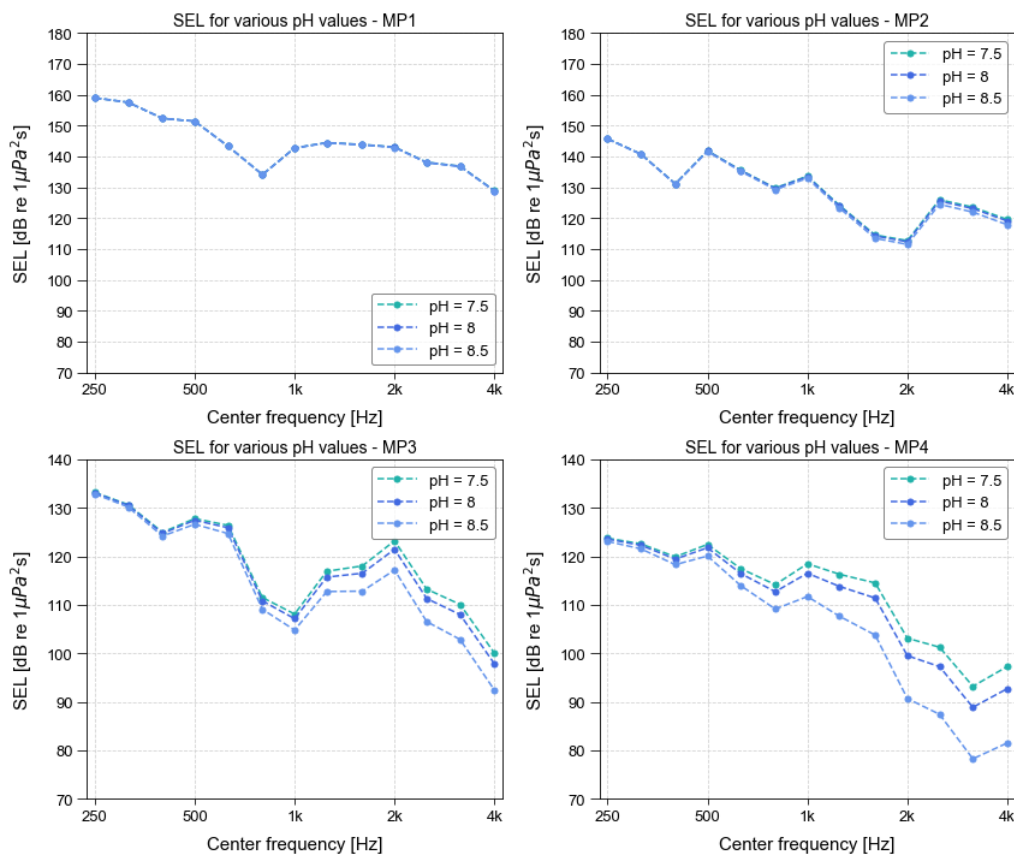
Figure D.3: The spread in Sound Exposure Level (SEL) in dB for the implemented geoacoustics properties of the sediment

D.4. Upper layer thickness

This section shows the predicted sound levels in the water for the seabed with a layer thickness of 160 m to 1.25 m. The results in the frequency spectrum at MP1 till MP4 are presented in Figure D.4, Figure D.5, Figure D.6 and Figure D.7. In Figure D.7 also the effect of different sediment types for the deeper layer are presented. For decreasing layer thickness the predicted sound levels increase and for increasing coarseness of the lower sediment layer the predicted sound levels increase.

Figure D.4: The Sound Exposure Level (SEL) per frequency band as simulated by the UAS at meausurement locations MP1, MP2, MP3 and MP4 for various sediment layer thicknessess upto 5 meter. This choice of thicknessess affects the SEL at the lower frequencies ranges ≤ 250Hz.
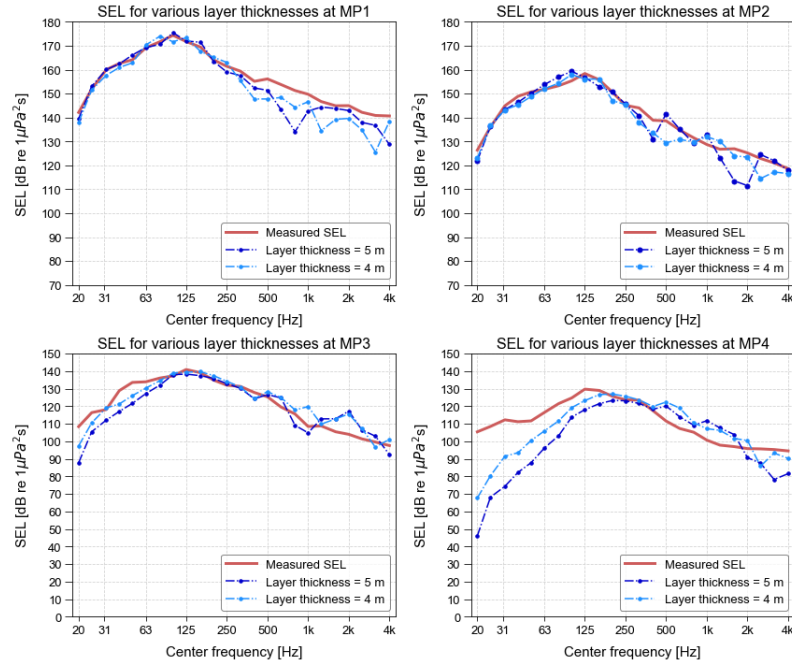
Figure D.5: The Sound Exposure Level (SEL) per frequency band as simulated by the UAS at meausurement locations MP1, MP2, MP3 and MP4 for various sediment layer thicknessess 5 m and 4 m.
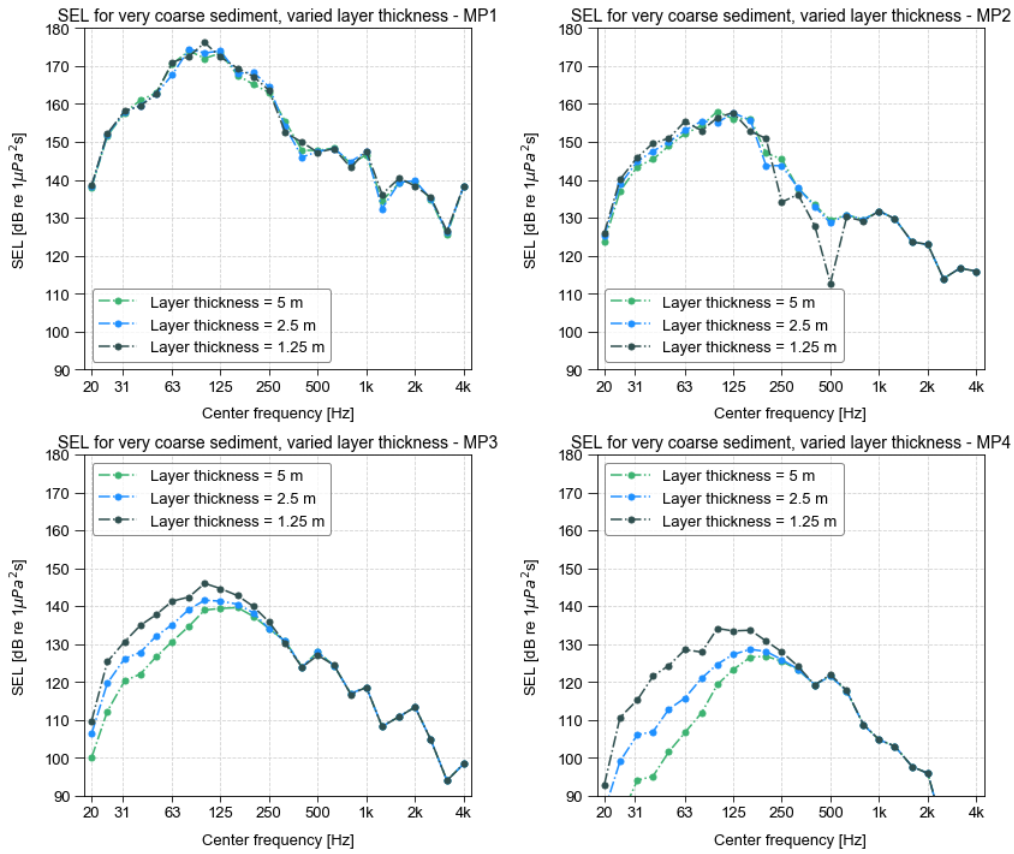
Figure D.6: The Sound Exposure Level (SEL) per frequency band as simulated by the UAS at meausurement locations MP1, MP2, MP3 and MP4 for various sediment layer 5 m , 2.5 m and 1.25 m
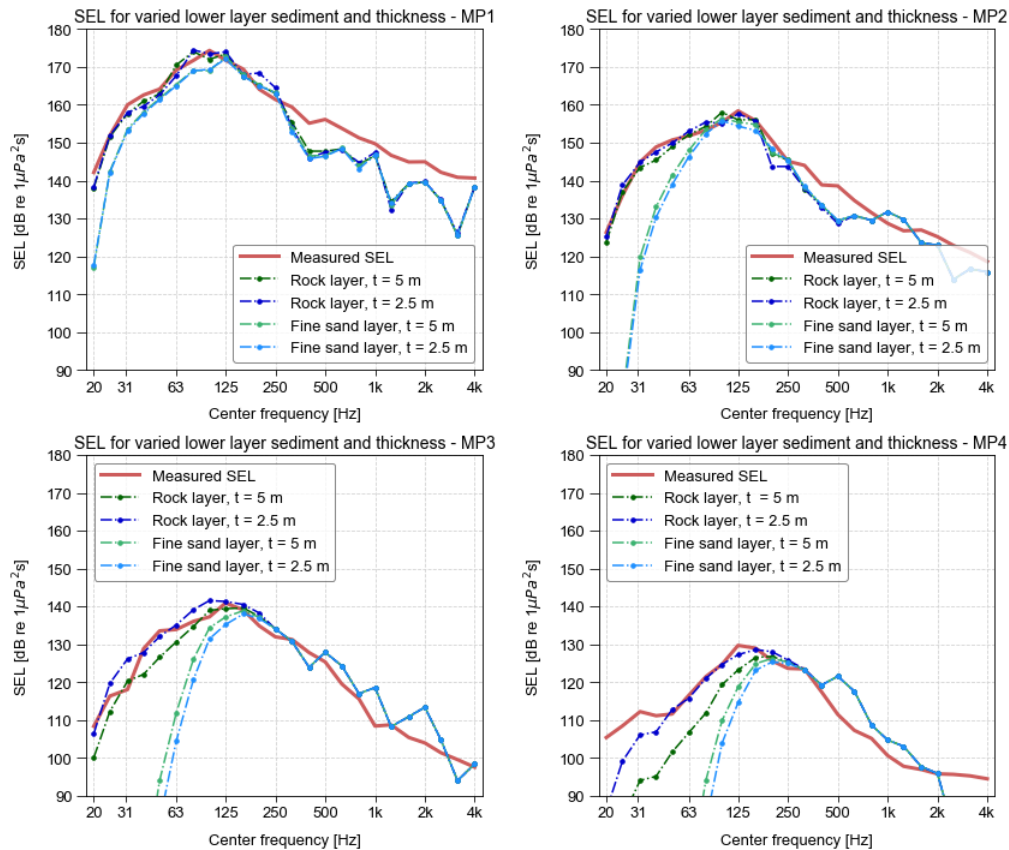
Figure D.7: The Sound Exposure Level (SEL) per frequency band as simulated by the UAS at meausurement locations MP1, MP2, MP3 and MP4 for various sediment layer thickness and sediment types

D.5. Temperature and Salinity

The effect of different values of the temperature and salinity of the water has been tested. The results in the frequency spectrum at MP1 till MP4 are presented in Figure D.8 and Figure D.9. The effect of both the temperature and salinity variations on the predicted sound levels is negligible.
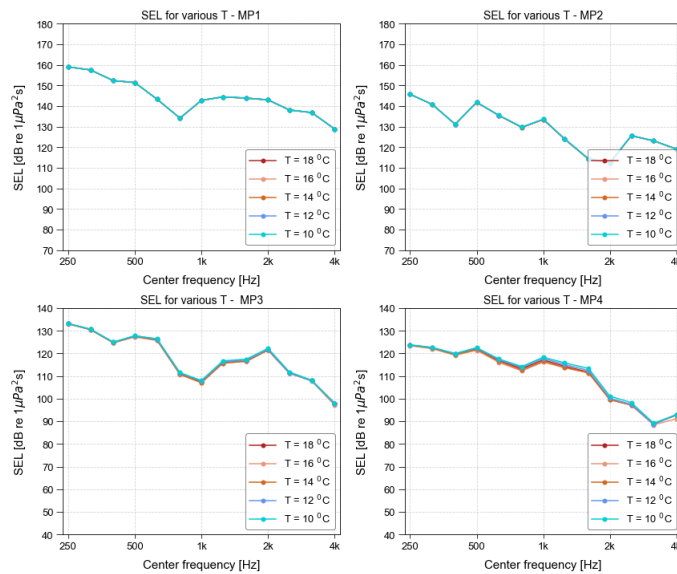
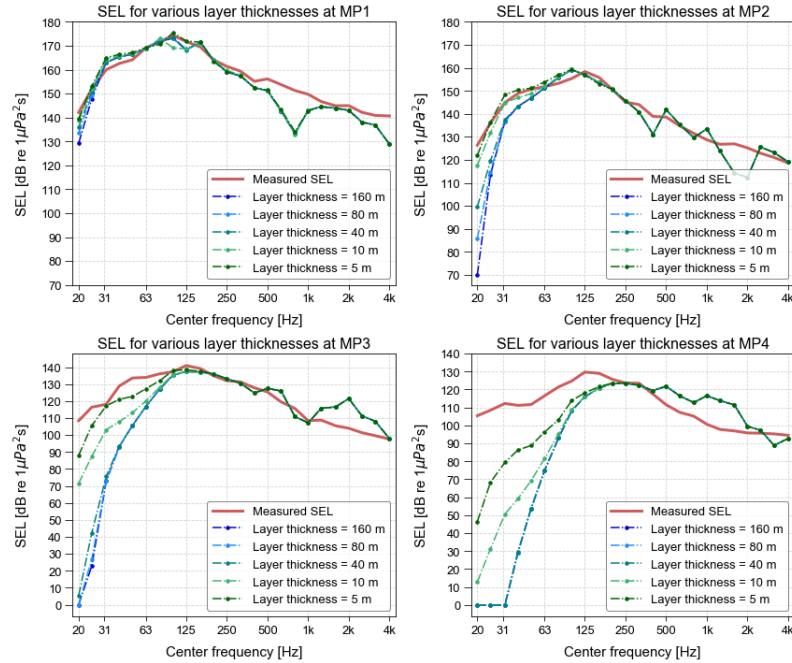Figure D.8: The Sound Exposure Level (SEL) per frequency band as simulated by the UAS at meausurement locations MP1, MP2, MP3 and MP4 for various values of the water temperature.

Figure D.9: The Sound Exposure Level (SEL) per frequency band as simulated by the UAS at meausurement locations MP1, MP2, MP3 and MP4 for various values of the salinity of the water.

D.6. Water depth

In the Gemini area the water level is dominated by the tides. In Binnerts et al. (2016b) a tidal variation of $\pm$ 0.80 meter at the location of monopile U8 is mentioned. Therefore the effect of various water levels on the SEL is studied. This tidal variation has negigible effect on the predicted sound levels.

Figure D.10: The total Sound Exposure Level (SEL) as simulated by the UAS at measurement locations MP1, MP2, MP3 and MP4 for two simulations with a different water depth.

Figure D.11: The total Sound Exposure Level (SEL) as simulated by the UAS at measurement location MP1, MP2, MP3 and MP4 for two simulation with different water depth.

Figure D.12: The total Sound Exposure Level (SEL) as simulated by the UAS at meausurement locations MP1, MP2, MP3 and MP4 for simulations with a different water depth.
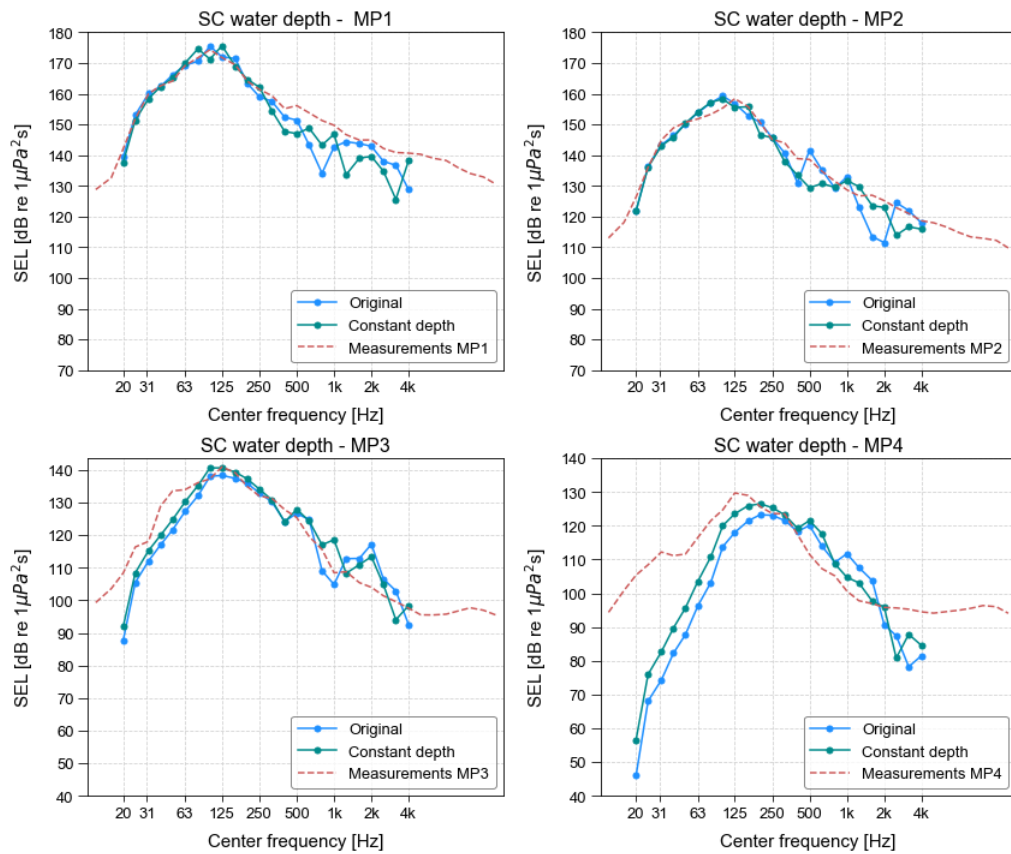
Figure D.13: The total Sound Exposure Level (SEL) as simulated by the UAS at measurement location MP1, MP2, MP3 and MP4 for simulation with different water depth.

D.7. Source spectrum

The sensitivity of the model to different source spectrums is analyzed. The the results (Figure D.14) obtained with the original source spectrum (blue line in Figure D.15) and the source spectrum obtained with data from wind park Q7 (Binnerts et al., 2016a) (green line in Figure D.15)are compared. The predicted total sound levels vary significantly. This highlights the difficulties associated with the point source represenation in the UAS.
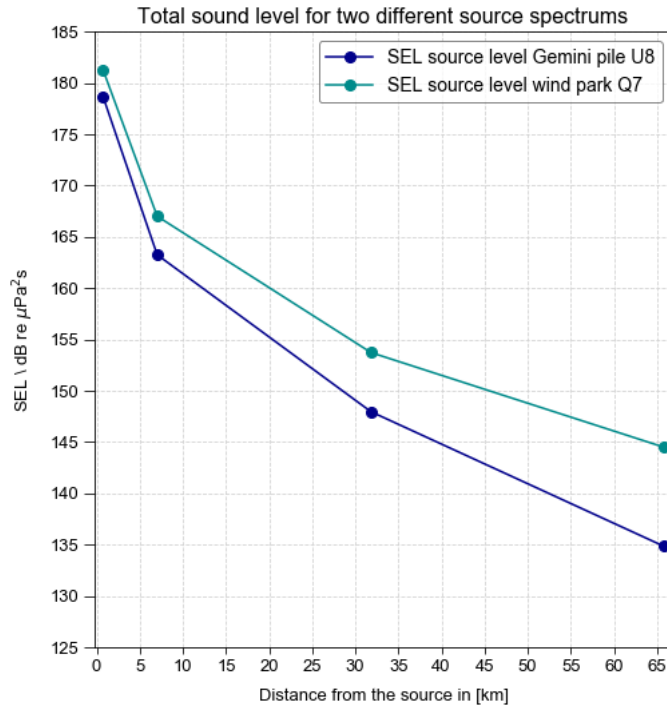
Figure D.14: The total SEL for two different source spectrums
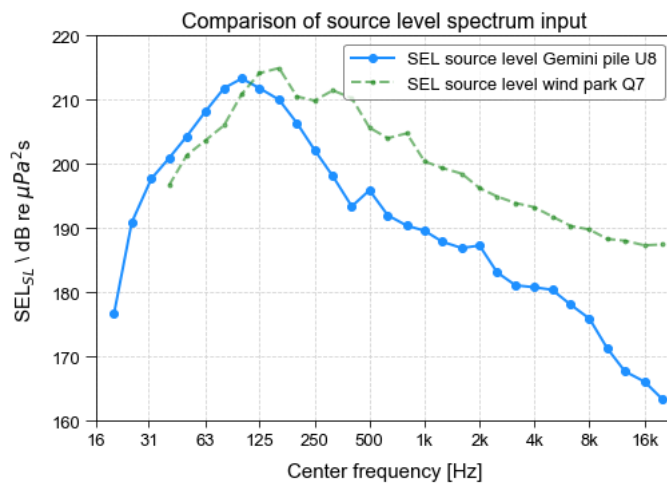
Figure D.15: The total SEL for two different source spectrums

D.8. Source depth

The effect of different depths of the point source has been tested. The results in the frequency spectrum at MP1 till MP4 are presented in Figure D.16 and Figure D.17. These results show the difficulty of a point source representation regarding its implemented depth.
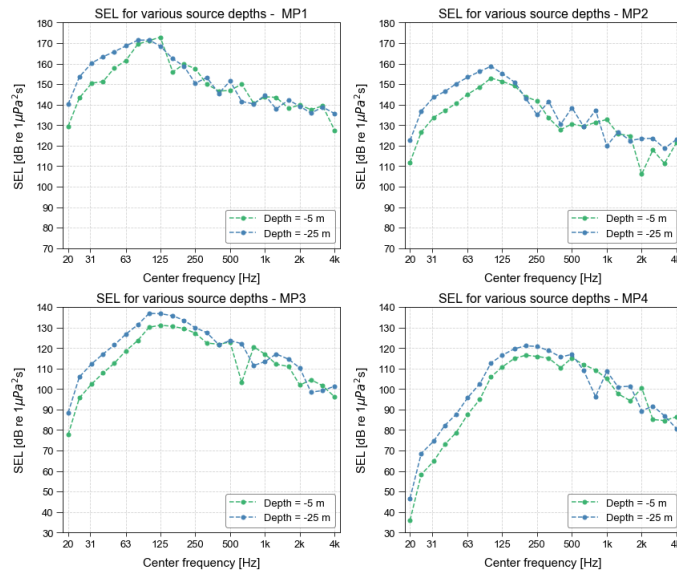
Figure D.16: The frequency distribution of the Sound Exposure Level (SEL) as simulated by the UAS at measurement location MP1, MP2, MP3 and MP4 for two simulation with different source depth.
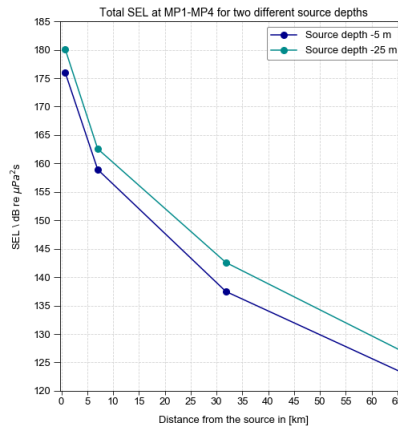
Figure D.17: The total Sound Exposure Level (SEL) as simulated by the UAS at measurement location MP1, MP2, MP3 and MP4 for two simulation with different source depth.

D.9. Receiver location

The receiver position used to produce the predicted results is based on the exact distance from the source in meters corresponding to measurement location MP1 till MP4 and the height of the heidrophone above the seabed, 2 meter and 10 meter respectively. Because the results in the UAS are provided per grid cell with dimensions $\Delta z = 1$, $\Delta r = 20$ m linear interpolation is used to determine the predicted results by the UAS on that exact location. This subsection investigates the effect of the linear interpolation on the results. To this end the receiver position is varied in depth and over range with $\pm$ 0.5 m and $\pm$ 20 m respectively.
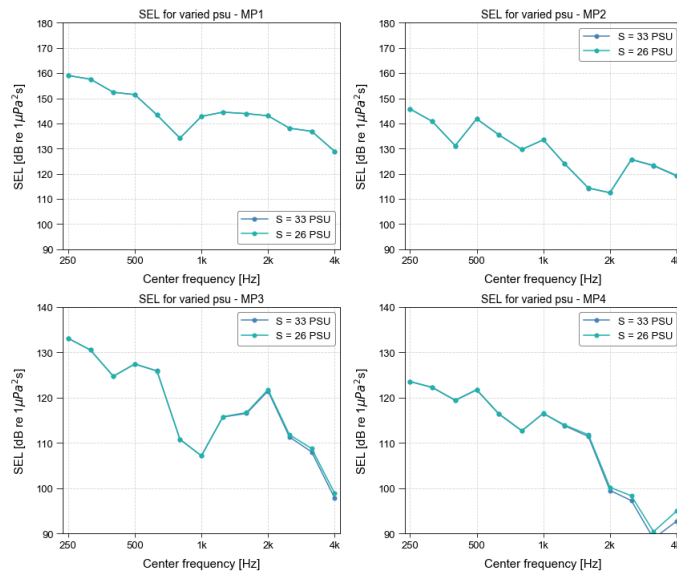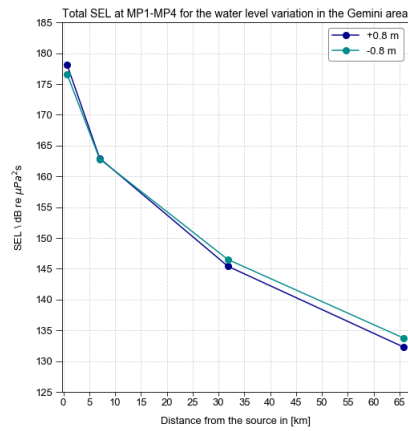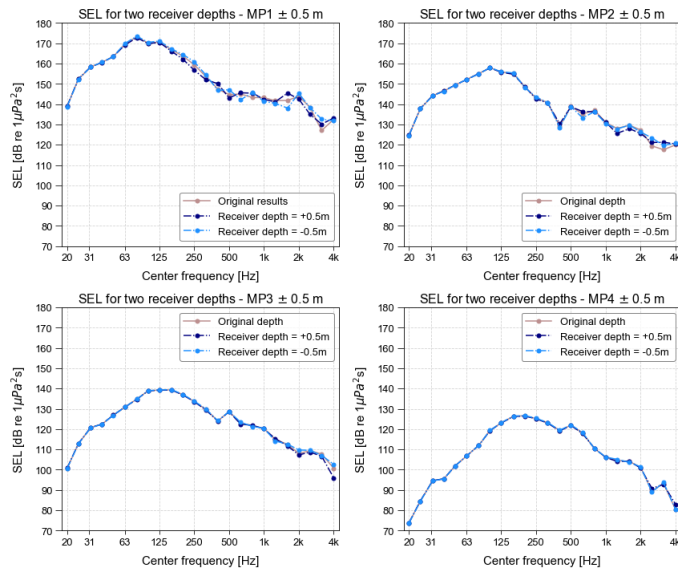

Figure D.18: The Sound Exposure Level (SEL) per frequency band as simulated by the UAS at measurement location MP1, MP2, MP3 and MP4 for two simulation with different receiver depth.

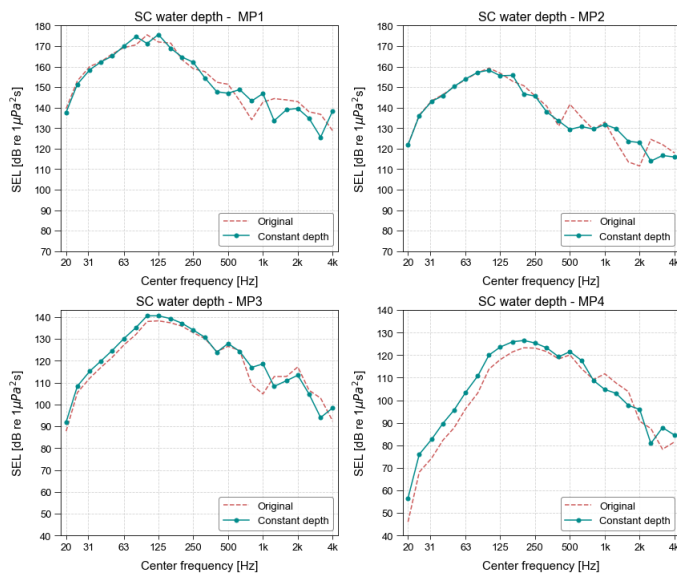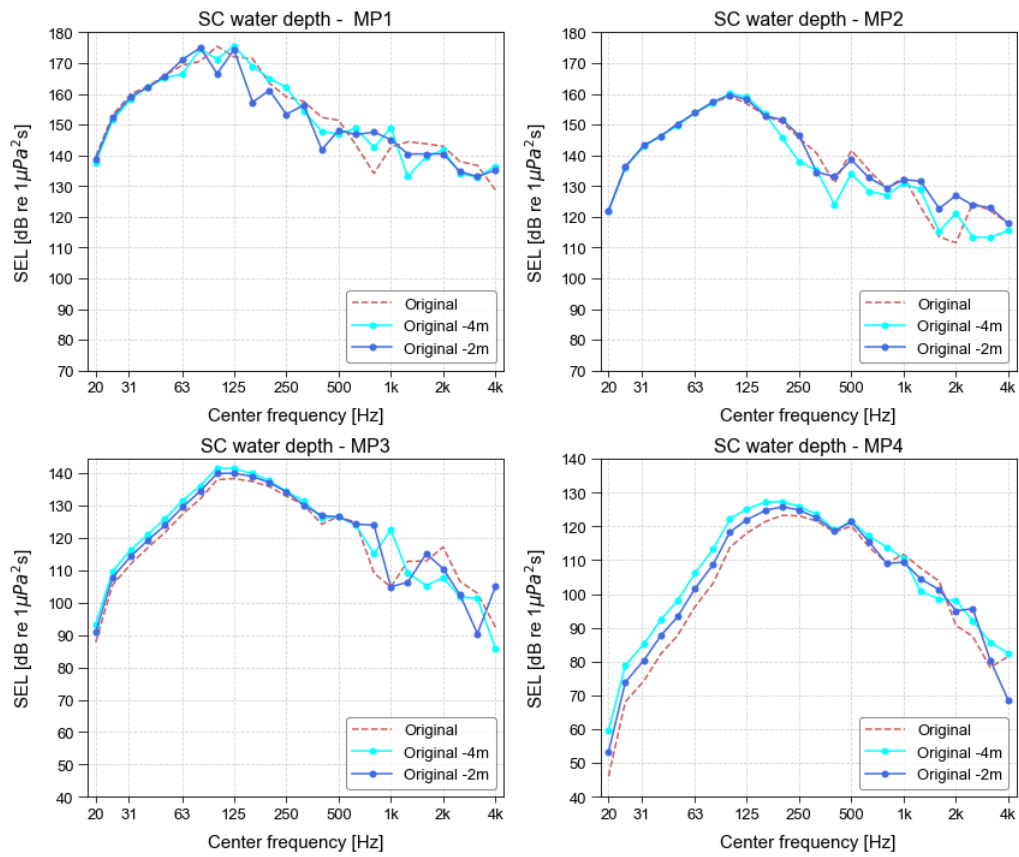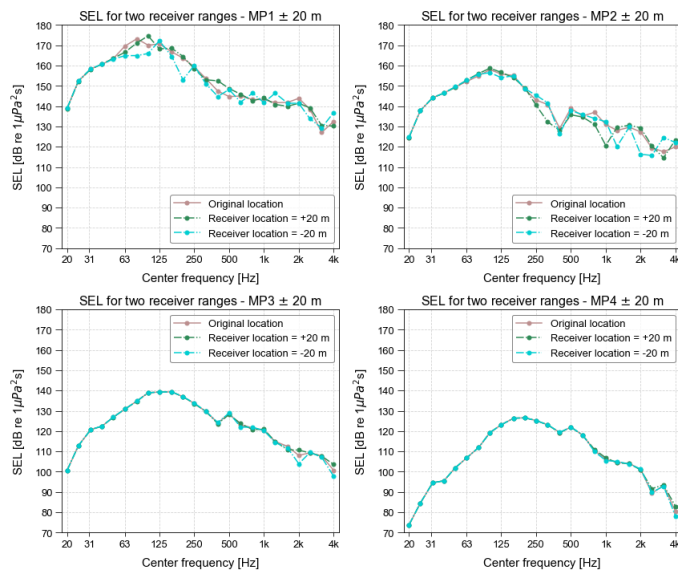Figure D.19: The Sound Exposure Level (SEL) per frequency band as simulated by the UAS at measurement location MP1, MP2, MP3 and MP4 for two simulation with different receiver distance from the source.

E

Jupyter Notebooks

Load Gemini data all frequencies

March 18, 2018

```
In [1]: import h5py
        import numpy as np
        import os

        root = r'C:\Checkouts\VOMSC\hyc\Afstuderen Onderwatergeluid\Data Gemini\Gemini\Gemini\(
```

```
In [2]: roots = [r'Gemini_MPU8_MP1\GM_MP1_1557_piling_nl.h5',r'Gemini_MPU8_MP2\GM_MP2_1536_pil:
        files = []
        for i in roots:
            file = os.path.join(root, i)
            f = h5py.File(file, 'r')
            files.append(f)
            print(os.path.exists(file))

        print(files)
```

```
True
True
True
True
True
True
True
True
[<HDF5 file "GM_MP1_1557_piling_nl.h5" (mode r)>, <HDF5 file "GM_MP2_1536_piling_nl.h5" (mode r
```

```
In [3]: #Define all measurement positions for 2m above seabed
        MP1_2 = files[0]['sel_data_singleblow/block0_values'][1261,:]
        MP2_2 = files[1]['sel_data_singleblow/block0_values'][8832,:]
        MP3_2 = files[2]['sel_data_singleblow/block0_values'][11415,:]
        MP4_2 = files[3]['sel_data_singleblow/block0_values'][875,:]
```

```
In [4]: #Define all measurement positions for 10m above seabed
        MP1_10 = files[4]['sel_data_singleblow/block0_values'][1261,:]
        MP2_10 = files[5]['sel_data_singleblow/block0_values'][8832,:]
        MP3_10 = files[6]['sel_data_singleblow/block0_values'][11415,:]
        MP4_10 = files[7]['sel_data_singleblow/block0_values'][875,:]
```

1

```
In [5]: MP_2 = [MP1_2,MP2_2,MP3_2,MP4_2]
        MP_10 = [MP1_10,MP2_10,MP3_10,MP4_10]

In [6]: #Define frequency axis
        FQ = [12,16,20,25,32,40,50,63,80,100,125,160,200,250,315,400,500,630,800,1000,1250,160(
        FQ_labels = ['12','16','20','25','32','40','50','63','80','100','125','160','200','250

In [7]: #Defines 4 array with SEL for all frequencies for every MP, 2 m above the seabed
        freq_all2 = []
        for i in range(len(MP_2)):
                x = MP_2[i]
                freq_all2.append(x)

In [8]: #Defines 4 array with SEL for all frequencies for every MP 10 m above the seabed
        freq_all10 = []
        for i in range(len(MP_10)):
                x = MP_10[i]
                freq_all10.append(x)
```

2

Interpolation of the MIKE Output files, Load Data and Plot both

March 18, 2018

```python
In [3]: import h5py
        import numpy as np
        import os

        import matplotlib.pyplot as plt
        %matplotlib inline

        from scipy import interpolate

        root = r'C:\Checkouts\VOMSC\hyc\Afstuderen Onderwatergeluid\Mike scripts'
```

```python
In [4]: file = os.path.join(root,r'hdf5_output\Run1.h5')
        os.path.exists(file)
```

```
Out[4]: True
```

```python
In [5]: f = h5py.File(file, 'r') # open read-only
```

```python
In [6]: #File settings
        filename = 'HR'
        outpath = r'C:\Users\HYC\Documents\00_Afstuderen Onderwatergeluid\05_Figures\Compare\D:
        Save = 'No'
        Close = 'Yes'
```

1 Load MIKE Output

```python
In [7]: D = {}
```

```python
In [8]: #Define x-axis
        D['xaxis'] = f['x-axis']
        D['xaxis'] = np.concatenate(D['xaxis'], axis=0)
        D['xaxis'] = D['xaxis'].astype(int)
```

```python
In [9]: #Define y-axis
        D['yaxis'] = f['y-axis']
        D['yaxis'] = np.concatenate(D['yaxis'], axis=0)
        D['yaxis'] = D['yaxis']
        D['yaxis'] = [(52-i)*-1 for i in D['yaxis']]
```

1

```
In [10]: #Define MIKE output in a list
         D['MIKEout_temp'] = []
         for i in f:
             D['MIKEout_temp'].append(f[i])

         D['MIKEoutput'] = D['MIKEout_temp'][0:-2]
```

2 2D interpolation of MIKE output

```
In [11]: #Define the interpolation parameters
         x = D['xaxis']
         y = D['yaxis']
         z = D['MIKEoutput']
```

```
In [12]: #Interpolate all the frequencies bands in list z
         mike_i = []
         for i in range(len(z)):
             i2d = interpolate.interp2d(x,y,z[i])
             mike_i.append(i2d)
```

```
In [13]: #Define array with all interpolated values at the MP's for all the frequency bands
         mike_def1 = []

         xnew1 = np.asarray([732, 7017])
         ynew1 = np.asarray([-32,-24])

         for i in range(len(mike_i)):
             i2d_new1 = mike_i[i](xnew1,ynew1)
             mike_def1.append(i2d_new1)

         mike_def2 = []

         xnew2 = np.asarray([31816, 65764])
         ynew2 = np.asarray([-32,-24])

         for i in range(len(mike_i)):
             i2d_new2 = mike_i[i](xnew2,ynew2)
             mike_def2.append(i2d_new2)

         #print(mike_def1)
         #print(mike_def2)
```

```
In [14]: mike_def = []

         for i in range(len(mike_def1)):
             s=np.concatenate((mike_def1[i],mike_def2[i]), axis=1)
             mike_def.append(s)
```

In [15]: *#Define array for the total sel and all frequencies bands seperate for MIKE output, x*
```
mike_tot = mike_def[24]
mike_feq = mike_def[0:24]
```

3 Load Gemini Data

In [16]: `root = r'C:\Checkouts\VOMSC\hyc\Afstuderen Onderwatergeluid\Data Gemini\Gemini\Gemini`

In [17]:
```
roots = [r'Gemini_MPU8_MP1\GM_MP1_1557_piling_nl.h5',r'Gemini_MPU8_MP2\GM_MP2_1536_pi1
files = []
for i in roots:
    file = os.path.join(root, i)
    f = h5py.File(file, 'r')
    files.append(f)
    print(os.path.exists(file))

print(files)
```

```
True
True
True
True
True
True
True
True
[<HDF5 file "GM_MP1_1557_piling_nl.h5" (mode r)>, <HDF5 file "GM_MP2_1536_piling_nl.h5" (mode r
```

In [18]:
```
#Define all measurement positions
MP1_2 = files[0]['sel_data_singleblow/block0_values'][1261,:]
MP2_2 = files[1]['sel_data_singleblow/block0_values'][8832,:]
MP3_2 = files[2]['sel_data_singleblow/block0_values'][11415,:]
MP4_2 = files[3]['sel_data_singleblow/block0_values'][875,:]
```

In [19]:
```
#Define all measurement positions for 10m above seabed
MP1_10 = files[4]['sel_data_singleblow/block0_values'][1261,:]
MP2_10 = files[5]['sel_data_singleblow/block0_values'][8832,:]
MP3_10 = files[6]['sel_data_singleblow/block0_values'][11415,:]
MP4_10 = files[7]['sel_data_singleblow/block0_values'][875,:]
```

In [20]:
```
MP_2 = [MP1_2,MP2_2,MP3_2,MP4_2]
MP_10 = [MP1_10,MP2_10,MP3_10,MP4_10]
```

In [21]: `DX = [732,7017,31816,65764]`

In [22]:
```
#Defines array with MP1-MP4 for total SEL and SEL at all frequencies 2 m above seabed
mp_all_2 = []
```

3

```
        for j in range(len(MP_2[0])):
            mp_j = []
            for i in range(len(MP_2)):
                x = MP_2[i][j]
                mp_j.append(x)
            mp_all_2.append(mp_j)
        #print(mp_all_2)
```

In [23]:
```
#Defines array with MP1-MP4 for total SEL and SEL at all frequencies 10 m above seabe
mp_all_10 = []
for j in range(len(MP_10[0])):
    mp_j = []
    for i in range(len(MP_10)):
        x = MP_10[i][j]
        mp_j.append(x)
    mp_all_10.append(mp_j)
#print(mp_all_10)
```

4   Plot data and MIKE output

In [25]:
```
plt.figure()
axs = plt.axes([0,0,2,1])
plt.plot(DX,mp_all_2[0], marker='o', markersize=5, linestyle='None', color ='r', label
plt.plot(DX,mp_all_10[0], marker='+', markersize=10, linestyle='None', color ='r', lal
plt.plot(DX,mike_def[24][0], marker='o', markersize=5, linestyle='None', color ='b', 
plt.plot(DX,mike_def[24][1], marker='+', markersize=10, linestyle='None', color ='b', 

plt.xticks(np.arange(0,66000,10000),np.arange(0,66, 10), fontsize =10)
plt.yticks(np.arange(100,210,20), fontsize = 10)

plt.title('SEL for MP1-MP4 for one-thid octave band center frequency ')
plt.ylabel('SEL \ dB re $\mu Pa^2$s')
plt.xlabel('Distance from the in meter')
plt.legend()
plt.close
```

Out[25]: <function matplotlib.pyplot.close>

Import MIKE Output and 2D interpolation of the results

March 18, 2018

```
In [1]: import h5py
        import numpy as np
        import os

        import matplotlib.pyplot as plt
        %matplotlib inline

        from scipy import interpolate

        root = r'C:\Checkouts\VOMSC\hyc\Afstuderen Onderwatergeluid\Mike scripts'

In [2]: file = os.path.join(root,r'hdf5_output\Run1.h5')
        os.path.exists(file)

Out[2]: True

In [3]: f = h5py.File(file, 'r') # open read-only

In [23]: #File settings
         filename = 'Run1'
         outpath = r'C:\Users\HYC\Documents\00_Afstuderen Onderwatergeluid\05_Figures\MIKE'
         Save = 'No'
         Close = 'Yes'
```

1   Load MIKE Output

```
In [5]: D = {}
        #Define x-axis
        D['xaxis'] = f['x-axis']
        D['xaxis'] = np.concatenate(D['xaxis'], axis=0)
        D['xaxis'] = D['xaxis'].astype(int)

In [6]: #Define y-axis
        D['yaxis'] = f['y-axis']
        D['yaxis'] = np.concatenate(D['yaxis'], axis=0)
        D['yaxis'] = D['yaxis']
        #D['yaxis'] = [(52-i)*-1 for i in D['yaxis']]
```

```
In [7]: #Define Results
        D['SELoverall'] = f['Freq_Total_dataset1']
        print(D['SELoverall'])

<HDF5 dataset "Freq_Total_dataset1": shape (51, 3301), type "<f8">
```

2 Plot MIKE SEL Overall

```
In [8]: #Define Nan values for plot
        D['SELplot'] = f['Freq_Total_dataset1']
        D['SELplot'] = np.concatenate(D['SELplot'], axis=0)
        D['SELplot'] = D['SELplot'].reshape(51,3301)
        D['SELplot'][D['SELplot'] <= 0] = np.nan
        d = np.ma.masked_where(np.isnan(D['SELplot']),D['SELplot'])
```

3 2D interpolation of MIKE output

```
In [27]: x = D['xaxis']
         y = D['yaxis']
         z = D['SELoverall']

In [28]: i2d = interpolate.interp2d(x,y,z)

In [29]: xnew1 = np.asarray([732, 7017])
         xnew2 = np.asarray([31816, 65764])
         ynew1 = np.asarray([-28,-20])
         ynew2 = np.asarray([-29,-21])
         SEL1 = i2d(xnew1,ynew1)
         SEL2 = i2d(xnew2,ynew2)
         SEL = np.concatenate((SEL1,SEL2), axis=1)
```

4 Load Gemini Data

```
In [13]: root = r'C:\Checkouts\VOMSC\hyc\Afstuderen Onderwatergeluid\Data Gemini\Gemini\Gemini`

In [14]: roots = [r'Gemini_MPU8_MP1\GM_MP1_1557_piling_nl.h5',r'Gemini_MPU8_MP2\GM_MP2_1536_pi]
         files = []
         for i in roots:
             file = os.path.join(root, i)
             f = h5py.File(file, 'r')
             files.append(f)
             print(os.path.exists(file))

         print(files)
```

2

```
True
True
True
True
True
True
True
True
[<HDF5 file "GM_MP1_1557_piling_nl.h5" (mode r)>, <HDF5 file "GM_MP2_1536_piling_nl.h5" (mode r
```

```
In [15]: #Define all measurement positions
         MP1_2 = files[0]['sel_data_singleblow/block0_values'][1261,:]
         MP2_2 = files[1]['sel_data_singleblow/block0_values'][8832,:]
         MP3_2 = files[2]['sel_data_singleblow/block0_values'][11415,:]
         MP4_2 = files[3]['sel_data_singleblow/block0_values'][875,:]
```

```
In [16]: #Define all measurement positions for 10m above seabed
         MP1_10 = files[4]['sel_data_singleblow/block0_values'][1261,:]
         MP2_10 = files[5]['sel_data_singleblow/block0_values'][8832,:]
         MP3_10 = files[6]['sel_data_singleblow/block0_values'][11415,:]
         MP4_10 = files[7]['sel_data_singleblow/block0_values'][875,:]
```

```
In [17]: MP_2 = [MP1_2,MP2_2,MP3_2,MP4_2]
         MP_10 = [MP1_10,MP2_10,MP3_10,MP4_10]
```

```
In [18]: DX = [732,7017,31816,65764]
         DX2 = [7017,31816,65764]
```

```
In [19]: #Defines array with MP1-MP4 for total SEL and SEL at all frequencies 2 m above seabed
         mp_all_2 = []
         for j in range(len(MP_2[0])):
             mp_j = []
             for i in range(len(MP_2)):
                 x = MP_2[i][j]
                 mp_j.append(x)
             mp_all_2.append(mp_j)
         #print(mp_all_2)
```

```
In [20]: #Defines array with MP1-MP4 for total SEL and SEL at all frequencies 10 m above seabed
         mp_all_10 = []
         for j in range(len(MP_10[0])):
             mp_j = []
             for i in range(len(MP_10)):
                 x = MP_10[i][j]
                 mp_j.append(x)
             mp_all_10.append(mp_j)
         #print(mp_all_10)
```

3

Load Mike Output (importing and interpolation for constant depth = 34m)

March 18, 2018

```python
In [27]: import h5py
         import numpy as np
         import os
         from scipy import interpolate

         root = r'C:\Checkouts\VOMSC\hyc\Afstuderen Onderwatergeluid\Mike scripts'
```

```python
In [28]: file = os.path.join(root,r'hdf5_output\Run1.h5')
         os.path.exists(file)
```

```python
Out[28]: True
```

```python
In [29]: f = h5py.File(file, 'r') # open read-only
```

1 Load MIKE output

```python
In [30]: D = {}
```

```python
In [31]: #Define x-axis
         D['xaxis'] = f['x-axis']
         D['xaxis'] = np.concatenate(D['xaxis'], axis=0)
         D['xaxis'] = D['xaxis'].astype(int)
```

```python
In [32]: #Define y-axis
         D['yaxis'] = f['y-axis']
         D['yaxis'] = np.concatenate(D['yaxis'], axis=0)
         D['yaxis'] = D['yaxis']
         D['yaxis'] = [(52-i)*-1 for i in D['yaxis']]
```

```python
In [33]: #Define MIKE output in a list
         D['MIKEout_temp'] = []
         for i in f:
             D['MIKEout_temp'].append(f[i])

         D['MIKEoutput'] = D['MIKEout_temp'][0:-2]
```

1

2   Interpolate MIKE output

```
In [34]: #Define the interpolation parameters
         x = D['xaxis']
         y = D['yaxis']
         z = D['MIKEoutput']
```

```
In [35]: #Interpolate all the frequencies bands in list z
         mike_i = []
         for i in range(len(z)):
             i2d = interpolate.interp2d(x,y,z[i])
             mike_i.append(i2d)
```

```
In [36]: #Define array with all interpolated values at the MP's for all the frequency bands
         mike_def1 = []

         xnew1 = np.asarray([732, 7017])
         ynew1 = np.asarray([-32,-24])

         for i in range(len(mike_i)):
             i2d_new1 = mike_i[i](xnew1,ynew1)
             mike_def1.append(i2d_new1)

         mike_def2 = []

         xnew2 = np.asarray([31816, 65764])
         ynew2 = np.asarray([-32,-24])

         for i in range(len(mike_i)):
             i2d_new2 = mike_i[i](xnew2,ynew2)
             mike_def2.append(i2d_new2)

         #print(mike_def1)
         #print(mike_def2)
```

```
In [37]: mike_def = []

         for i in range(len(mike_def1)):
             s=np.concatenate((mike_def1[i],mike_def2[i]), axis=1)
             mike_def.append(s)
```

```
In [38]: #Define array for the total sel and all frequencies bands seperate for MIKE output, x
         mike_tot = mike_def[24]
         mike_feq = mike_def[0:24]
```

```
In [39]: print(mike_tot)
```

```
[[ 177.04279785  162.68316879  144.9399292   130.81810608]
 [ 178.65596924  163.23671036  147.94463806  134.83974915]]
```

2